STRUCTURAL ANALYSIS AND 3D KINEMATIC RESTORATION OF THE SOUTHERN
SUDBURY BASIN, ONTARIO.

By IRIS LENAUER, B.Sc., M.Sc.

A dissertation submitted to the School of Graduate Studies in partial fulfillment of the
requirements for the Degree of Doctor of Philosophy.

McMaster University DOCTOR OF PHILOSOPHY (2012) Hamilton, Ontario (School of Geography and Earth Sciences)

TITLE: Structural analysis and 3D kinematic restoration of the southern Sudbury Basin, Ontario
AUTHOR: Iris Lenauer, B.Sc. (University of Vienna, Austria), M.Sc. (University of Vienna, Austria)
SUPERVISOR: Dr. Ulrich Riller
NUMBER OF PAGES: ix, 121

ABSTRACT

This thesis addresses the spatial distribution of structures and deformation geometry in the southern Sudbury Basin, Ontario, a synclinal fold basin. Major components are low-temperature fabric development in the Sudbury Igneous Complex (SIC), the relation between fabrics and fold structures in Huronian rocks, and kinematic modeling of deformation of the southern Sudbury Basin. These topics lead to a synthetic model of the structural history of the SIC and its host rocks. Analysis of structures in the Norite layer of the SIC shows that this unit deformed under a single deformation regime and variable rheological conditions. This is evident by foliation planes, folded granitoid dikes, brittle shear faults and ductile high-strain zones. Brittle deformation preceded the formation of foliation planes and caused hydrolytic weakening of the Norite. Bulk thinning led to steepening of lithological contacts and igneous layering in the SIC. Structures in Huronian rocks and Sudbury Breccia display components of post-impact deformation that cannot be accounted for by thrusting along a high-strain zone, the so-called South Range Shear Zone, and by large-scale folding of the SIC. Shape change of the SIC from a convex outward to concave inward geometry led to basin-concentric shortening, the formation of a buckle fold of the SIC and axial-planar fabrics in Huronian rocks. Mutually perpendicular fabric orientations compatible with overall NW-SE shortening indicate that discordant foliations can form as a consequence of local strain perturbations near lithological contacts. Kinematic modelling of deformation based on field-based structural data tests the validity of trishear fault propagation folding as a possible deformation mechanism for the southern Sudbury Basin. Trishear deformation of the central South Range accounts for angular discordances between the upper and basal contacts of the SIC, local overturning of southern SIC, steepening of foliation planes, strain gradients in the Sudbury Basin, and thickness variations of SIC layers. Implications are shallowly dipping SIC layers both at greater depths and above the current erosion level, translation of Huronian rocks, and thinning in a section of the trishear zone manifested at surface by the South Range Shear Zone.

Table of Contents

v

List of Figures

List of Tables

1.   Introduction

1.1 The geological significance of the Sudbury Impact Structure

The Sudbury Impact Structure is one of the largest known terrestrial impact structures on Earth, and one of the few that exposes an impact melt sheet. The Sudbury Impact Structure represents a geologically unique study area as it is the only impact structure exposing a crystalline melt sheet that is affected by significant tectonometamorphic overprint. The impact structure has drawn the attention of geologists since its discovery as a contiguous melt sheet in the mid-19th century as it is of extraordinary economic and scientific significance. For one, the Sudbury area hosts abundant Ni-Cu-PGE deposits, making it one of the largest Ni-producing districts world-wide. Future economic prosperity of the Sudbury area is dependent on a continuation of exploration of hitherto unknown ore deposits, at greater depth and greater radial distance to the prospective melt sheet, the crystalline layered rock formed due to the impact. Even though the Sudbury Impact Structure has been the subject of extensive geological, mineralogical, petrological, and geochemical studies, many aspects of its formation and modification by deformation are still disputed.

The energy set free by the impact allowed for the generation of a large melt sheet, the Sudbury Igneous Complex (SIC), which cooled and differentiated into chemically and petrographically distinct layers. Due to density variations and gravitational effects, rocks hosting abundant metal sulphides were the first to settle upon cooling of the SIC and are, thus, situated at the base of this impact melt (Golightly, 1994). The melt sheet subsequently differentiated into layers traditionally known as the Norite, Quartz Gabbro and Granophyre, which form the Main Mass of the SIC. Ore-bearing material is also localized in dikes in the fractured host rocks of the SIC. These so-called Offset Dikes represent the parental quartz dioritic composition for the melt sheet (Lightfoot et al., 2001). A discontinuous layer of mafic to ultramafic inclusion-bearing gabbro-noritic to noritic rock, the so-called Sublayer (Pattison, 1979; Lightfoot et al. 1997), the basal layers of the SIC, the Offset Dikes and the immediate host rocks of the SIC pose the prime target of current mining activities.

The Sudbury Basin, which comprises the synformal SIC, impact-melt breccias of the Onaping Formation and a post-impact sedimentary fill, is crudely elliptical in map view (Fig. 1.1). The long axis of the Basin strikes NE-SW and extends 60 km – twice as long as the short axis. The SIC segments are termed the North, South and East Ranges, which are connected by the synclinal NE- and SE-lobes and a fold closure in the SW (Fig. 1.1). The SIC in each of the Ranges exhibits distinct characteristics in terms of its thickness, dips of lithological contacts, and structural overprint. The North Range SIC is marked by well-preserved cumulate magmatic fabric (Naldrett and Hewins, 1984) and a low degree of metamorphic overprint. In contrast, the South Range of the Sudbury Basin displays a zone of highly strained rocks, the so-called South Range Shear Zone (Rousell, 1975; Shanks and Schwerdtner, 1991a; Fig. 1.1), which crosscuts the SIC and the adjacent Onaping Formation. Thus, the intensity of deformation is higher in the South Range than in the North Range.

Notwithstanding the abundance of published literature, the geological complexity of the Sudbury Basin is a reason why major scientific questions are still left unanswered. The current

interpretations of the three-dimensional geometry of the SIC are based upon geophysical measurements and drill holes. Outcrop studies are extensive, but have been generally focused on petrologic and geochemical aspects. Thus, a detailed examination of exposed structural elements is necessary to analyze the geometric evolution of the Sudbury Basin. Previous studies systemically document fabrics in the SIC and the Onaping Formation (Rousell, 1975; Shanks, 1991; Shanks and Schwerdtner, 1991a; Cowan, 1996; Klimczak et al., 2007). Borehole data provides information on the vertical extent of deformation and surface data supplies extensive spatial coverage. Understanding the geometry of the SIC basal contact and its immediate host rocks is critical for mineral exploration. Furthermore, deciphering the current shape of the SIC can provide information on the original geometry of the impact melt sheet, which adds to our knowledge of impact processes in general.
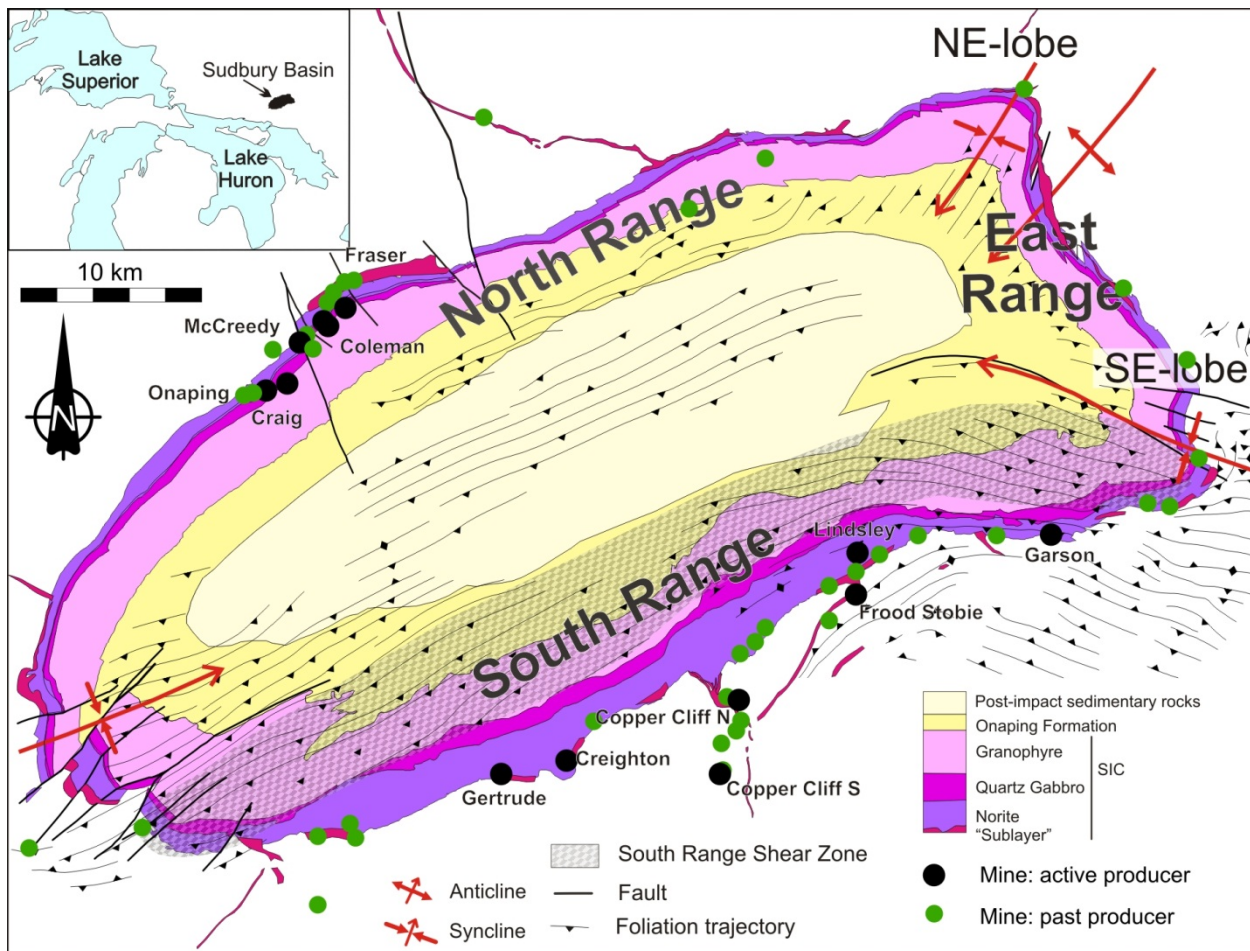
Figure 1.1: Map-view geometry of the SIC and post-impact sedimentary rocks. The map shows foliation trajectories (modified from Cowan et al., 1999) as well as major faults and fold structures. The location of past and actively producing mines are taken from Ames et al. (2005).

1.2 Unresolved questions regarding the deformation of the South Range

Although abundant investigations had the rocks of the Sudbury Impact Structure as their focus, the geometry of the SIC at depth and the effects of post-impact deformation are still a matter of debate. The size of the original impact crater and the volume, thickness and lateral extent of the melt sheet, remain poorly constrained. These crater characteristics are obscured due to erosion and post-impact tectonic overprint. In particular, the orientation, magnitude and timing of the deformation of the SIC, more specifically its South Range, are poorly constrained. In detail, quantities of deformation such as the rotational components, amounts of layer-parallel shortening, and fault displacements of the SIC have not been recorded systematically. It is also unclear where deformation localized and how it manifests itself in the affected lithologies. The aim of this thesis lies in enhancing our understanding of the geometric relationships of lithological contacts, structures and mineral fabrics in the SIC and its host rocks to better quantify post-impact deformation.

The geometry and kinematics of post-impact deformation are critical for assessing the original shape of the SIC. As a significant portion of the SIC has been eroded, the primary geometry and size of the Sudbury Impact Structure are largely a matter of debate. For example, the size of the preserved melt sheet, the position of the exposed SIC in the initial crater, and the initial crater geometry are largely unknown. Pre-deformation geometry and the primary shape of the SIC were the subject of numerical modeling studies (Ivanov and Deutsch, 1999; Ivanov, 2005), paleomagnetic (Morris, 1984) and structural work (Shanks and Schwerdtner, 1991b). The synformal geometry of the SIC is either a primary feature (Cowan, 1999) or a consequence of sagging during cooling of the melt sheet (Peredery and Morrison, 1984). It is also proposed that the crater was originally circular and that the SIC ponded on a roughly horizontal crater floor (Grieve et al., 1991; Therriault et al., 2002). More recent structural studies suggest that the synclinal geometry of the SIC is due to post-impact, non-cylindrical folding (Cowan and Schwerdtner, 1994; Riller et al., 1998; Riller, 2005; Klimczak et al., 2007; Halls, 2009; Dreuse et al., 2010).

The elliptical plan-view shape of the SIC indicates that the overall geometry of post-impact tectonic overprint is dominated by shortening parallel to the short axis of the Basin. Due to the basin asymmetry it is apparent, however, that the current plan-view shape of the SIC cannot be the product of pure cylindrical folding. The Basin abounds in heterogeneities, in particular in terms of geometry and thickness of SIC layers. Upon closer examination, the term "ellipse-shaped" does not adequately describe the plan-view shape of the SIC, because of the NE- and SE-lobes, and the southwestern fold closure (Fig. 1.1). Fabric analysis of the SIC and its adjacent rocks in the NE-lobe led to the conclusion that the NE-lobe represents a fold structure (Klimczak et al., 2007). The SE-lobe is marked by pervasive foliation and the SIC in the southwestern fold closure is segmented by a series of NW-striking faults. In the South Range the contacts of the SIC show local deviations from their overall NE-SW strike, in particular in the eastern South Range where SIC contacts strike E-W (Fig. 1.1). The protrusions of SIC in the central South Range into its host rocks appear incompatible with the overall NW-SE shortening directions (Shanks and Schwerdtner, 1991a) forming the first-order fold representing the Sudbury Basin.

Furthermore, it needs to be explored whether local buckle folding has any effect on thickness variations of SIC layers.

Additionally, the degree of deformation of the Norite of the South Range SIC has not yet been adequately addressed. The Norite layer is steeply inclined and yet appears to record little to no pervasive strain fabrics. For example, in the eastern part of the South Range the contact between the SIC and its host rocks dips at a high angle and is in places overturned (Fig. 1.1). The deviation in dip angle of the basal SIC contact away from the initially horizontal position suggests that the SIC has been affected by tectonic overprint. A subhorizontal geometry likely represents the primary shape of the melt sheet as shown by numerical models and observations on lunar and terrestrial crater morphologies (French, 1998). The rotation of the SIC to a steeply inclined position needs to be reconciled with the observation that the South Range Norite preserves igneous cumulate texture (Naldrett and Hewins, 1984) and apparently displays low levels of ductile strain (Thomson et al., 1985; Riller, 2005) and systematic geochemical trends (Lightfoot and Zotov, 2005). No mechanism for folding or straining a crystalline rock without forming metamorphic mineral fabric has yet been proposed that could explain the shape change of the South Range SIC. Based on seismic reflection data it has been proposed that the South Range SIC is imbricated on a series of SE-dipping faults (Milkereit et al., 1992). At surface, however, the SIC contacts can be traced continuously throughout most of the Sudbury Basin and less offset is observed on faults in the Basin than the magnitude required to achieve apparent S-dipping faulted contacts in the seismic images. A mechanism needs to be found that can reconcile the steep dips of the basal SIC with an apparent paucity of strain-induced mineral fabrics in the Norite. In general, it is unclear under which tectonic conditions substantial amounts of reorientations of lithological contacts can be accommodated while preserving cumulate igneous mineral fabrics.

A series of metavolcanic and metasedimentary rocks of the Huronian Supergroup form the host rocks to the South Range of Sudbury Basin. These rocks show evidence of amphibolite-grade tectonometamorphic overprint associated with the intrusion of granitoid rocks in the basal strata (Riller and Schwerdtner, 1997). In the vicinity of the granitoid intrusives the Huronian rocks are folded in a complex manner. The metasedimentary strata of the Huronian Supergroup south of the SIC are thrown into km-scale anti- and syncline folds. Although peak metamorphism and deformation are generally attributed to the Blezardian Orogeny (Riller and Schwerdtner, 1997), evidence of pervasive younger deformation events remains elusive. There is little documentation of distinct fabric generations or of crosscutting relationship. Although there is isolated evidence of post-impact deformation in the host rocks of the SIC documented in impact breccia (e.g. Scott and Spray, 1999), associating mineral fabrics to a distinct orogenic event has proven difficult.

Lithological contacts in the South Range SIC generally dip toward the Basin centre and, thus, to the NW. The SIC layers lie directly adjacent to steeply SE-dipping and S-facing metavolcanic and metasedimentary rocks. This reversal in stratigraphy from the SIC to the Huronian rocks was first noted by Cooke (1948). Rotating the South Range SIC to an initial subhorizontal geometry requires tilting of these rocks to the SE. Using solid-body rotation to restore the initial geometry of the SIC together with its host rocks leads to the overturning of the Huronian rocks prior to the emplacement of the SIC. Furthermore, tilting of the wall rock does not correlate well with geometry of the ore bodies, which are shaped as gravity-controlled vertical fingers (Lightfoot

and Farrow, 2002). Consequently, solid-body rotation of the SIC together with its host rocks as one coherent unit does not adequately explain the formation of the Sudbury Basin. A deformation mechanism needs to be identified that can accomplish differential deformation of the South Range SIC and the Huronian rocks.

This thesis is geared towards deciphering deformation in the southern Sudbury Basin and attempts to define the mechanisms characterizing post-impact shape change of the SIC and the orientation of the strain and paleo-stress fields. Benefits of the study lie in enhancing knowledge on the effects of deformation at lithological interfaces, the interaction of ductile fabrics and brittle faults, and restoration of strain, rotation and displacement of an originally horizontal marker layer, given by the impact melt sheet. Deciphering the three dimensional geometry of SIC and its host rocks has significant economic implications in understanding the location and geometry of ore deposits associated with the Sudbury Basin.

References

Ames, D.E., Davidson, A., Buckle, J.L., Card, K.D., 2005. Geology, Sudbury Bedrock Compilation, Ontario. Geological Survey of Canada, Open File 4570, scale 1:50 000.

Cooke, H.C., 1948. Regional structure of the Lake Huron-Sudbury area. *In:* Structural Geology of Canadian ore deposits, Canadian Institute of Mining and Metallogeny, 580-589.

Cowan, E.J., 1996. Deformation of the Eastern Sudbury Basin. Ph.D. thesis, University of Toronto, Toronto, 366p.

Cowan, E.J., 1999. Magnetic fabric constraints on the initial geometry of the Sudbury Igneous Complex: a folded sheet or a basin-shaped igneous body? Tectonophysics 307, 135-162.

Cowan, E.J., Schwerdtner W.M. 1994. Fold origin in the Sudbury basin. *In*: Lightfoot, P.C., Naldrett, A.J. (Eds.), Proceedings of the Sudbury - Noril'sk Symposium, Special Volume 5. Ontario Geological Survey, 45-55.

Cowan, E.J., Riller, U., Schwerdtner, W.M., 1999. Emplacement geometry of the Sudbury Igneous Complex: Structural examination of a proposed impact melt-sheet. *In*: Dressler, B.O., Sharpton, V.L., Large Meteorite Impacts and Planetary Evolution II. GSA Special Paper 339. Geological Society of America, Boulder, 399–418.

Dreuse, R., Doman, D., Santimano, T., Riller, U., 2010. Crater floor topography and impact melt sheet geometry of the Sudbury impact structure. Terra Nova, 22, 463-469.

Golightly, J.P., 1994. The Sudbury Igneous Complex as an Impact Melt: Evolution and Ore Genesis. *In:* Lightfoot, P.C., Naldrett, A.J. (Eds.), Proceedings of the Sudbury-Noril'sk Symposium. OGS Special Volume 5, 105-118.

Grieve, R., Stöffler, D., Deutsch, A., 1991. The Sudbury Structure - controversial or misunderstood. Journal of Geophysical Research 96, 22753-22764.

Halls, H.C., 2009. A 100 km-long paleomagnetic traverse radial to the Sudbury Structure, Canada and its bearing on Proterozoic deformation and metamorphism of the surrounding basement. Tectonophysics 474, 493-506.

Ivanov, B.A., 2005. Numerical Modeling of the Largest Terrestrial Meteorite Craters. Solar System Research 39, 381–409.

Ivanov, B.A., Deutsch, A., 1999. Sudbury impact event: Cratering mechanics and thermal history. *In*: Dressler, B. O., Sharpton, V. L. (Eds.), Large Meteorite Impacts and Planetary Evolution II. The Geological Society of America, Washington, D.C., 389-398.

Klimczak, C., Wittek, A., Doman, D., Riller, U., 2007. Fold origin of the NE-lobe of the Sudbury Basin, Canada: Evidence from heterogeneous fabric development in the Onaping Formation and the Sudbury Igneous Complex. Journal of Structural Geology 29, 1744-1756.

French B. M., 1998. Traces of Catastrophe: A Handbook of Shock-Metamorphic Effects in Terrestrial Meteorite Impact Structures. LPI Contribution No. 954, Lunar and Planetary Institute, Houston. 120 pp.

Lightfoot, P.C., Keays, R.R., Doherty, W., 2001. Chemical evolution and origin of nickel sulfide mineralization in the Sudbury Igneous Complex, Ontario. Ontario Geological Survey, Open File Report 5959, 231 p.

Lightfoot, P.C., Farrow, C.E.G., 2002. Geology, geochemistry, and mineralogy of the Worthington offset dike: a genetic model for offset dike mineralization in the Sudbury Igneous Complex. Economic Geology 97, 1419-1446.

Lightfoot, P.C., Zotov, I.A., 2005. Geology and Geochemistry of Sudbury Igneous Complex, Ontario, Canada: Origin of Nickel Sulfide Mineralization Associated with an Impact-Generated Melt Sheet. Geology of Ore Deposits 47, 349-381.

Milkereit, B., Green, A., Sudbury Working Group, 1992. Deep geometry of the Sudbury structure from seismic reflection profiling. Geology 20, 807-811.

Morris, W.A., 1984. Paleomagnetic constraints on the Magmatic, Tectonic, and Metamorphic History of the Sudbury Basin Region. *In*: Pye, E. G., Naldrett, A. J., Giblin, P. E. (Eds.), The Geology and Ore Deposits of the Sudbury Structure. Special Publication 1. Ontario Geological Survey, Toronto, 411-429.

Naldrett, A.J., Hewins, H.R., 1984. The Main Mass of the Sudbury Igneous Complex. *In:* Pye, E.G., Naldrett, A.J., Giblin, P.E. (Eds.), The Geology and Ore Deposits of the Sudbury Structure. Special Publication 1, Ontario Geological Survey, Toronto, 235-252.

Pattison, E.F., 1979. The Sudbury Sublayer. Canadian Mineralogist 17, 257-274.

Peredery, W.V., Morrison, G.G., 1984. Discussion of the Origin of the Sudbury Structure. *In* Pye, E.G., Naldrett, A.J., Giblin, P.E. (Eds.), The Geology and Ore Deposits of the Sudbury Structure. Special Publication 1, Ontario Geological Survey, Toronto, 491-511.

Riller, U., 2005. Structural characteristics of the Sudbury Impact Structure, Canada: impact-induced and orogenic deformation – a review. Meteoritics and Planetary Science 40, 1723-1740.

Riller, U., Schwerdtner, W., 1997. Mid-crustal deformation at the southern flank of the Sudbury Basin, central Ontario, Canada. Geological Society of America Bulletin 109, 841-854.

Rousell, D.H., 1975. Origin of foliation and lineation in Onaping Formation and deformation of Sudbury Basin. Canadian Journal of Earth Sciences 12, 1379-1395.

Scott, R.G., Spray, J.G., 1999. Magnetic fabric constraints on friction melt flow regimes and ore emplacement direction within the South Range Breccia Belt, Sudbury Impact Structure. Tectonophysics 307, 163-189.

Shanks, W. S., 1991. Deformation of the central and southern portions of the Sudbury Structure. Ph.D. thesis, University of Toronto, Toronto, 145p.

Shanks, W.S., Schwerdtner, W.M., 1991a. Structural analysis of the central and southwestern Sudbury Structure, Southern Province, Canadian Shield. Canadian Journal of Earth Sciences 28, 411-430.

Shanks, W.S., Schwerdtner, W.M., 1991b. Crude quantitative estimates of the original northwest-southeast dimension of the Sudbury Structure, southcentral Canadian Shield. Canadian Journal of Earth Sciences 28, 1677-1686.

Thomson, M.L., R.L. Barnett, Fleet, M.E., Kerrich, R., 1985. Metamorphic assemblages in the South-Range Norite and the footwall mafic rocks near the Kirkwood Mine, Sudbury, Ontario. The Canadian Mineralogist 23, 173-186.

Therriault, A., Fowler, A., Grieve, R., 2002. The Sudbury Igneous Complex: A differentiated impact melt sheet. Economic Geology and the Bulletin of the Society of Economic Geologists 97, 1521-1540.

2.   Geology and deformation of the Sudbury Igneous Complex

2.1.   Lithological overview of the Sudbury Igneous Complex

The Sudbury Igneous Complex (SIC) is the relic of a 2.5 to 3.0 km-thick layered crystalline sheet (Therriault et al., 2002). The SIC is made up of the basal gabbroic to noritic Sublayer, which is overlain respectively by layers that are traditionally labelled Norite, Quartz Gabbro and Granophyre. These three layers form what is commonly referred to as the Main Mass of the SIC (Naldrett and Hewins, 1984). The composition of the SIC is high in SiO_2 and is bimodal, marked by the low-silica Norite (ca. 56 % SiO_2) and the silica-rich Granophyre (ca. 70% SiO_2) (Lightfoot et al., 2001; Lightfoot and Zotov, 2005). These layers are separated by a transition layer known as the Quartz Gabbro. The transition between the layers is gradational in terms of mineral and chemical composition. The composition of the parental melt is evident from the so-called Offset Dikes (Grant and Bite, 1984; Lightfoot et al., 2001). The quartz diorite Offset Dikes protrude up to 30km into the host rocks of the SIC (Grant and Bite, 1984), tapering in width with increasing distance from the Main Mass. Dikes are oriented radially and concentrically to the base of the SIC and are mostly subvertical (Grant and Bite, 1984).

The South Range Norite is composed of a cumulus phase of plagioclase and hypersthene and intercumulus augite, quartz, magnetite and ilmenite (Naldrett and Hewins, 1984). In the Quartz Gabbro, relative proportions of hypersthene decrease, and augite, quartz, magnetite, ilmenite and apatite increase. The Granophyre is composed predominantly of micrographic intergrowth of quartz and feldspar and of tabular plagioclase grains. In areas where it is least deformed, the composition of the South Range Granophyre is akin to its counterpart in the North Range. Variations between the SIC of the North and South Ranges are most pronounced in the mineral content of the Norite. Quartz-rich Norite forms the lower portion of Norite in the South Range. In the North Range, this layer is formed by a hypersthene-rich cumulate. Crystal cumulate and igneous lamination are igneous fabrics preserved in the SIC (Naldrett et al., 1972) and possibly indicate the orientation of the paleo-horizontal surface assuming the formation of cumulus fabrics is induced by gravitational settling (e.g. Irvine, 1987).

The SIC layers are characterized by igneous and by metamorphic mineral shape fabrics, the spatial density and orientation of which vary with location. The metamorphism of mineral fabrics varies from greenschist-facies in the North Range to lower amphibolite-facies in the South Range (Card, 1978; Thomson et al., 1985; Fleet et al., 1987). The extent to which the South Range Norite was affected by deformation has not been studied in detail. Large portions of the South Range Norite are reported to be unstrained (Riller, 2005) and display igneous mineral fabrics characterized by a granular texture and hypidiomorphic plagioclase and hypersthene (Naldrett and Hewins, 1984; Thomson et al., 1985). Naldrett et al. (1970) document metamorphic alteration of the Norite from the East Range and the South Range. In these areas Thomson et al. (1985) distinguish between the Black Norite, in which hypersthene and augite are preserved, and the Green Norite, which shows a metamorphic mineral assemblage of amphibole, epidote, biotite, albite and quartz. This mineral assemblage is consistent with prograde metamorphism to amphibolite facies, known from Huronian host rock of the South Range (Fleet et al., 1987).

Ore deposits related to the SIC are predominantly situated at the basal contact of the SIC, in quartz diorite dikes protruding into the adjacent rocks, and in the host rocks. Over 50% of the deposits are in the Contact Sublayer, one quarter in Offset Dikes, and 15% in the Frood Stobie Breccia Belt and less than 10% as veins in the host rock (Ames and Farrow, 2007). Ore deposits in the Sudbury Basin are tallied at a total of past production together with present resources of 1500 Mt showing average grades of 1% Ni, 1% Cu and 1 g/t Pd+Pt (Farrow and Lightfoot, 2002).

Ore deposits, especially those in the South Range, show evidence of post-emplacement deformation (Rousell, 1975; Cochrane, 1984; Owen and Coats, 1984). Particularly in the southeastern Sudbury Basin deposits display shear structures and are offset by faults. The Copper Cliff Offset Dike, which extends southward into the host rocks of the SIC in the central South Range, is segmented by faults (Cochrane, 1984). Faults affecting the ore deposits in the South Range Breccia Belt are associated with schist, and fault gouge (Davis, 1984). The Breccia Belt also shows abundant oblate magnetic fabrics (Scott and Spray, 1999). In the eastern South Range the wall rocks to the mineralized zones are strongly foliated and brecciated, displaying fault gouge at the basal contact of the Norite (Owen and Coats, 1984; Mukwakwami et al., 2012). Ductile deformation under greenschist-facies metamorphic conditions is observed from the Worthington Offset Dike (Hecht et al., 2008). In summary, Offset Dikes and ore deposits are affected by both ductile and brittle deformation.

2.2. *The Formation of the Sudbury Impact Structure*

It is commonly accepted that the SIC formed as a result of the effects of a meteorite impact into the Paleoproterozoic crust at 1.85 Ga (Pye et al., 1984; Grieve et al., 1991; Grieve, 1994; Deutsch et al., 1995). The impact origin was first proposed by Dietz (1964), who suggested that a meteorite impact produced a crater and formed an impact melt sheet. The main arguments documenting the Sudbury Impact Structure as the result of a hypervelocity meteorite impact are: high Ir-content in the melt-breccia of the Onaping Formation, abundance of pseudotachylite bodies decreasing with distance from Sudbury Basin, shatter cones, and shock metamorphism in minerals (Guy-Bray et al., 1966; French, 1967; French, 1968; French, 1970; Dence, 1972; Peredery, 1972; Grieve, 1994). The SIC and features in its adjacent rocks formed by impact processes are referred to as the Sudbury Impact Structure.

Overlying the Main Mass SIC is the Onaping Formation, an impact melt-breccia breccia whose clast sizes decrease overall upwards (French, 1967; Rousell, 1975). The Onaping Formation also contains fallback breccia (Grieve et al., 2010), which is the product of rocks uplifted above the expanding transient cavity by a vapor plume and subsequently deposited back into the impact crater. This impact-related breccia is generally composed of variously sized target rock fragments and glass. In the Sudbury Impact Structure, the Onaping Formation is composed of shocked lithic fragments and a range of originally vitric phases (Grieve et al., 2010). The glassy phases are pervasively devitrified as the consequence of hydrothermal events (Ames et al., 1998). Individual units of the Onaping Formation are marked by the presence of carbon material and chloritic alteration. The Onaping Formation constitutes a fundamental argument for the impact origin of the Sudbury Structure as it hosts impact diamonds and shock metamorphic quartz, feldspar and zircon (Masaitis et al., 1999; French, 1967; Peredery, 1972; Dressler et al., 1996; Bohor et al., 1993; Krogh et al., 1993).

The events involved in the formation of the Sudbury Impact Structure commenced with the impact of a ca. 10 km diameter meteorite impacting the Paleoproterozoic and Archean crust (Grieve and Cintala, 1992; Grieve, 1994). The kinetic energy of the impact formed a transient crater by excavating and displacing the target rocks (Dressler and Reimold, 2001). Approximately $3 - 4 \times 10^4$ km^3 molten target rocks (Ivanov, 2005) filled the transient cavity, the base of which reached a depth of 30 km (Grieve, 1994; Deutsch et al., 1995). Additionally to the formation of a transient cavity and melt, target rocks were brecciated (Grieve, 1994). At a later stage of crater formation the crater floor was uplifted and formed a central uplift and peak rings (Melosh, 1989). Subsequently, inward-moving clast-rich melt and suevite covered the top of melt sheet, forming what is now known as the Onaping Formation (Grieve, 1994; Grieve et al., 2010).

Most authors assume that the geometry of the impact melt sheet was initially subhorizontal, disregarding corrugations in the crater floor such as embayments (e.g., Grieve et al. 1991, Lightfoot et al., 1997; Therriault et al., 2002; Deutsch et al., 1995). However, structural observations lead Shanks and Schwerdtner (1991) to believe that the SIC had an original funnel-shaped geometry. Magnetic and structural fabric observations by Cowan (1999) suggest an initially parabolic emplacement geometry, analogous to a basin shape described by Morris (1984) based on primary magnetic remanence directions. The formation of the Main Mass is

attributed to shock-induced melting of crustal material and subsequent impact melt ponding in a crater with a subhorizontal crater floor (Grieve et al., 1991; Grieve, 1994; Deutsch et al., 1995; Therriault et al., 2002; Zieg and Marsh, 2005; Dreuse et al., 2010).

Cooling of the SIC is marked by heat conduction at its base and top, forming a thermal aureole in the surrounding rocks. The duration of cooling of the Main Mass SIC is evidenced in the difference of crystallization ages between norite at varying levels in the igneous stratigraphy (Davis, 2008). The cooling time is estimated to be up to 10 000 years (Prevec and Cawthorn, 2002; Zieg and Marsh, 2005). During this time frame, host rock debris was incorporated and compositional gradients were produced by in situ differentiation (Dickin et al., 1996; Ivanov and Deutsch, 1999). The processes involved in the differentiation include fractional crystallization (Ebel and Naldrett, 1996; Warren et al., 1996; Lavrenchuk et al., 2010), or the separation of two superheated immiscible liquids (Golightly, 1994; Zieg and Marsh, 2005). Distinct pulses of melt intrusion have also been proposed to account for compositionally distinct phases of the SIC (e.g. Morris, 1981; Chai and Eckstrand, 1993; Ariskin et al., 1999).

In summary, the most prominent feature of the Sudbury Impact Structure is the SIC which formed from an impact melt sheet. Features in the host rocks of the SIC include Offset Dikes and brecciated and shock metamorphosed host rocks. The composition of the Offset Dikes indicated their intimate relationship to the Main Mass SIC and they were likely formed by melt seeping into fractures in the crater floor (Grant and Bite, 1984). The dike-like pseudotachylite bodies, also known as the Sudbury Breccia, occur in the basement rocks around and up to 50 km away from the SIC (Dressler, 1984; Rousell et al., 2003). Pseudotachylite bodies decrease in size and abundance with increasing distance from the SIC (Speers, 1957). The composition of the matrix and the clasts composing the bodies varies according to location and are within compositional range of the local host rocks (Dressler, 1984). A combination of shock loading (Rousell et al., 2003; Lafrance et al., 2008; Lafrance and Kamber, 2010), in situ melting and comminution (Scott and Spray, 2000), and impact melt drainage (Riller et al., 2010) are likely the key processes involved in the formation of the Sudbury Breccia.

2.3.   Deformation history of the Sudbury area and regional tectonic setting

The Sudbury Basin extends over the boundary between the Superior and the Southern Province of the Canadian Shield, which constitute the host rocks of the SIC (Fig. 2.1). The North and East Ranges are underlain by high-grade metamorphic and granitoid rocks of the Archean Superior Province (Card et al., 1972). These rocks consist of the Levack Gneiss Complex of supracrustal and intrusive units (Card, 1994). Between the formation of granulites at approximately 2.71 Ga (Krogh et al. 1984) and deformation and metamorphism under upper amphibolite-facies metamorphic conditions at around 2.65 Ga (Krogh et al. 1984), these rocks were uplifted from 28 to 21 km depth to shallow crustal levels of 11 to 5 km (James et al., 1992). At this depth the rocks of the Levack Gneiss Complex recrystallized at the contact of, and imparted by, the SIC. A contact metamorphic aureole is documented in the North Range SIC (Lakomy 1990).

The Levack Gneiss was intruded by granitoid magma of the Cartier pluton at 2.64 Ga (Meldrum et al., 1997) and by the Matachewan dike swarm at 2.45 Ma (Heaman, 1997). The Cartier pluton

mostly shows little internal structure (Meldrum et al., 1997). Ductile fabrics are observed in an E-W ductile shear zone which lies approximately 15 km NW of the basal SIC in the North Range, the so-called Benny Deformation Zone, (Fueten et al., 1992; Kellett and Rivard, 1996). The Matachewan dike swarm is demagnetized in the Benny Deformation Zone and altered with southward decreasing intensity (Siddorn and Halls, 2002). In the vicinity of the North Range SIC, however, little altered dikes are preserved (Siddorn and Halls, 2002). Brittle deformation in the North Range and its host rocks SIC is documented by mainly left-lateral offset of the SIC along faults of the NNW-striking Onaping Fault System (Buchan and Ernst, 1994).

The South Range of the SIC is in contact with metavolcanic and metasedimentary rocks of the Huronian Supergroup of the Southern Province, which show a deformation history distinct from the Archean rocks underlying the North Range. The Huronian rocks were deposited onto Archean rocks between 2.45 Ga (age of the Copper Cliff Rhyolite: Krogh et al., 1984) and 2.21 Ga (age of Nipissing Diabase: Noble and Lightfoot, 2002). During this time interval Huronian metasedimentary rocks were deposited, deformed and metamorphosed to amphibolite facies metamorphism and intruded by felsic plutons, notably the Creighton and Murray Plutons, which border the southern flank of the Sudbury Basin (Card et al. 1972; Card 1978; Riller and Schwerdtner, 1997; Riller et al., 1999).

Deformation of the Huronian rocks is attributed to 2.4 to 2.2 Ga Blezardian tectonism and the 1.89 to 1.83 Ga Penokean orogeny (Riller et al., 1997). The formation of the Eastern Penokean Orogen is documented from the Lake Superior region (Sims et al., 1985) where it is attributed to a frontal collision of island arc terrains with the southern margin of the Superior Province (Sims et al., 1985; 1989). Proterozoic accretion in the Lake Huron ages is implied by Nd model ages in the Neoproterozoic Grenville Province rocks (Dickin and McNutt, 1989). The Penokean Orogeny commences at about 1.89 Ga (Sims, 1989) with ocean closure, subduction and associated arc volcanism, and at 1.875 Ga terranes began accreting onto the stable Superior Craton (Van Schmus, 1980). By 1.85 Ga the greater part of oceanic crust had been subducted and the orogeny turned into a continent-continent collision with the consequent formation of foreland basins and fold-and-thrust-belts in the Great Lakes region (Schulz and Cannon, 2007). Tectonometamorphic events of the Penokean Orogeny are relevant for the Sudbury Structure as the emplacement age of the SIC coincides with the time frame of orogenic activity.

Deformation of the SIC commenced likely during its cooling (Riller et al., 1996; Rosenberg and Riller, 2000; Ivanov, 2005; Klimczak et al., 2007), but peak metamorphism of the SIC is thought to have occurred under prograde conditions (Fleet et al., 1987). New geochronologic and thermochronologic evidence suggests that significant post-impact deformation and metamorphism of Huronian rocks occurred at about 1.76 to 1.74 Ga (Piercey et al., 2007) and was likely associated with the emplacement of 1.74 Ga granitoid plutons between the rocks of the Huronian Supergroup and rocks of the Grenville Province (Easton, 2000). Radiometric dating of deformation zones at the base of the South Range Norite yield a 1.65 Ga age for the formation of syntectonic minerals (Bailey et al., 2004). Post-impact metamorphic and deformation are thus not limited to a single orogenic event.

Proximity and orientation of the long axis of the Sudbury Basin to the NE-striking Grenville Front led some workers to invoke that the Basin was shaped by late Proterozoic Grenvillian

tectonism (Dietz, 1964; Card et al., 1984; Fueten and Redmond, 1997; Spray et al., 2004). Additional evidence for the presence of Grenville age deformation event is given by the offset of diabase dikes of the 1.23 Ga (Gates and Hurley, 1973) Sudbury swarm (Tschirhart and Morris, 2012). Nevertheless, these diabase dikes appear unstrained in the Sudbury area (Brocoum and Dalziel, 1974), thereby indicating that this youngest deformation event likely occurred at a shallow crustal level.
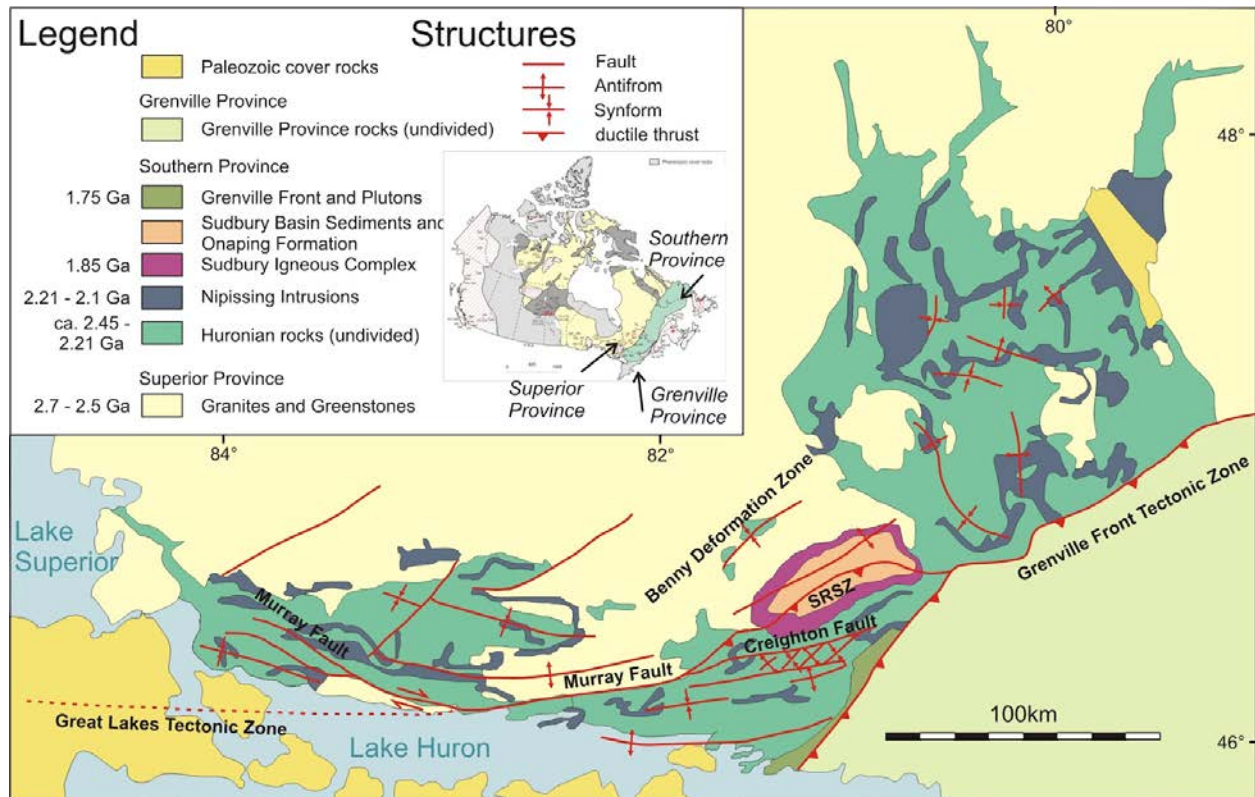
Figure 2.1: The Sudbury Basin in its regional setting at the boundary between the Superior, Southern and Grenville Provinces (after Sims et al., 1981). SRSZ = South Range Shear Zone.

References

Ames, D.E., Farrow C.E.G., 2007. Metallogeny of the Sudbury Mining Camp, Ontario. *In*: Goodfellow, W.D. (Ed.), Mineral Deposits of Canada: A Synthesis of Major Deposit-Types, District Metallogeny, the Evolution of Geological Provinces, and Exploration Methods. Geological Association of Canada, Mineral Deposits Division, Special Publication 5, p. 329-350.

Ames, D.E., Watkinson, D.H., Parrish, R.R., 1998. Dating of a regional hydrothermal system induced by the 1850 Ma Sudbury impact event. Geology 26, 447-450.

Ariskin, A., Deutsch, A., Ostermann, M., 1999. Sudbury Igneous Complex: Simulating phase equilibria and in situ differentiation for two proposed parental magmas. *In*: Dressler, B. O., Sharpton, V. L. (Eds.), Large Meteorite Impacts and Planetary Evolution II. The Geological Society of America, Washington, D.C., 373-388.

Bailey, J., Lafrance, B., McDonald, A., Fedorowich, J., Kamo, S., Archibald, D., 2004. Mazatzal-Labradorian-age (1.7-1.6 Ga) ductile deformation of the South Range Sudbury impact structure at the Thayer Lindsley mine, Ontario. Canadian Journal of Earth Sciences 41, 1491-1505.

Bohor, B.F., Betterton, W.J., Krogh, T.E., 1993. Impact shocked zircons: Discovery of shock-induced textures reflecting increasing degrees of shock metamorphism. Earth and Planetary Science Letters 119, 419–424.

Brocoum, S., Dalziel, I., 1974. Sudbury Basin, Southern Province, Grenville Front, and Penokean Orogeny - Discussion. Geological Society of America Bulletin 85, 1571-1580.

Buchan, K.L., Ernst, R.E., 1994. Onaping fault system: age constraints on deformation of the Kapuskasing structural zone and units underlying the Sudbury Structure. Canadian Journal of Earth Sciences 31, 1197-1205.

Card, K.D., 1978. Geology of the Sudbury-Manitoulin Area, District of Sudbury and Manitoulin; Ontario Geological Survey, Report 166, 238 p.

Card, K.D., 1994. Geology of the Levack gneiss complex, the northern footwall of the Sudbury structure, Ontario. *In:* Canadian Shield: Geological Survey of Canada, Current Research 1994-C, 269-278.

Card, K.D., Church, W.R., Franklin, J.M., Robertson, J.A., West, G.F., Young, G.M., 1972. The Southern Province. *In*: Price, R.A., Douglas, R.J.W. (Eds.), Variations in Tectonic Style in Canada. Geological Association of Canada Special Paper 8, 335-380.

Card, K.D., Gupta, P.H., McGrath, P.H., Grant, F.S. 1984. The Sudbury Structure: Its Regional Geological and Geophysical Setting. *In*: Pye, E.G., Naldrett, A.J., Giblin P.E (Eds.), The Geology and Ore Deposits of the Sudbury Structure. Special Publication 1, Ontario Geological Survey, Toronto, 25–43.

Chai, G. and Eckstrand, O.R. 1993. Origin of the Sudbury Igneous Complex, Ontario – differentiated of two separate magmas; Geological Survey of Canada, Paper 93-1E, p. 219-230.

Cochrane, L.B., 1984. Ore deposits of the Copper Cliff Offset. *In*: Pye, E.G., Naldrett, A.J., Giblin P.E (Eds.), The Geology and Ore Deposits of the Sudbury Structure. Special Publication 1, Ontario Geological Survey, Toronto, 347–359.

Cowan, E.J., 1999. Magnetic fabric constraints on the initial geometry of the Sudbury Igneous Complex: a folded sheet or a basin-shaped igneous body? Tectonophysics 307, 135-162.

Davis, D.W., 2008. Sub-million-year age resolution of Precambrian igneous events by thermal extraction -thermal ionization mass spectrometer Pb dating of zircon: Application to crystallization of the Sudbury impact melt sheet. Geology 38, 383-386.

Davis, G.C, 1984. Little Stobie Mine: A South Range Contact Deposit. *In*: Pye, E.G., Naldrett, A.J., Giblin P.E (Eds.), The Geology and Ore Deposits of the Sudbury Structure. Special Publication 1, Ontario Geological Survey, Toronto, 361–369.

Dence, M.R., 1972. Meteorite impact craters and the structure of the Sudbury Basin. *In:* Guy-Bray, J. (Ed.), New Developments of the Sudbury Geology. Special Paper 10. Geological Association of Canada, Toronto, 7-18.

Deutsch, A., Grieve, R. A. F., Avermann, M., Bischoff, L., Brockmeyer, P., Buhl, D., Lakomy, R., Müller-Mohr, V., Ostermann, M., Stöffler, D., 1995. The Sudbury Structure (Ontario, Canada): A tectonically deformed multi-ring impact basin. Geologische Rundschau 84, 697-709.

Dickin, A.P., McNutt, R.H., 1989. Nd model age mapping of the southeast margin of the Archean foreland in the Grenville province of Ontario. Geology 17, 299-302.

Dickin, A.P., Artan, M.A., Crocket, J.H., 1996. Isotopic evidence for distinct crustal sources of North and South Range ores, Sudbury Igneous Complex. Geochimica et Cosmochimica Acta 60, 1605–1613.

Dietz, R., 1964. Sudbury Structure as an Astrobleme. Journal of Geology 72, 412-434.

Dressler, B.O., 1984. The effects of the Sudbury event and the intrusion of the Sudbury Igneous Complex on the footwall rocks of the Sudbury Structure. *In*: Pye, E.G., Naldrett, A.J., Giblin, P.E., (Eds), The Geology and Ore Deposits of the Sudbury Structure. Special Publication 1, Ontario Geological Survey, Toronto, 97-136.

Dressler, B.O., Reimold, W.U., 2001. Terrestrial impact melts. Earth Science Reviews 56, 205-284.

Dressler, B.O., Weiser, T., Brockemeyer, P., 1996. Recrystallized impact glass of the Onaping Formation and the Sudbury Igneous Complex, Sudbury structure, Ontario, Canada. Geochimica et Cosmochimica Acta 60, 2019-2036.

Dreuse, R., Doman, D., Santimano, T., Riller, U., 2010. Crater-floor topography and impact melt sheet geometry of the Sudbury impact structure, Canada. Terra Nova 22, 463-469.

Easton, R.M. 2000. Metamorphism of the Canadian Shield, Ontario, Canada. II. Proterozoic metamorphic history. Canadian Mineralogist 38, 319-344.

Ebel, D.S., Naldrett, A.J., 1996. Fractional crystallization of sulfide ore liquids at high temperature. Economic Geology 91, 607-621.

Farrow, C.E.G., Lightfoot, P.C., 2002. Sudbury PGE revisited: Toward an Integrated model. *In* Cabri, L.J., (Ed.), The Geology, Geochemistry, Mineralogy and Mineral Beneficiation of Platinum-Group Elements: Canadian Institute of Mining, Metallurgy and Petroleum, Special Volume 54, 13-130.

Fleet, M.E., Barnett, R.L., Morris, W.A., 1987. Prograde metamorphism of the Sudbury igneous complex. Canadian Mineralogist 25, 499-514.

French, B.M., 1967. Sudbury Structure Ontario: Some Petrographic Evidence for an Origin by Meteorite Impact. Science 156, 1094-1098.

French, B.M., 1968. Sudbury Structure, Ontario: some petrographic evidence for an origin by meteorite impact. *In:* French, B.M., Short, N.M., (Eds.), Shock Metamorphism of Natural Materials. Mono Book Corporation, Baltimore, 383-412.

French, B.M., 1970. Possible relations between meteorite impact and igneous petrogenesis, as indicated by the Sudbury structure, Ontario, Canada. Bulletin Volcanologique 34, 466-517.

Fueten, F., Redmond, D.J., 1997. Documentation of a 1450 Ma contractional orogeny preserved between the 1850 Ma Sudbury Impact Structure and the 1 Ga Grenville orogenic front, Ontario, Canada. Geological Society of America Bulletin 109, 268-279.

Fueten, F., Seabright, R., and Morris, B. 1992. A structural transect across the Levack Gneiss – Cartier Batholith complex, northwest of the Sudbury Structure. *In:* Lithoprobe Abitibi–Grenville Transect Workshop, 15–16 Dec. 1992, Montréal. Lithoprobe Report 33, pp. 11–15.

Gates, T.M., Hurley, P.M., 1973. Evaluation of Rb-Sr dating methods applied to the Matachewan, Abitibi, Mackenzie, and Sudbury dike swarms in Canada. Canadian Journal of Earth Sciences 10, 900-919.

Golightly, J.P., 1994. The Sudbury Igneous Complex as an Impact Melt: Evolution and Ore Genesis. *In:* Lightfoot, P.C., Naldrett, A.J. (Eds.), Proceedings of the Sudbury-Noril'sk Symposium. OGS Special Volume 5, 105-118.

Grant, R.W., Bite, A., 1984. The Sudbury Quartz Diorite Offset Dikes. *In:* Pye, E.G., Naldrett, A.J., Giblin, P.E., (Eds.) The Geology and Ore Deposits of the Sudbury Structure. Special Publication 1, Ontario Geological Survey, Toronto, 275-300.

Grieve, R.A.F., 1994. An impact model of the Sudbury Structure. *In:* Lightfoot, P.S., Naldrett, A.J., (Eds.), Proceedings of the Sudbury-Noril'sk Symposium: Ontario Geological Survey Special Volume 5, p.245-270.

Grieve, R.A.F., Cintala, M.J., 1992. An analysis of differential impact melt-crater scaling and implications for the terrestrial cratering record. Meteoritics 27, 526-538.

Grieve, R., Stöffler, D., Deutsch, A., 1991. The Sudbury Structure - controversial or misunderstood. Journal of Geophysical Research 96, 22753-22764.

Grieve, R.A.F., Ames, D.E., Morgan, J.V., Artemieva, N., 2010. The evolution of the Onaping Formation at the Sudbury impact structure. Meteoritics and Planetary Science 45, 759-782.

Guy-Bray, J.V., and geological staff, 1966. Shatter cones at Sudbury. Journal of Geology 74, 243-245.

Heaman, L.M., 1997. Global mafic magmatism at 2.45 Ga: Remnants of an ancient large igneous province? Geology 25, 299-302.

Hecht, L., Wittek, A., Riller, U., Mohr, T., Schmitt, R.T., Grieve, R.A.F., 2008. Differentiation and emplacement of the Worthington Offset Dike of the Sudbury impact structure, Ontario. Meteoritics and Planetary Science 43, 1659-1679.

Irvine, T.N., 1987. Layering and related structures in the Duke Island and Skaergaard Intrusions: similarities, differences, and origins. *In:* Parsons, I. (Ed.), Origins of Igneous Layering. D. Reidel, Dordrecht, 185-246.

Ivanov, B.A., Deutsch, A., 1999. Sudbury impact event: Cratering mechanics and thermal history. *In*: Dressler, B. O., Sharpton, V. L. (Eds.), Large Meteorite Impacts and Planetary Evolution II. The Geological Society of America, Washington, D.C., 389-398.

Ivanov, B.A., 2005. Numerical Modeling of the Largest Terrestrial Meteorite Craters. Solar Systems Research 39, 381-407.

James, R. S., Sweeney, J. M., Peredery, W. 1992. Thermobarometry of the Levack gneiss-footwall rocks to the Sudbury Igneous Complex (SIC). Lithoprobe: Abitibi-Greenville transect. pp. 179–182.

Kellett, R.L., Rivard, B., 1996. Characterization of the Benny deformation zone, Sudbury, Ontario. Canadian Journal of Earth Sciences, 33, 1256–1267.

Klimczak, C., Wittek, A., Doman, D., Riller, U., 2007. Fold origin of the NE-lobe of the Sudbury Basin, Canada: Evidence from heterogeneous fabric development in the Onaping Formation and the Sudbury Igneous Complex. Journal of Structural Geology 29, 1744-1756.

Krogh T.E., Davis D.W., Corfu F., 1984. Precise U-Pb zircon and Baddeleyite Ages for the Sudbury Area. *In*: Pye, E.G., Naldrett, A.J., Giblin, P.E. (Eds.), The Geology and Ore Deposits of the Sudbury Structure. Special Publication 1, Ontario Geological Survey, Toronto, 431-446.

Krogh, T.E., Kamo, S.L., Bohor, B.F., 1993. Shock metamorphosed zircons with correlated U-Pb discordance and melt rocks with concordant protolith ages indicate an impact origin for the Sudbury structure. *In* Hart, S., Basu, A., (Eds.), Earth Processes: Reading the isotopic code. American Geophysical Union Monograph 95, 343-353.

Lafrance, B., Legault, D., Ames, D.E., 2008. The formation of the Sudbury breccia in the North Range of the Sudbury Impact Structure. Precambrian Research 165, 107-119.

Lafrance, B., Kamber, B.S., 2010. Geochemical and microstructural evidence for in situ formation of the pseudotachylitic Sudbury Breccia by shock-induced compression and cataclasis. Precambrian Research 180, 237-250.Lakomy, R., 1990. Implications for cratering mechanics from a study of the Footwall breccia of the Sudbury impact structure, Canada. Meteoritics 25, 195–207.

Lavrenchuk, A., Latypov, R., Lightfoot, P.C., 2010. The Sudbury Igneous Complex, Canada: Numerical Modeling Confirms Fractionation of a Single Parental Magma. Ontario Geological Survey, Miscellaneous Release–Data 269, 11th Platinum Symposium, 4p.

Lightfoot, P. C., Keays, R. R., Morrison, G. G., Bite, A., Farrell, K. P., 1997. Geochemical relationships in the Sudbury igneous complex; origin of the main mass and offset dikes. Economic Geology and the Bulletin of the Society of Economic Geologists 92, 289-307.

Lightfoot, P.C., Keays, R.R., Doherty, W., 2001. Chemical evolution and origin of nickel sulfide mineralization in the Sudbury Igneous Complex, Ontario. Ontario Geological Survey, Open File Report 5959, 231 p.

Lightfoot, P.C., Zotov, I.A., 2005. Geology and Geochemistry of Sudbury Igneous Complex, Ontario, Canada: Origin of Nickel Sulfide Mineralization Associated with an Impact-Generated Melt Sheet. Geology of Ore Deposits 47, 349-381.

Masaitis, V.L., Shafranovsky, G.I., Grieve, R.A.F., Langenhorst, F., Peredery, V., Therriault, A. M., Balmasov, E.L., Fedorova, I.G., 1999. Impact diamonds in the suevitic breccias of the Black Member of the Onaping Formation, Sudbury structure. Ontario, Canada. *In* Dressler, B.O., Sharpton, V.L., (Eds.), Large meteorite impacts and planetary evolution II. GSA Special Paper 339, Geological Society of America, Boulder, 317–321.

Meldrum, A., Abdel-Rahman, A.-F.M, Martin, R.F., Wodicka, N., 1997. The nature, age and petrogenesis of the Cartier Batholith, northern flank of the Sudbury structure, Ontario, Canada. Precambrian Research 82, 265–285.

Melosh, H.J., 1989. Impact cratering: A geologic process. Oxford University Press, New York, 245 p.

Morris, W.A., 1981. Intrusive and Tectonic History of the Sudbury Micropegmatite: The Evidence from Paleomagnetism. Economic Geology 76, 791-804.

Morris, W.A., 1984. Paleomagnetic constraints on the Magmatic, Tectonic, and Metamorphic History of the Sudbury Basin Region. *In*: Pye, E. G., Naldrett, A. J., Giblin, P. E. (Eds.), The Geology and Ore Deposits of the Sudbury Structure. Special Publication 1. Ontario Geological Survey, Toronto, 411-429.

Mukwakwami, J., Lafrance, B., Lesher, C.M., 2012. Back-Thrusting and Overturning of the Southern Margin of the 1.85 Ga Sudbury Igneous Complex at the Garson Mine, Sudbury, Ontario. Precambrian Research 196-197, 81-105.

Naldrett, A.J., Bray, J.G., Gasparrini, E L., Podolsky, T., Rucklidge, J C., 1970. Cryptic Variation and the Petrology of the Sudbury Nickel Irruptive. Economic Geology and the Bulletin of the Society of Economic Geologists 65, 122-274.

Naldrett, A.J., Greenman, L., Hewins, R.H., 1972. The Main Irruptive and the Sublayer at Sudbury, Ontario. Proceedings of the 24th International Geological Congress, Montreal, 206-214.

Naldrett, A.J., Hewins, R.H., 1984. The Main Mass of the Sudbury Igneous Complex. *In*: Pye, E.G., Naldrett, A.J., Giblin, P.E. (Eds.), The Geology and Ore Deposits of the Sudbury Structure. Special Publication 1. Ontario Geological Survey, Toronto, 235-252.

Noble, S.R., Lightfoot, P.C., 1992. U–Pb baddeleyite ages of the Kerns and Triangle Mountain intrusions, Nipissing Diabase, Ontario. Canadian Journal of Earth Sciences 29, 1424-1429.

Owen, D.L., Coats, C.J.A., 1984. Falconbridge and East mines. *In*: Pye, E.G., Naldrett, A.J., Giblin, P.E. (Eds.), The Geology and Ore Deposits of the Sudbury Structure. Special Publication 1. Ontario Geological Survey, Toronto, 371-378.

Pattison, E.F., 1979. The Sudbury Sublayer. Canadian Mineralogist 17, 257-274.

Peredery, W.V., 1972. Chemistry of fluidal glasses and melt bodies in the Onaping formation. *In:* Guy-Bray, J. (Ed.), New developments in Sudbury Geology. Special Paper 10. Geological Association of Canada, Toronto, 49–59.

Piercey, P., Schneider, D.A., Holm, D.K., 2007. Geochronology of Proterozoic metamorphism in the deformed Southern Province, northern Lake Huron region, Canada. Precambrian Research 157, 127-143.

Prevec, S.A., and Cawthorn, R.G. 2002. Thermal evolution and interaction between impact melt sheet and footwall: a genetic model for the contact sublayer of the Sudbury Igneous Complex. Canada. Journal of Geophysical Research 107, 2176-2190.

Pye, E.G., Naldrett, A.J., Giblin, P.E. (Eds.), The Geology and Ore Deposits of the Sudbury Structure. Special Publication 1. Ontario Geological Survey, Toronto, 603 p.

Riller, U., 2005. Structural characteristics of the Sudbury Impact Structure, Canada: impact-induced and orogenic deformation – a review. Meteoritics and Planetary Science 40, 1723-1740.

Riller, U., Cruden, A.R., Schwerdtner, W.M., 1996. Magnetic fabric and microstructural evidence for a tectono-thermal overprint of the early Proterozoic Murray pluton, central Ontario, Canada. Journal of Structural Geology 18, 1005-1016.

Riller, U., Schwerdtner, W., 1997. Mid-crustal deformation at the southern flank of the Sudbury Basin, central Ontario, Canada. Geological Society of America Bulletin 109, 841-854.

Riller, U., Schwerdtner, W., Halls, H., Card, K., 1999. Transpressive tectonism in the eastern Penokean orogen, Canada. Consequences for Proterozoic crustal kinematics and continental fragmentation. Precambrian Research 93, 51-70.

Riller, U., Lieger, D., Gibson, R.L., Grieve, R.A.F., Stöffler, D., 2010. Origin of large-volume pseudotachylite in terrestrial impact structures. Geology 38, 619-622.

Rosenberg, C.L., Riller, U., 2000. Partial-melt topology in statically and dynamically recrystallized granite. Geology 28, 2-7.

Rousell, D.H., 1975. Origin of foliation and lineation in Onaping Formation and deformation of Sudbury Basin. Canadian Journal of Earth Sciences 12, 1379-1395.

Rousell, D.H., Fedorowich, J.S., Dressler, B.O., 2003. Sudbury Breccia (Canada): a product of the 1850 Ma Sudbury Event and host to footwall Cu-Ni-PGE deposits. Earth Science Reviews 60, 147-174.

Scott, R.G., Spray, J.G., 1999. Magnetic fabric constraints on friction melt flow regimes and ore emplacement direction within the South Range Breccia Belt, Sudbury Impact Structure. Tectonophysics 307, 163-189.

Scott, R.G., Spray, J.G., 2000. The South Range Breccia Belt of the Sudbury Impact Structure: A possible terrace collapse feature. Meteoritics and Planetary Science 35, 505-520.

Schulz, K., Cannon, W., 2007. The Penokean orogeny in the Lake Superior region. Precambrian Research 157, 4-25.

Shanks, W.S., Schwerdtner, W.M., 1991. Structural analysis of the central and southwestern Sudbury Structure, Southern Province, Canadian Shield. Canadian Journal of Earth Sciences 28, 411-430.

Siddorn, J.P., Halls, H.C., 2002. Variation in plagioclase clouding intensity in Matachewan dykes: evidene for the exhumation history of the northern margin of the Sudbury Igneous Complex. Canadian Journal of Earth Sciences 39, 933-942.

Sims, P.K., Card, K.D., Lumbers, S.D., 1981. Evolution of early Proterozoic basins of the Great Lakes region. *In*: Campbell, F.H.A. (Ed.), Proterozoic Basins of Canada. Geological Survey of Canada Paper 81-10, 379-397.

Sims, P.K., Peterman, Z.E., Schulz, K.J., 1985. The Dunbar gneiss-granitoid dome: Implication for early Proterozoic tectonic evolution of northern Wisconsin. Geological Society of America Bulletin 96, 1101-1112.

Sims, P.K., Van Schmus, W.R., Schulz, K.J., Peterman, Z.E., 1989. Tectono-stratigraphic evolution of the Early Proterozoic Wisconsin magmatic terranes of Penokean Orogen. Canadian Journal of Earth Sciences 26, 2145-2158.

Speers, E.C., 1957. The age relation and origin of common Sudbury Breccia. Journal of Geology 65, 497-514.

Spray, J.G., Butler, H.R., Thompson, L.M, 2004. Tectonic influences on the morphometry of the Sudbury impact structure: Implications for terrestrial cratering and modeling. Meteoritics and Planetary Science 39, 287-301.

Therriault, A., Fowler, A., Grieve, R., 2002. The Sudbury Igneous Complex: A differentiated impact melt sheet. Economic Geology and the Bulletin of the Society of Economic Geologists 97, 1521-1540.

Thomson, M.L., R.L. Barnett, Fleet, M.E., Kerrich, R., 1985. Metamorphic assemblages in the South-Range Norite and the footwall mafic rocks near the Kirkwood Mine, Sudbury, Ontario. The Canadian Mineralogist 23, 173-186.

Tschirhart, P., Morris, W.A. 2012. Grenville age deformation of the Sudbury impact structure: evidence from magnetic modelling of the Sudbury diabase dyke swarm. Terra Nova 24, 213-220.

Van Schmus, W.R., 1980. Chronology of igneous rocks associated with the Penokean orogeny in Wisconsin. *In*: Morey, G. B., Hanson, G. (Eds.), Selected Studies of Archean Gneisses and Lower Proterozoic Rocks, Southern Canadian Shield. Geological Society of America, pp. 159-168.

Warren, P.H., Claeys, P., Cedillo-Pardo E., 1996.Mega-impact melt petrology (Chicxulub, Sudbury, and the Moon): Effects of scale and other factors on potential for fractional

crystallization and development of cumulates. Geological Society of America Special Papers 307, 105-124.

Zieg, M.J., Marsh, B.D., 2005. The Sudbury Igneous Complex: Viscous emulsion differentiation of a superheated melt sheet. Geological Society of America Bulletin 117, 1427-1450.

3.   Fabric evolution and deformation in the South Range Norite

3.1.   Introduction

The formation of brittle shear faults in orogenic belts is usually considered to postdate ductile fabric development (e.g., Watts and Williams, 1979). As such, shear fractures are interpreted to record late stages of orogenic deformation. However, in initially isotropic rocks, notably granitoid bodies, brittle fractures have been documented to coalesce into zones of brittle-ductile or ductile deformation (Segall and Simpson, 1986; Bürgmann and Pollard, 1994; Tourigny and Tremblay, 1997; Pennacchioni, 2005). Thus, brittle faults may form during or even precede ductile deformation in granitoid rocks. As evidence for the existence of precursor brittle fractures is likely erased by subsequent pervasive crystal plastic deformation in orogenic belts (Means, 1989), the significance of small-scale shear fractures for accomplishing regional deformation of igneous rock bodies may have been largely underestimated. Despite the evidence for the development of isolated ductile shear zones from brittle precursor faults in granitoid rocks, it remains to be elucidated to what extent this process operates in mafic igneous rocks. Moreover, the kinematic effects of such fabric development on the geometry of deformed (mafic) igneous sheets have received little attention by structural analysts. Here we report on the genetic relationship between brittle and ductile fabric development and its influence on the melt sheet geometry using the Sudbury Igneous Complex, Canada, as an example. Because the Complex is layered, well-exposed and heterogeneously deformed, it lends itself excellently for this study.

The Sudbury Basin (Brocoum and Dalziel, 1974; Pye et al., 1984) is considered as the central portion of the Sudbury Impact Structure (Butler, 1994; Riller 2005; Grieve et al., 2008). The Basin is made up of the Main Mass of the Sudbury Igneous Complex (SIC), the relic of an impact melt sheet (Grieve et al., 1991; Deutsch et al., 1995) dated at 1.85 Ga (Krogh et al., 1984), clast-melt breccias of the overlying Onaping Formation (Peredery and Morrison, 1984; Grieve et al., 2010), and post-impact sedimentary rocks (Fig. 3.1). Cu-Ni sulphide deposits are concentrated chiefly at the base of the SIC in the so-called Sublayer and adjacent rock (e.g., Keays and Lightfoot, 2004; Ames et al., 2007) and made the Sudbury Basin a world-class mining camp.

The synformal geometry of the SIC has been attributed to sagging of the melt sheet upon cooling (Peredery and Morrison, 1984) or is considered as primary (Cowan et al., 1999). More recent structural studies suggest, however, that this geometry is due to post-impact, non-cylindrical folding (Cowan and Schwerdtner, 1994; Riller et al., 1998; Riller, 2005; Klimczak et al., 2007; Halls, 2009; Dreuse et al., 2010). Due to the highly variable crater floor topography (Dreuse et al., 2010), the orientation of the lower SIC contact, notably of the southern Sudbury Basin, cannot be used to constrain rotation magnitudes of the SIC. Furthermore, internal contacts of the SIC are non-parallel at surface (Fig. 3.1). In particular, it is unclear whether this configuration constitutes the original orientation of the lithological contacts, or whether deformation modified the contact geometry.
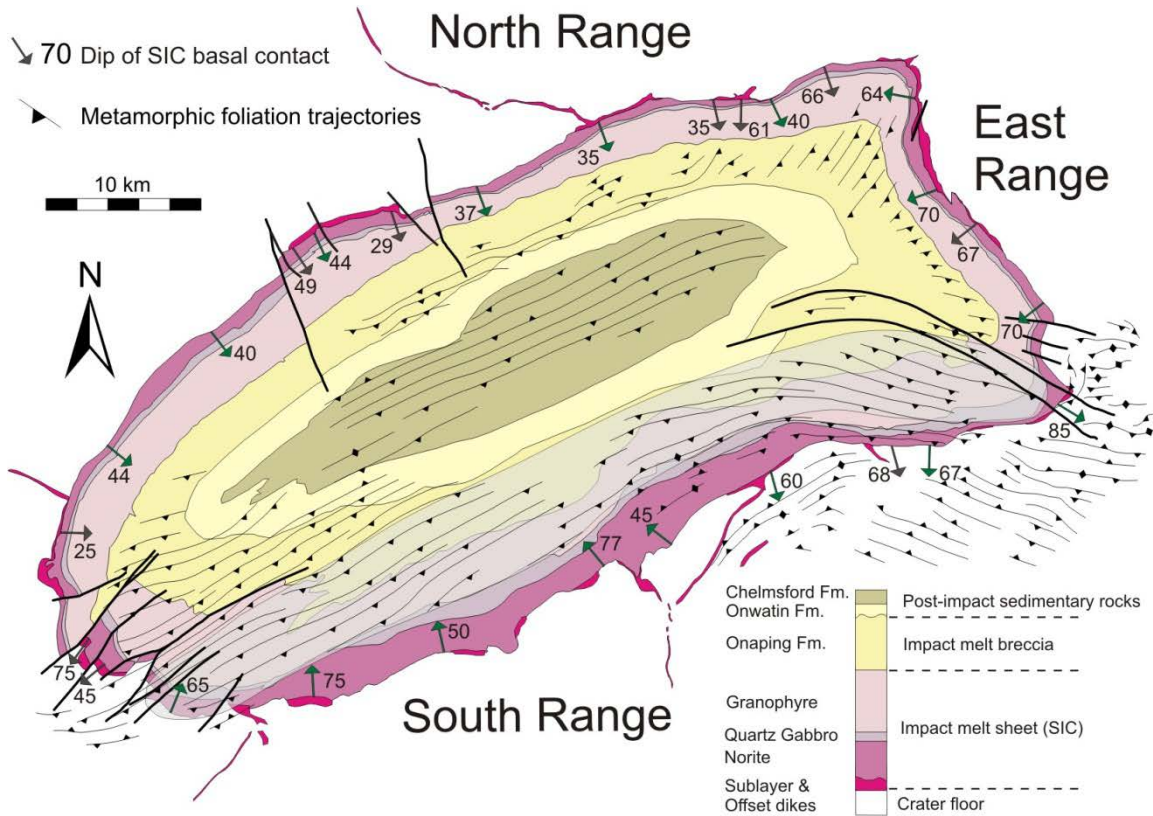
Figure 3.1: Simplified geological map of the Sudbury Basin showing first-order structural characteristics (modified from Cowan et al., 1999). Dip magnitudes (numbers) of basal SIC contact segments are from Ames et al. (2005) and Dreuse et al. (2010) (green and black arrows, respectively).

To better understand the mechanisms of fabric development, including rotational components of deformation, in the southern SIC, we analyzed the orientation and spatial distribution of igneous and metamorphic mineral fabrics as well as outcrop-scale fold structures in the field. These analyses are complemented by inversion of small-scale, brittle-ductile shear faults from which we infer shortening directions during deformation of the SIC and its host rocks. Collectively, these data allow us to characterize the deformation mechanisms by which the SIC changed shape and its mechanical behavior during deformation. This study pertains directly to understanding the deformation of, and strain localization in, mafic melt sheets at upper crustal levels.

3.2.   *Tectonic Background Setting*

At surface, the SIC forms morphological ranges, i.e., the North Range, the South Range and the East Range (Fig. 3.1). The North Range and the East Range are underlain by high-grade metamorphic and granitoid rocks of the Archean Superior Province (Card et al., 1972). These rocks formed at approximately 2.71 Ga and were affected by upper amphibolite- to granulite-facies metamorphism at around 2.65 Ga (Krogh et al. 1984). The South Range of the SIC overlies metavolcanic and metasedimentary rocks of the Huronian Supergroup which were deposited onto Archaean rocks between 2.45 Ga (age of the Copper Cliff Formation: Krogh et al., 1984) and 2.21 Ga (Nipissing diabase intrusion: Corfu and Andrews, 1986). During this time interval Huronian metasedimentary rocks were deposited, deformed and metamorphosed to

amphibolite facies and intruded by felsic plutons, notably the Creighton and Murray Plutons, which border the southern flank of the Sudbury Basin (Card et al. 1972; Card 1978; Riller and Schwerdtner, 1997; Riller et al., 1999).

The SIC and Huronian rocks were affected by various Proterozoic pulses of deformation. Deformation of the SIC commenced likely during its cooling (Klimczak et al., 2007) but peak metamorphism and deformation of the SIC is thought to have occurred under prograde conditions (Fleet et al., 1987). New geochronologic and thermochronologic evidence suggests that significant post-impact deformation and metamorphism of Huronian rocks occurred at about 1.76 to 1.74 Ga (Piercey et al., 2007) and was likely associated with the emplacement of 1.74 Ga granitoid plutons (Easton, 2000). Deformation zones at the base of the South Range Norite were dated at ca. 1.65 Ga (Bailey et al., 2004). Proximity and orientation of the long axis of the Sudbury Basin to the NE-striking Grenville Front led some workers to invoke that the Basin was shaped by late Proterozoic Grenvillian tectonism (Dietz, 1964; Card et al., 1984; Fueten and Redmond, 1997; Spray et al., 2004). This is, however, at variance with the presence of unstrained diabase dikes of the 1.23 Ga Sudbury swarm (Gates and Hurley, 1973) in the Sudbury area (Brocoum and Dalziel, 1974). Thus, the precise age of Basin formation is still uncertain.

3.3.   Structural characteristics of the Sudbury Basin

The Main Mass of the SIC is made up of petrographically distinct layers that are traditionally known as Norite, Quartz Gabbro and Granophyre (Fig. 3.1). Collectively, these layers are characterized by igneous and metamorphic mineral shape fabrics, the intensity and orientation of which vary with location. Much of the Sudbury Basin and adjacent Huronian host rocks were affected by deformation, the metamorphic grade of which varies from greenschist-facies in the North Range to lower amphibolite-facies in the South Range (Card, 1978; Thomson et al., 1985; Fleet et al., 1987). This led to the development of mesoscopic planar (S) and linear (L) mineral shape fabrics, the intensity of which decrease generally toward the north in the Sudbury area.

Except at the NE-lobe and SE-lobe of the Sudbury Basin (Fig. 3.1), planar metamorphic mineral shape fabrics strike parallel to the long axis of the Basin and are either subvertical or dip southward (Cowan, 1996). In the lobes, the shape fabrics are axial-planar to the plan view curvature of the SIC (Cowan, 1999) pointing to a fold origin of the two lobes (Cowan and Schwerdtner, 1994; Riller, 2005; Klimczak et al., 2007). In post-impact sedimentary rocks, planar fabrics developed as a slaty cleavage that is axial planar to doubly plunging, open similar and concentric folds of bedding planes (Rousell, 1984).

The South Range Shear Zone (SRSZ), a SE-dipping ductile deformation zone, is the most prominent structural element of the Sudbury Basin (Rousell, 1975; Shanks and Schwerdtner, 1991). Mineral fabrics of the shear zone display L-S geometry and formed mostly at, or near, the contact of the Granophyre and Onaping Formation (Fig. 3.1). Reverse sense-of-shear on the SRSZ translated the South Range approximately 8 to 13 km toward the NW (Shanks and Schwerdtner, 1991). The SRSZ formed apparently under lower amphibolite-facies metamorphic conditions and was overprinted by small-scale, brittle-ductile shear faults, which formed at mid greenschist-facies metamorphic conditions (Fleet et al., 1987).

The extent to which the South Range Norite was affected by deformation has not been studied in detail. Large portions of the South Range Norite are reported to be unstrained (Riller, 2005) and display igneous mineral fabrics characterized by a granular texture and hypidiomorphic plagioclase and hypersthene (Naldrett and Hewins, 1984; Thomson et al., 1985). The intercumulus mineral phases consist of augite, hornblende, quartz, titanomagnetite and biotite (Thomson et al., 1985). Naldrett et al. (1970) document metamorphic alteration of the Norite from the East Range and the South Range. In these areas Thomson et al. (1985) distinguishes between the Black Norite, in which hypersthene and augite are preserved, and the Green Norite, which shows a metamorphic mineral assemblage of amphibole, epidote, biotite, albite and quartz. This mineral assemblage is consistent with prograde metamorphism to amphibolite facies, known from Huronian host rock of the South Range (Fleet et al., 1987).

3.4.   *Results*

3.4.1.   Igneous fabrics

Igneous mineral fabrics of the South Range Norite are planar and consist of subhedral plagioclase, orthopyroxene and to some extent amphibole. Collectively, the fabric defined by these mineral phases is reminiscent of a cumulus texture (Fig. 3.2a). Plagioclase has andesine composition, shows twin lamellae, and is zoned, evident by the increase in sodium content towards crystal margins (Fleet & Barnett, 1978). Similarly, amphibole is zoned, apparent by cores of green hornblende rimmed by blue-green hornblende (Fleet & Barnett, 1978). It is noteworthy that none of these mineral phases form a mineral lineation.

Minerals indicative of metamorphism and hydrothermal alteration are known to have affected much of the South Range Norite. For example, epidote and scapolite occupy grain boundaries, notably between plagioclase and amphibole, replace plagioclase cores and coat fractures (Thomson et al., 1985). Similarly, talc replaces hypersthene cores and is found in fractures cutting bronzite. Hypersthene is rimmed by actinolitic hornblende and brown edenite is selectively replaced by blue-green actinolitic hornblende (Fleet et al., 1987). Chlorite, epidote and quartz decorate brittle fractures (see section 4.4). Despite metamorphic transformation of the Norite at the grain scale, primary igneous fabrics are generally preserved well enough to be visible in outcrop (Fleet et al., 1987).

Although often faint in outcrop, igneous layering can be observed throughout the South Range Norite. The orientation of planar igneous fabrics was mapped in the South Range Norite at 276 stations (Figs. 3.3a, 3.4a, b). For a better appraisal of along-strike fabric variation, the orientation of planar igneous fabrics was grouped into two zones, the Western Zone and the Eastern Zone, defined by NE-SW strike and E-W strike of SIC contacts, respectively (Fig. 3.3a). Assuming that layering in the SIC formed by gravitational settling (Naldrett et al., 1970) and was subhorizontal prior to deformation, inclined planar igneous fabrics can be used to infer total rotation magnitudes of the South Range SIC. Planar igneous fabrics dip moderately toward the NW in the Western Zone (Fig. 3.4a) and toward the N in the Eastern Zone (Fig. 3.4b) and strike parallel to SIC contacts (Fig. 3.3a). The dip of planar igneous fabrics suggests that the South Range SIC was tilted by approximately 40° to 60° toward the NW in the Western Zone and about the same magnitude toward the N in the Eastern Zone (Figs. 3.4a, b).
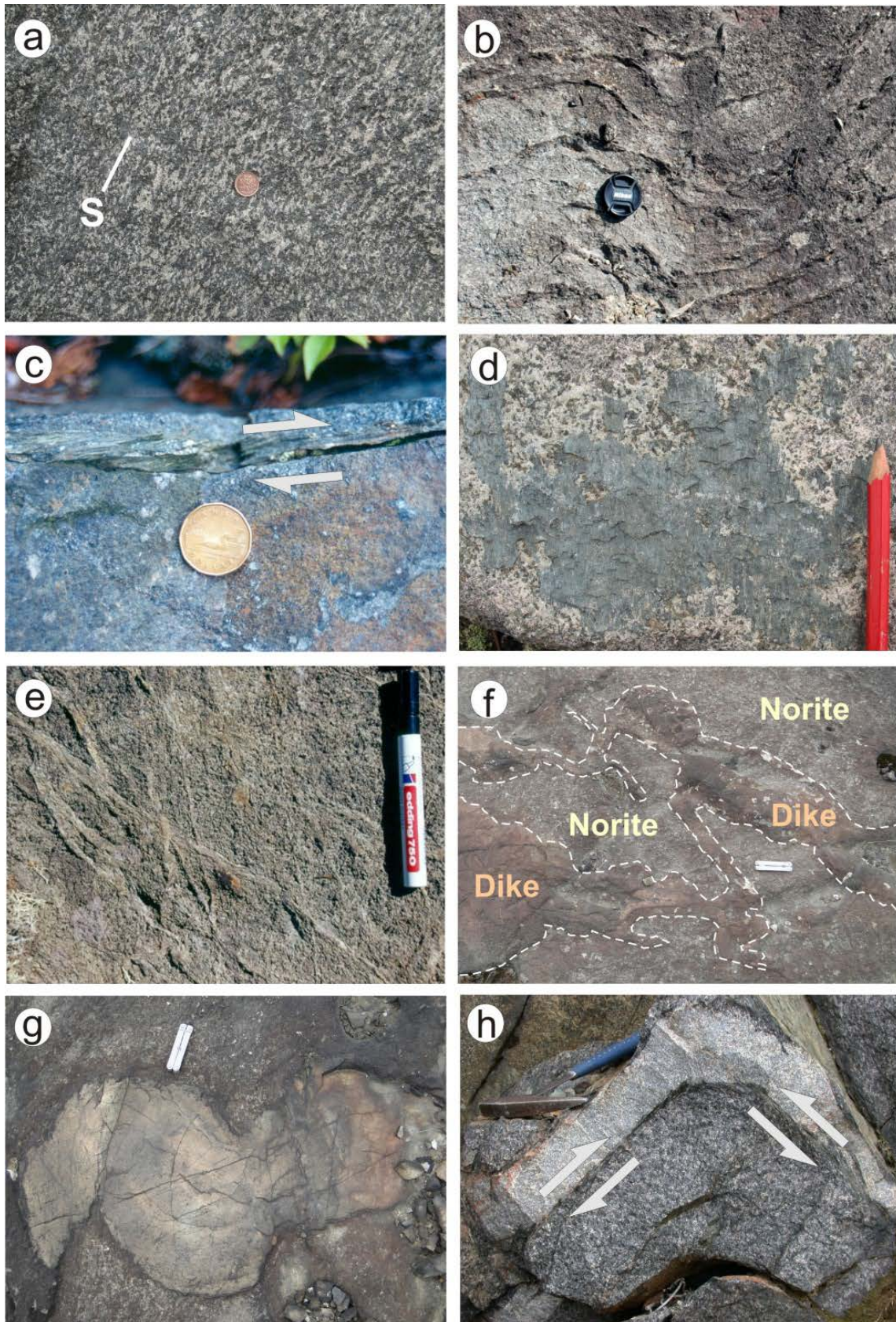
Figure 3.2 (previous page): Structural field characteristics of the South Range SIC. (a) Trace of planar igneous mineral fabrics (S) in Quartz Gabbro defined by subhedral plagioclase (white) and pyroxene transformed to actinolite (dark green). (b) Folded brittle shear faults in Norite. (c) Small-scale, brittle-ductile shear zone in Norite in profile plane. Note obliquity between metamorphic foliation defined by chlorite flakes and the zone margins. Half-arrows indicate sense-of-slip. (d) Brittle shear fault surface decorated by chlorite fibres. (e) Anastomosing pattern of small-scale chloritic shear zones in Norite. (f) Irregular shaped granitoid dike in Norite. Stippled lines delineate dike margins. (g) Buckled granitoid dike in Norite. Pocket knife is parallel to the trace of the shape-preferred orientation of metamorphic minerals in the Norite. (h) Folded granitoid dike in Quartz Gabbro. The dike margins of the fold limbs are reused as brittle-ductile slip surfaces. Half arrows indicate sense-of-slip. Note cuspate-lobate contact geometry in (g) and (h).
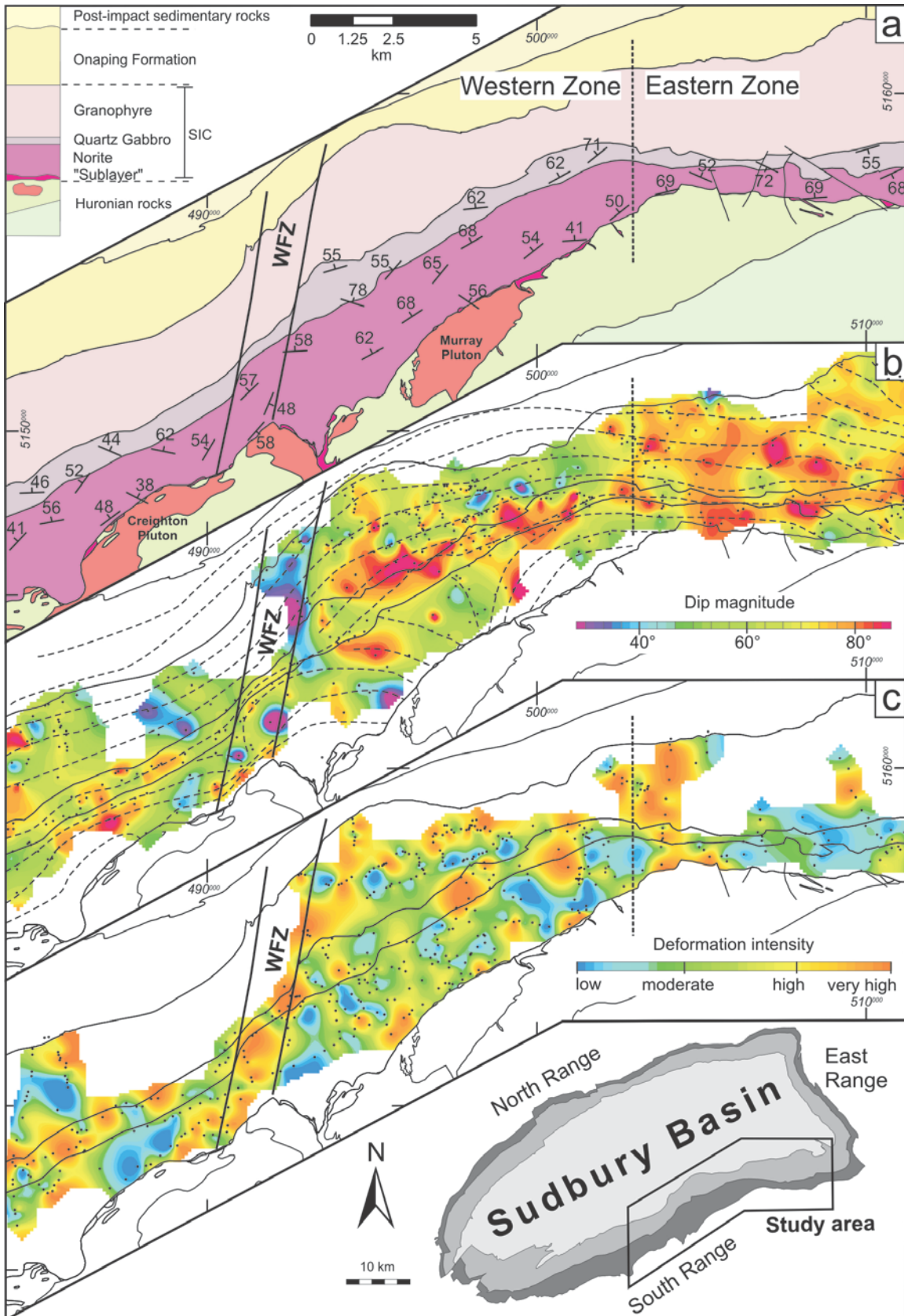
Figure 3.3: Caption on following page.
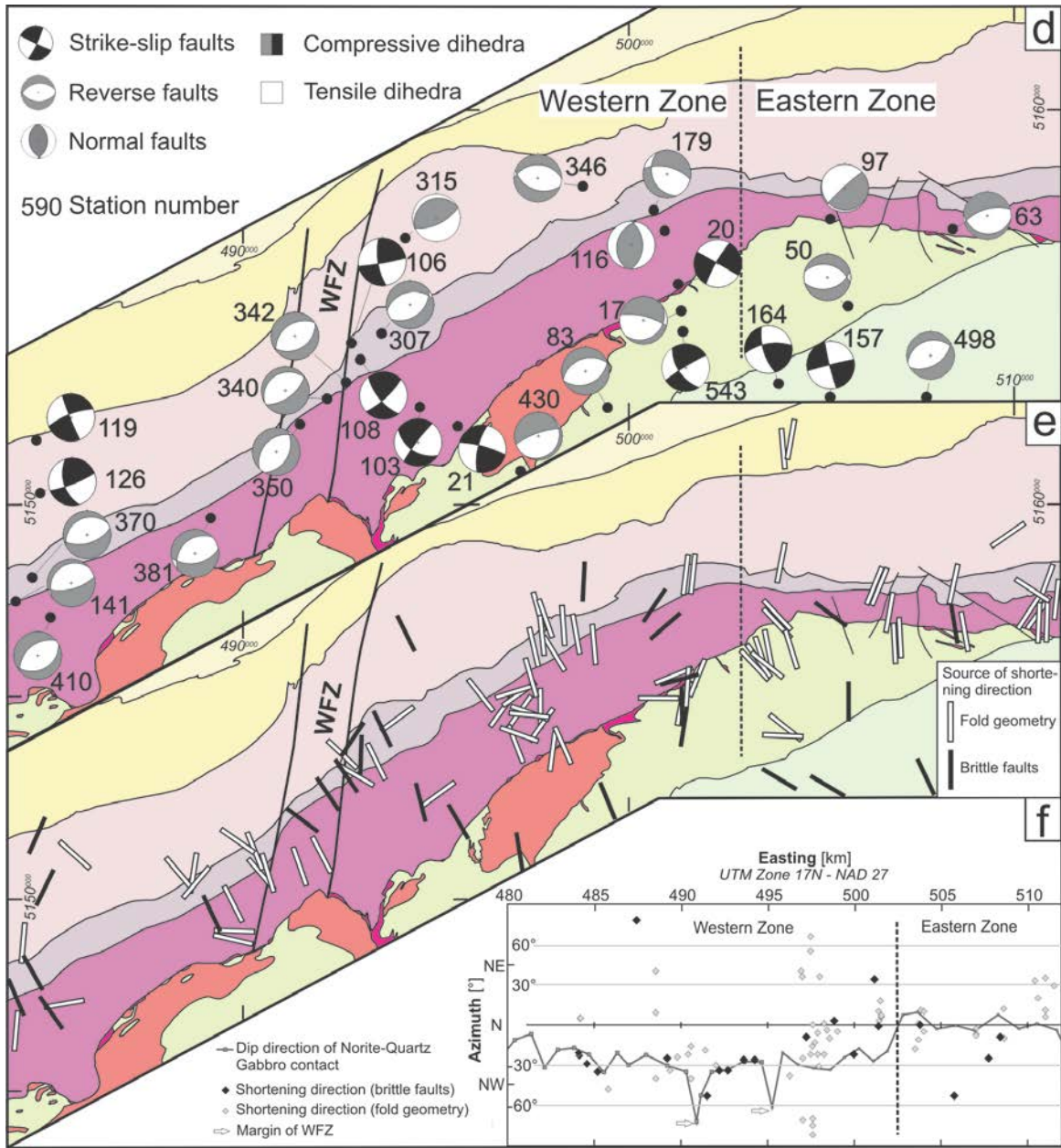
Figure 3.3: Structure of the study area in the South Range SIC. WFZ: Whitewater Lake Fault Zone. (a) Simplified geological map showing averages of dip directions (symbols) and dip magnitudes (numbers) of igneous layering. (b) Strike trajectories of inclined planar metamorphic shape fabrics (including data by Ames et al., 2005) overlain on contoured dip magnitudes of fabrics. Note the large variation in fabric strike in the basal Norite as opposed to that at the contact of the Granophyre with the Onaping Formation. (c) Variation in intensity of metamorphic mineral fabrics. For definition and explanation of fabrics see text. Contours in (b) and (c) were created with a minimum curvature algorithm using a cell size of 100 m. Dots in (b) and (c) show location of stations the contouring is based on. (d) Map showing dihedra of shortening and extension inferred from the inversion of brittle shear faults using the Numerical Dynamic Analysis. Station numbers correspond to numbering of diagrams and principal strain axes shown in Figure 5 and Table 1, respectively. (e) Directions of shortening inferred from brittle-fault analysis and fold geometry of granitoid dikes, projected onto the map plane. (f) Graph showing the along-strike variation in dip direction (azimuth) of the contact between Norite and Quartz Gabbro and shortening directions. The x-axis marks Easting coordinates. Note parallelism of shortening directions with dip direction of contact.

31
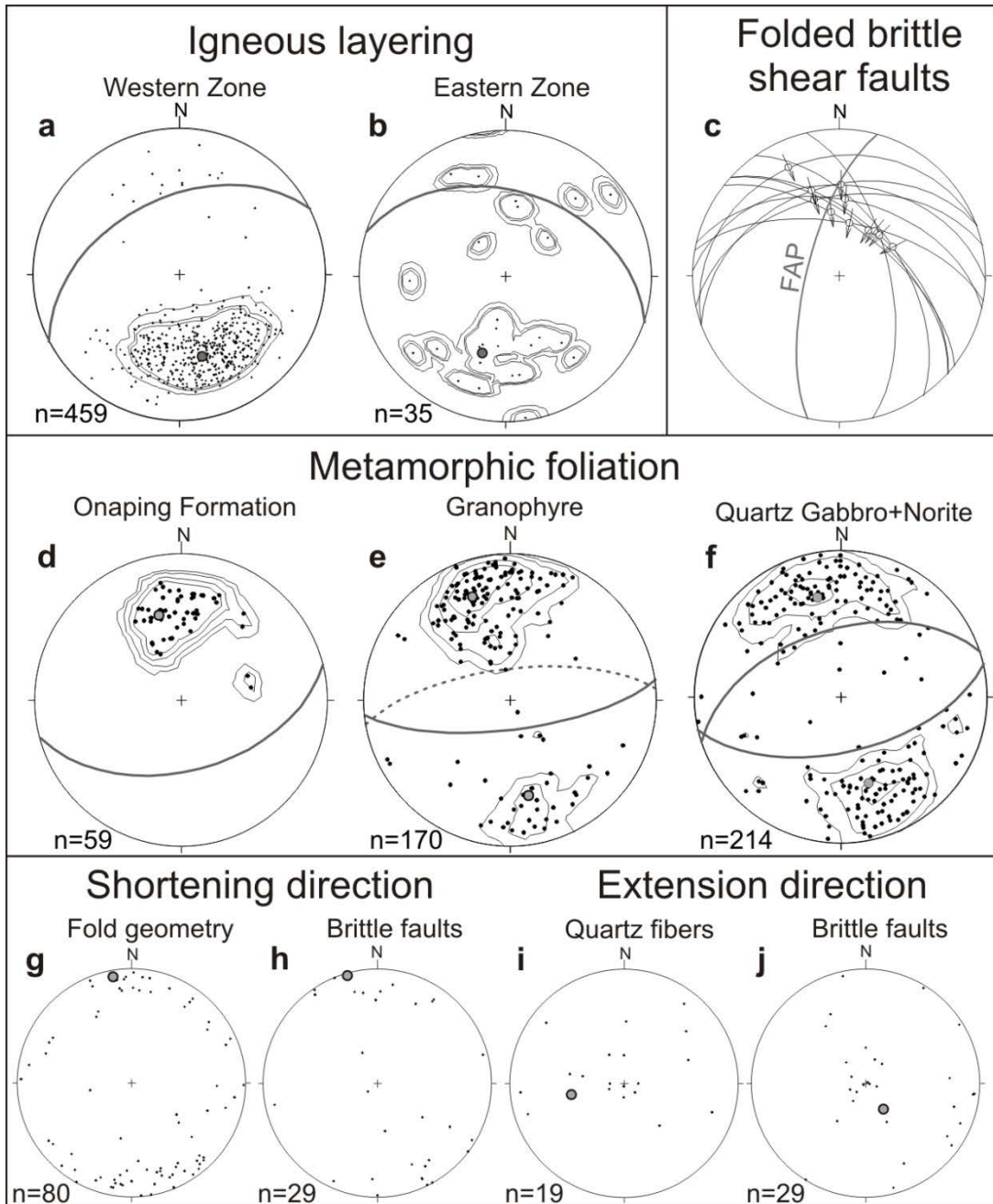
Figure 3.4: Lower-hemisphere, equal-area projections of magmatic and metamorphic fabric elements of the South Range SIC. Large grey circles indicate means and n the respective number of measurements. (a) Poles to magmatic layering in the Western Zone. (b) Poles to magmatic layering in the Eastern Zone. (c) Orientation of folded brittle fault plane segments (great circles), respective sense-of-slip of hanging wall (arrows) and fold-axial plane (FAP). (d) Poles to metamorphic foliation in the Onaping Formation. (e) Poles to metamorphic foliation in the Granophyre. (f) Poles to metamorphic foliation in the Quartz Gabbro and Norite. Foliation planes in (d) to (f) are from the Western Zone. (g) Poles to fold-axial planes of granitoid dikes. (h) Shortening directions inferred from brittle shear faults. (i) Orientation of quartz fibers. (j) Extension directions inferred from brittle shear faults. Note co-linearity of mean directions in (g) and (h), and (i) and (j), respectively.

3.4.2. Metamorphic fabrics

The South Range SIC and adjacent Onaping Formation display metamorphic mineral fabrics, the orientations of which were recorded at a total of 349 stations (Figs. 3.3b, 3.4d, e, f). Except for in the South Range Shear Zone (Shanks and Schwerdtner, 1991), the mineral fabrics in the SIC have planar geometry and are either defined by the shape-preferred orientation of amphibole and potassium feldspar or by biotite and chlorite (Figs. 3.2c, d). In outcrops, in which both metamorphic mineral assemblages are present, fabrics defined by chlorite and biotite display the same orientation as fabrics made up mostly of amphibole. This allowed us to reliably distinguish between metamorphic mineral fabrics and igneous layering, as the latter is defined by subhedral plagioclase and orthopyroxene in the South Range Norite. Moreover, distinction between the two fabric types is corroborated by the fact that the Onaping Formation is devoid of planar igneous fabrics and that the orientation of metamorphic mineral fabrics in the Onaping is akin to that mapped in the South Range SIC (Fig. 3.4d, e, f). Metamorphic and igneous mineral fabrics may be present in the same outcrops but generally display different orientations.

The orientation of planar metamorphic fabrics varies with position in the South Range SIC, notably in the Norite (Fig. 3.3b). Near the contact of the Onaping Formation with the Granophyre, which lies within the SRSZ (Fig. 3.1), and at the upper and lower contacts of the Quartz Gabbro, fabrics dip moderately to steeply southward and strike parallel to these contacts (Figs. 3.4d, e, f). By contrast, the strike of planar mineral fabrics in the Norite, notably close to its basal contact, is highly variable and often at high angles to the SIC-footwall contacts (Fig. 3.3b). The variation in planar fabric orientation can be explained by the map-scale strain gradient associated with the SRSZ. Specifically, away from the SRSZ, i.e., in the basal Norite, highly variable fabric orientations point to low levels of map-scale strain as opposed to high strain levels indicated by the more uniform orientation of planar fabrics in the SRSZ.

In the Western Zone, foliation planes in the Onaping Formation dip at moderate angles uniformly to the S (Fig. 3.4d). In the adjacent Granophyre two clusters of foliation orientations are apparent (Fig. 3.4e). Here, a well-defined cluster indicates steeply south-dipping foliation planes, whereas a less pronounced one represents steeply north-dipping planes. A bimodal orientation of foliation planes, i.e., steeply north- and steeply southward dipping planes, is well apparent in the Norite and Quartz Gabbro (Fig. 3.4f). Thus, metamorphic foliation seems to change systematically from a conjugate pattern in the Norite and Quartz Gabbro to uniformly south-dipping planes in the Onaping Formation. This points to a progressive change from co-axial to non-coaxial deformation toward the SRSZ.

Metamorphic fabric development varies with location in the South Range. Fabric development can be assessed by the number of shear planes per area in a given outcrop (Fig. 3.5) and ranges from isolated, few millimeter-wide deformation zones (Figs. 3.2c, d, 3.5a) to pervasively foliated rock (Fig. 3.2g). At low spatial density, shear fractures are spaced decimeters to meters apart and are observed to be planar (Fig. 3.5a). In these locations, intersections between fractures are at high angles to each other and show little offset (Fig. 3.5a). At higher spatial densities, shear fractures are conjugate to each other and connect to millimeter- to centimeter-wide ductile shear zones (Fig. 3.5b, c). The foliation in these zones is mostly defined by the shape-preferred orientation of chlorite and biotite, and is oblique to shear zone margins (Fig. 3.2c).
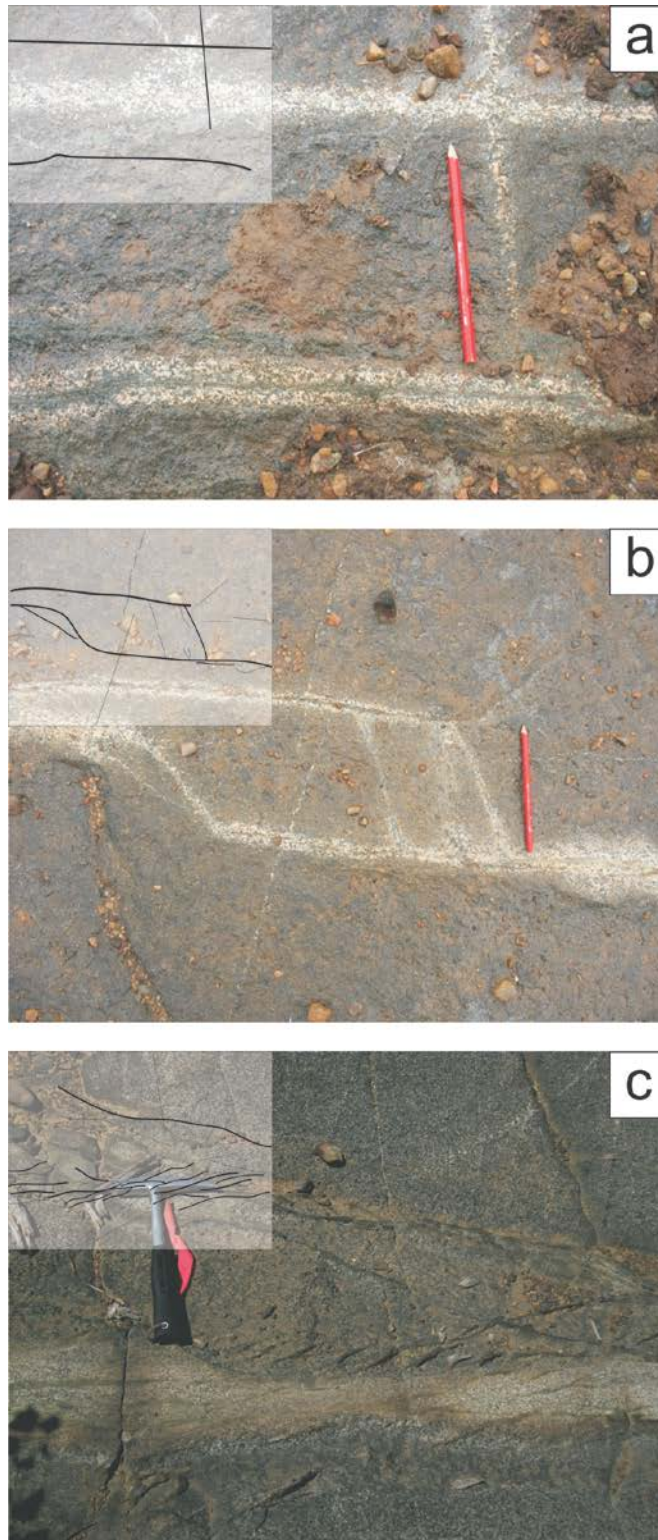
Figure 3.5: Outcrop photos showing variable fracture densities and the coalescence of shear fractures into shear zones with increasing deformation intensity. Shear fractures are well evident by alteration halos. (a) Widely spaced fractures oriented at high angles to each other. (b) Isolated fractures coalescing to thin shear zone. (c) Shear zone characterized by sigmoidal brittle-ductile shear fractures in an outcrop containing a high fracture density.

The variation in metamorphic fabric development can be used to crudely map deformation intensity in the South Range SIC (Fig. 3.3c). Outcrops characterized by the sporadic presence of thin seams of metamorphic minerals, notably chlorite fibers, which nucleate in and decorate brittle shear fractures (Fig. 3.2d), form zones of low deformation intensity. Outcrops replete with centimeter-wide shear zones form zones of moderate deformation intensity. The shear zones often have anastomosing geometry (Fig. 3.2e) and coalesce to form meter-wide foliated zones in areas of high deformation intensity. Outcrops characterized by pervasive metamorphic foliation form zones of very high deformation intensity.

Heterogeneity in metamorphic fabric development as seen on the outcrop scale is also evident on the map scale. Here, deformation intensity varies on the hundred-meter to kilometer scale (Fig. 3.3c). In places, outcrops characterized by high deformation intensity connect to kilometer-scale zones of continuous deformation. In particular, there is a laterally coherent NNE-striking zone of enhanced deformation north of the eastern Creighton Pluton (Fig. 3.3a, c), henceforth referred to as the Whitewater Lake Fault Zone (WFZ). On outcrop scale the WFZ is characterized by pervasive, subvertical and symmetric anastomosing planar metamorphic mineral fabrics, which are devoid of mineral lineations. The zone transects the Quartz Gabbro where its upper and lower contacts deviate from their overall ENE strike toward the NE (Fig. 3.3a). The strike separation displayed by these contacts agrees with the sigmoidal curvature of metamorphic foliation trajectories associated with the WFZ (Fig. 3.3b) and may indicate a sinistral shear component resolved on the WFZ. Thus, the WFZ forms a broad zone of continuous deformation that displaces the South Range SIC.

3.4.3. Folded granitoid dikes

The South Range Norite contains dike- and pod-like bodies of granitoid composition that range in thickness from a few millimeters to decimeters and can be traced up to tens of meters. The bodies are likely derived from the nearby ca. 2.3 Ga Creighton and Murray Plutons (Fig. 3.3a). The shapes of the granitoid bodies are highly irregular and have wispy apophyses (Fig. 3.2f), reminiscent of magma mingling. This suggests that the granitoid bodies intruded the Norite as back injections when the Norite was a melt.

The granitoid bodies are tightly to isoclinally folded. The folds are associated with an axial-planar fabric in the adjacent host rock (Fig. 3.2g) that is chiefly defined by the shape-preferred orientation of amphibole and biotite. The margins of folded dikes are lobate, whereas the host rock displays cusps (Fig. 3.2g, h). This indicates that the dikes were mechanically more competent than the host rock during folding. However, the dikes retained their structural coherence during this deformation, which indicates continuous deformation during shape change of the granitoid dikes.

Assuming that the folds of the granitoid dikes formed due to shortening orthogonal to their fold-axial planes, i.e., in the direction of the poles to these planes, local shortening directions for the South Range SIC were determined at 55 stations (Fig. 3.4g). Shortening directions in the Western Zone are mostly NW-SE and in agreement with left-lateral strike separation of SIC contacts on the WFZ, whereas shortening in the Eastern Zone is rather N-S (Fig. 3.3e). Thus, the shortening

directions inferred from folded granitoid dikes are crudely orthogonal to the strike of the SIC contacts (Figs. 3.3e, f).

3.4.4.   Brittle deformation

Small-scale brittle shear faults are pervasively developed in the South Range SIC and adjacent Huronian rocks. The fault planes are mostly decorated by chlorite fibers (Fig. 3.2d) and sporadically by fibrous quartz, calcite and biotite. In places, faults are associated with fault gouge or cohesive cataclasite. The sense-of-slip on the faults was determined by the polarity of stair-stepping geometry displayed by the mineral fibers, secondary Riedel fractures and displaced passive markers, such as granitoid dikes.

The orientation of 372 brittle fault surfaces and their respective striations were measured at 29 stations (Fig. 3.6, Table 3.1). The sense-of-slip was reliably determined for 200 fault surfaces. The fault populations consist chiefly of moderately SE- and NW-dipping conjugate reverse faults and N-S striking strike-slip faults (Fig. 3.6). Based on the orientation of fault surfaces, the orientation of mineral fibers and the sense-of-slip, principal axes of paleostress or infinitesimal strain can be calculated for a given fault population (Angelier, 1979). As displacement on the brittle fault surfaces is minimal, we interpret principal paleostress axes in terms of paleostrain axes.

The presence of conjugate fault sets calls for an analytical method that considers each fault plane individually. As some stations displayed a low number of fault planes with a reliable sense of slip, the application of analytical methods searching for the best-fit reduced stress tensor is limited. For each fault population per station, the infinitesimal shortening and extension directions (Table 3.1) were calculated using the Numerical Dynamic Analysis (NDA: Spang, 1972). This method assigns to each fault plane a shear strain magnitude of 1. Furthermore, the angle between the maximum principal strain axes and the fault plane is identical for each fault population. For our analysis, we chose an angle of 30° between the maximal principal strain direction and the maximum resolved shear strain, which is within the limits of experimentally obtained values for this angle (Byerlee, 1968).

For each fault plane a set of shortening and extension directions is calculated in tensor form. The sum of all tensors divided by the number of fault planes results in the deviatoric strain tensor. The eigenvector and the eigenvalue of this tensor define the orientation of the principal reciprocal strain directions ($\lambda_1 > \lambda_2 > \lambda_3$) and the strain ratio ($R_{strain}$). In addition, NDA gives the number of fault planes whose measured slip senses are opposite to the ones predicted by a particular solution ("nev" in Table 3.1).

Shortening axes plunge shallowly north- or southward at almost all stations (Figs. 3.4h, 3.6). The direction of extension is vertical in 16 stations, sub-horizontal at 10 stations and hybrid at 3 (Figs. 3.3d, 4j, 3.6). Subvertical extension during brittle deformation is also indicated by the orientation of fibrous quartz in extension veins (Fig. 3.4i). Analogous to the shortening directions inferred from granitoid dikes, shortening directions based on inversion of brittle shear faults are crudely orthogonal to the strike of SIC contacts and compatible with left-lateral displacement on the WFZ (Fig. 3.3d, e).

Finally, it should be noted that brittle fault surfaces in the Norite of the Eastern Zone are sporadically folded (Fig. 3.2b). Fault planes decorated with quartz and chlorite are spaced several centimeters apart and display open folds. As a consequence of folding, mineral fibers on individual folded fault planes are fanning around the respective fold hinge zone (Fig. 3.4c). This suggests that brittle faulting preceded in places continuous deformation accomplished by folding and foliation development.

Station	Easting	Northing	λ1	λ2	λ3	R_{Strain}	#hf	nev	skip
17	501398	5154995	359/28	099/18	217/56	0.35	24	0	16
20	501438	5154449	075/05	305/83	165/06	0.72	16	1	10
21	495904	5151735	150/17	314/72	058/04	0.29	18	3	11
50	503787	5157118	180/02	089/15	216/75	0.83	12	0	7
63	508415	5157102	351/21	257/09	146/67	0.57	9	0	4
83	499974	5152541	338/01	068/02	230/88	0.62	7	1	2
97	505765	5157393	127/49	228/09	325/39	0.60	24	4	13
103	494624	5152482	346/19	225/56	086/27	0.41	21	0	16
106	492853	5154140	034/13	246/75	126/08	0.53	14	1	9
108	493081	5153715	002/21	197/69	095/05	0.10	13	0	3
116	501305	5155672	229/81	005/06	096/06	0.87	18	3	6
119	484749	5151557	204/07	325/77	113/11	0.48	10	0	6
126	484446	5149476	026/24	244/61	123/16	0.62	8	1	3
141	484147	5147448	157/24	251/09	000/64	0.53	9	0	5
157	504039	5153825	121/04	280/86	031/02	0.50	5	0	1
164	502588	5154106	121/27	306/63	212/02	0.66	7	0	3
179	501165	5157901	034/15	297/26	151/59	0.72	5	0	1
307	493626	5154397	154/01	063/12	248/78	0.33	10	1	6
315	494258	5156862	334/66	064/00	154/24	0.18	11	0	5
340	492216	5152694	146/20	055/03	317/70	0.52	19	0	14
342	492714	5153124	326/02	236/02	098/87	0.48	14	0	10
346	498842	5158206	183/17	275/06	022/72	0.42	10	0	3
350	491513	5152040	127/01	037/09	225/81	0.50	12	0	6
370	484583	5148069	151/00	241/02	056/88	0.83	14	0	7
381	489212	5149620	155/08	247/16	040/72	0.68	19	0	12
410	485203	5147183	325/06	235/06	102/82	0.79	16	1	10
430	497233	5150617	171/55	069/09	333/33	0.51	9	1	4
498	507750	5152161	155/09	064/07	295/79	0.50	6	0	2
543	501416	5154448	009/14	248/64	105/21	0.25	12	0	5

Table 3.1: Quantities of brittle deformation inferred from Numerical Dynamic Analysis. Orientation of shortening (λ_1) and extension (λ_3) axes is given as dip direction/dip. R_{Strain} is the strain ratio, # denotes the number of fault planes per station and nev *is the number of fault planes whose measured slip senses are opposite to the ones predicted by a particular solution.*
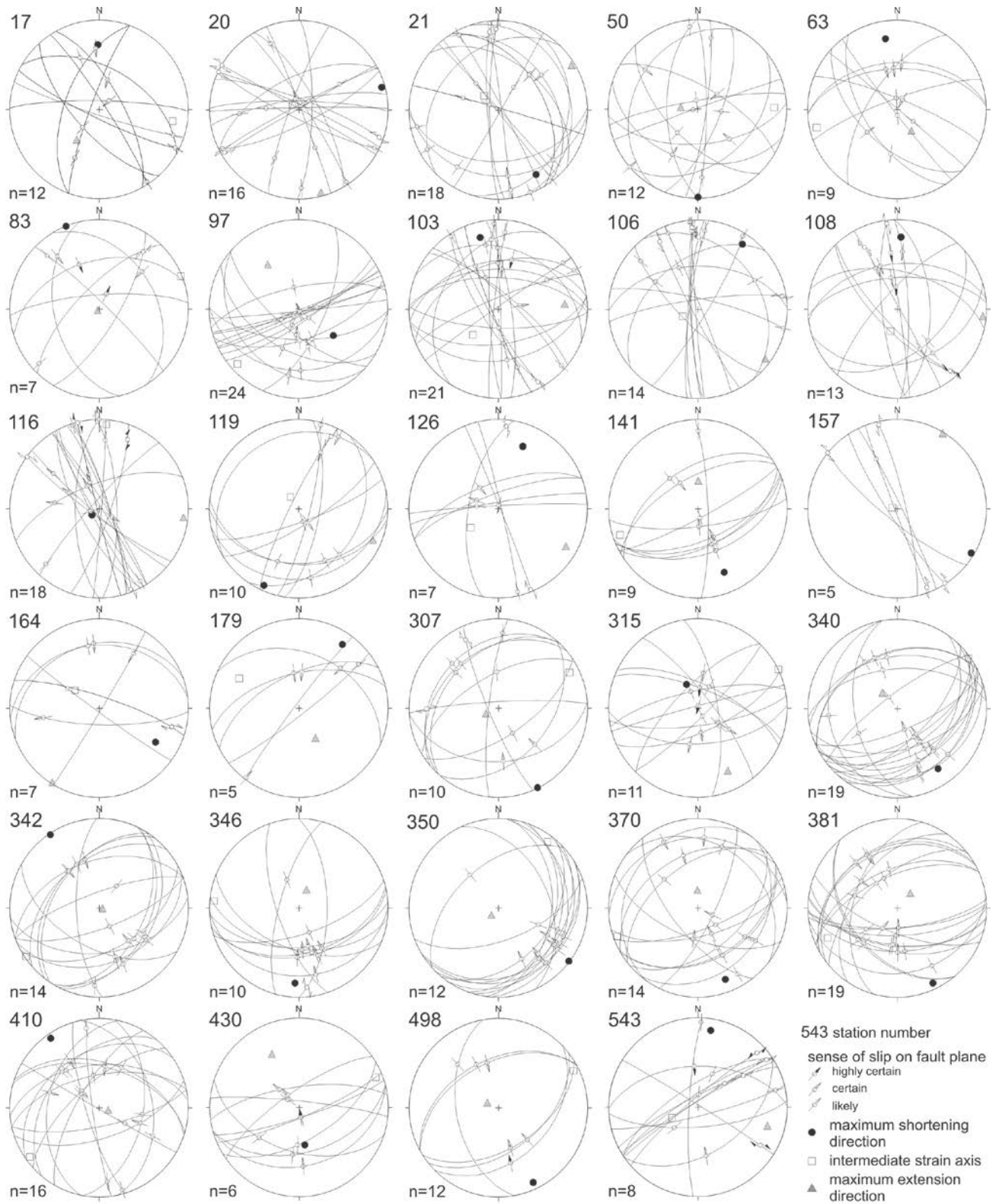
Figure 3.6: Lower-hemisphere equal-area projections showing the orientation of brittle faults (great circles) and respective sense-of-slip of hanging walls (arrows) as well as principal strain axes inferred from Numerical Dynamic Analysis (Table 3.1).

3.5.   Structural interpretation

This structural analysis indicates that the South Range SIC, notably the Norite, underwent heterogeneous deformation, evident by the development and spatial distribution of centimeter- to the kilometer-scale structures. Specifically, we examined the orientation of (1) planar metamorphic mineral fabrics, (2) quartz fibres in extension veins, (3) folds in granitoid dikes, (4) small-scale brittle shear faults and (5) kilometer-scale deformation zones. The orientation and kinematics of these structures indicate that the South Range SIC underwent substantial layer-parallel stretching and layer-normal shortening, i.e., thinning.

There is a marked variation in shortening directions evident from fault-slip analysis, fold geometry of granitoid dikes and orientation of planar metamorphic shape fabrics that correlates with the strike of the SIC contacts (Figs. 3.3b, e, f). Specifically, shortening directions are oriented N-S in the E-W trending Eastern Zone, whereas the NE-SW trending Western Zone is dominated by NW-SE trending shortening directions. Thus, shortening directions are approximately perpendicular to the SIC contacts, whereas extension directions are mostly vertical (Fig. 3.3d). This geometry of local shortening and extension axes corroborates thinning of the South Range SIC.

The shortening and extension axes inferred from the orientation of metamorphic foliation surfaces, geometry of granitoid dikes, kinematics of brittle-ductile shear faults and orientation of quartz fibers in extension fractures are largely collinear (Fig. 3.4). Thus, the strain fabrics formed under variable rheological conditions (see below), but under a single deformation regime during progressive shortening. However, it remains to be ascertained whether deformation of the South Range SIC under these conditions occurred during cooling (Riller, 2005; Klimczak et al., 2007) or during prograde regional metamorphism (Thomson et al., 1985) of the SIC.

The presence of folded brittle-ductile fault planes in the Norite suggests that discontinuous deformation of the SIC preceded continuous deformation in many places. This is also evident by anastomosing, chlorite- and biotite-coated shear fractures coalescing to form ductile shear zones in the Norite and Quartz Gabbro (Fig. 3.2e). Collectively, this indicates that zones of pervasive foliation development formed initially from localized brittle shear faults (e.g., Pennacchioni, 2005). Evidently, brittle faults in the Norite and Quartz Gabbro lead to localized hydration and transformation of mafic minerals to chlorite and biotite in fault rock. This indicates low- to middle greenschist-facies metamorphic conditions during deformation. Such low-temperature, hydrolytic weakening (Kronenberg et al., 1990) caused widening of brittle shear fractures to hydrated shear faults that ultimately coalesced into broad ductile deformation zones during progressive deformation (Figs. 3.5, 3.7). This mechanism of metamorphic foliation development by coalescence of hydrated brittle-ductile shear bands has also been documented in initially isotropic granitoid rock (Choukroune and Gapais, 1983; Christiansen and Pollard, 1997).

Bulk NW-SE shortening in the South Range SIC is compatible with large-scale folding of the SIC and the kinematics of the SRSZ. The SRSZ may have formed independently of folding (Milkereit et al., 1992; Wu et al., 1994; Boerner et al., 2000) or as a consequence of folding-induced strain (Card and Jackson, 1995). The map-scale variation in orientation of metamorphic foliation (Fig. 3.3b) and the northward increase in non-coaxiality of deformation (Figs. 3.4 d, e,

f) suggest that deformation in the South Range SIC is kinematically related to the formation of the SRSZ. The fact that only a single deformation regime can be discerned from the strain fabrics may, therefore, indicate that large-scale folding of the SIC occurred contemporaneously with activity of the SRSZ (Fig. 3.7). This hypothesis agrees with the observed predominance of symmetric strain fabrics in the South Range SIC indicating flattening strains (Fig. 3.4e, f). Bulk thinning of the SIC as the main mechanism of deformation is compatible with geochemical profiles across the South Range SIC. These profiles are characterized by systematic variations in chemical trends showing no marked discontinuities (Lightfoot, 2009). Also, analogue experiments by Riller et al. (2010) suggest that the formation of the SRSZ is a mechanical consequence of folding of the SIC (Card and Jackson, 1995).

The deformation fabrics recorded in the South Range Norite have important implications for understanding the magnitude and mechanism of rotation in the South Range. The total magnitude of rotation of the South Range SIC, as inferred from the orientation of igneous layering in the Norite, ranges from 40° to 60° (Fig. 3.4a). However, not all of this rotation magnitude may have been taken up by solid-body rotation, i.e., tilting of the South Range SIC. Layer-parallel thinning can enhance the dip of pre-existing inclined material surfaces, such as lithological contacts and primary layering, by shearing-induced rotation (inset in Fig. 3.7). This may well have enhanced the inclination of SIC contacts and igneous layering during N-S shortening in the South Range. Thus, the actual tilt component of the South Range at the current level of erosion is expected to be smaller than indicated by the inclination of igneous layering in the Norite (60°: Figs. 3.4a, 3.7). Accordingly, variable magnitudes of thinning can account for the observed difference in contact dips between the South Range and the North Range. Notably, dip magnitudes of SIC contacts are larger for the South Range than for the North Range (Fig. 3.1). Structural elements in the South Range SIC suggest that it constitutes the short, but highly strained, limb of an asymmetric, NW-verging km-scale anticline-syncline pair of the SIC (Fig. 3.7).
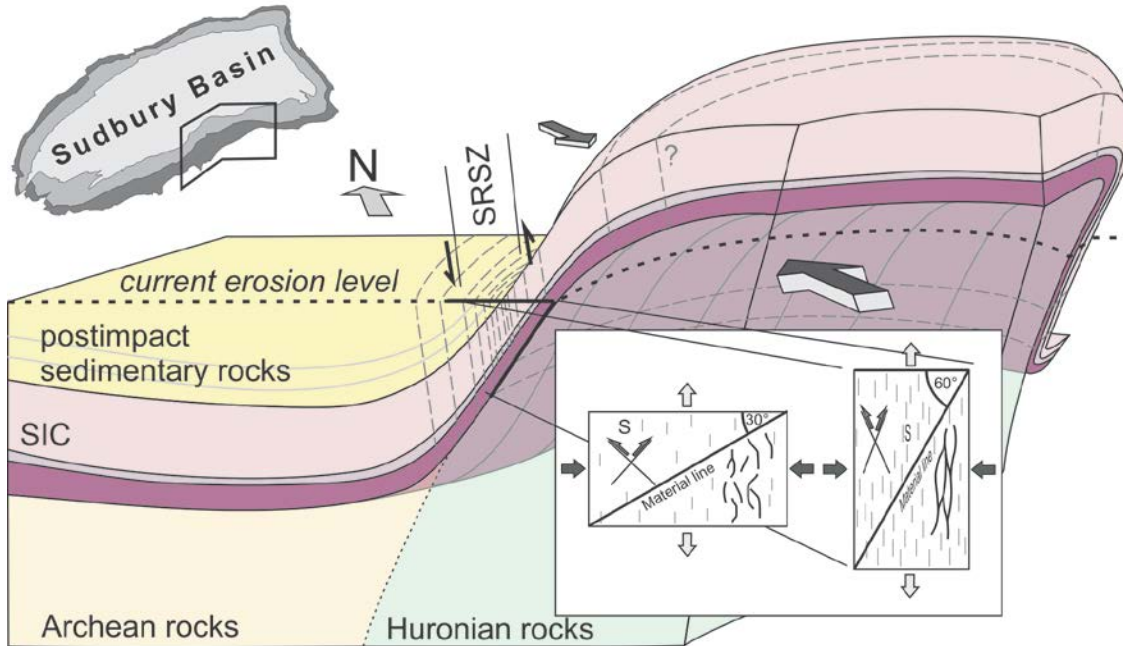
Figure 3.7: Conceptual model showing structural characteristics of the deformed South Range SIC. The South Range Shear Zone (SRSZ) forms as a consequence of fold-induced strain that leads to thinning of the SIC in the steep short limb of an asymmetric anticline-syncline pair. Traces of foliation surfaces are shown as grey stippled lines. Inset shows the shear-induced rotation of material surfaces, such as conjugate shear faults, anastomosing brittle-ductile shear zones, foliation surfaces (S) and inclined contacts, after 40% of bulk coaxial shortening (dark arrows) and respective extension (light arrows). Note steepening of material line representing the basal SIC contact by about 30° as a consequence of overall thinning of the SIC and reduction in the angle between conjugate structures. The orientation of foliation surfaces does not change with respect to the principal axes of bulk strain.

3.6.   Conclusions

Deformation in the South Range SIC, notably the Norite and Quartz Gabbro, was taken up by centimeter- to kilometer-scale structures, notably planar metamorphic mineral fabrics, tight to isoclinal folds in granitoid dikes, small-scale brittle shear faults and first-order ductile high-strain zones. Deformation was heterogeneous and occurred under variable rheological conditions but evidently under a single deformation regime. This suggests that shape change of the South Range SIC was achieved during folding of the SIC and concomitant reverse sense-of-shear on the SRSZ. Locally, brittle deformation preceded the development of pervasive planar metamorphic mineral fabrics and caused hydrolytic weakening of initially isotropic Norite and Quartz Gabbro. As a consequence, these units were thinned, which likely had a profound influence on the geometry and kinematics of deformation in the South Range SIC during overall NW-SE shortening. Most importantly, thinning of the South Range SIC enhanced the inclination of its contacts and igneous layering. This suggests that the actual tilt component of the South Range is smaller than the maximum rotation (60°) of the Norite as indicated by the dip of its igneous layering. Variable magnitudes of thinning of the SIC can account for differences in contact inclination of the North Range and the South Range. The structure of the latter is compatible with that of the short limb of a NW-verging, asymmetric fold.

3.7.   Summary

Compared to felsic igneous rocks the genetic relationship between brittle and ductile fabric development and its influence on the geometry of deformed mafic melt sheets has received little attention in structural analyses. This study explored these relationships using the Sudbury Igneous Complex (SIC) as an example. The SIC is the relic of a layered impact melt sheet that was transformed into a fold basin, the Sudbury Basin, during Paleoproterozoic deformation at the southern margin of the Archean Superior Province. I studied brittle and ductile strain fabrics on the outcrop and map scales in the southern Sudbury Basin, notably in the Norite and Quartz Gabbro layers of the SIC. Here, deformation is heterogeneous and occurred under variable rheological conditions, evident by the development of brittle shear fractures, brittle-ductile shear zones and pervasive ductile strain. The mineral fabrics formed under low- to middle greenschist-facies metamorphism, whereby brittle deformation caused hydrolytic weakening and ductile fabric development. Principal strain axes inferred from all structural elements are collinear and point to a single deformation regime that led to thinning of SIC layers during progressive deformation. Ductile fabric development profoundly influenced the orientation of SIC material planes, such as lithological contacts and magmatic mineral fabrics. More specifically, these planar structural elements are steep where the SIC underwent large magnitudes of thinning, i.e., in the south limb of the Sudbury Basin. Here, the actual tilt component of material planes is likely smaller than its maximum total rotation (60°) inferred from inclined igneous layering in the Norite. My field-based study shows that ductile fabric development from brittle faults can have a profound influence on the shape change of igneous melt sheets and may be more significant than previously appreciated.

References

Angelier, J., 1979. Determination of the mean principle directions of stresses for a given fault population. Tectonophysics T17-T26.

Ames, D.E., Davidson, A., Buckle, J.L., Card, K.D., 2005. Geology, Sudbury Bedrock Compilation, Ontario. Geological Survey of Canada, Open File 4570, scale 1:50 000.

Ames, D.E., Farrow, C.E.G., 2007. Metallogeny of the Sudbury Mining Camp, Ontario. *In*: Goodfellow, W.D. (Ed.), Mineral deposits of Canada- A synthesis of Major Deposit types, District Metallogeny, the Evolution of Geological Provinces and Exploration Methods, Geological Association of Canada Special Publication 5, 329-350.

Bailey, J., Lafrance, B., McDonald, A., Fedorowich, J., Kamo, S., Archibald, D., 2004. Mazatzal-Labradorian-age (1.7-1.6 Ga) ductile deformation of the South Range Sudbury impact structure at the Thayer Lindsley mine, Ontario. Canadian Journal of Earth Sciences 41, 1491-1505.

Boerner, D.E., Milkereit, B., Wu, J., Salisbury, M., 2000. Seismic images and three-dimensional architecture of a Proterozoic shear zone in the Sudbury Structure (Superior Province, Canada). Tectonics 19, 397-405.

Brocoum, S., Dalziel, I., 1974. Sudbury Basin, Southern Province, Grenville Front, and Penokean Orogeny - Discussion. Geological Society of America Bulletin 85, 1571-1580.

Butler, H., 1994. Lineament analysis of the Sudbury multiring impact structure. Geological Society of America Special Paper 293, 319-329.

Bürgmann, R., Pollard, D.D., 1994. Strain accommodation about strike-slip-fault discontinuities in granitic rock under brittle-to-ductile conditions. Journal of Structural Geology 16, 1655-1674.

Byerlee, J. D., 1968. Brittle ductile transition in rock. Journal of Geophysical Research 73, 4741-4750.

Card, K.D., 1978. Geology of the Sudbury-Manitoulin Area, District of Sudbury and Manitoulin; Ontario Geological Survey, Report 166, 238 p.

Card, K.D., Church, W.R., Franklin, J.M., Robertson, J.A., West, G.F., Young, G.M., 1972. The Southern Province. In: Price, R.A., Douglas, R.J.W. (Eds.), Variations in Tectonic Style in Canada. Geological Association of Canada Special Paper 8, 335-380.

Card, K.D., Gupta, P.H., McGrath, P.H., Grant, F.S. 1984. The Sudbury Structure: Its Regional Geological and Geophysical Setting. In: Pye, E.G., Naldrett, A.J., Giblin P.E (Eds.), The Geology and Ore Deposits of the Sudbury Structure. Special Publication 1, Ontario Geological Survey, Toronto, 25–43.

Card, K.D., Jackson, S.L, 1995. Tectonics and metallogeny of the Early Proterozoic

Huronian fold belt and the Sudbury structure of the Canadian shield, Field Trip Guide Book, Geological Survey of Canada, Open File 3139, 55p.

Choukroune, P., Gapais, D., 1983. Strain pattern in the Aar granite (Central Alps): Orthogneiss developed by bulk inhomogeneous flattening. Journal of Structural Geology 5, 411-418.

Christiansen, P.P., Pollard, D.D., 1997. Nucleation, growth and structural development of mylonitic shear zones in granitic rock. Journal of Structural Geology 19, 1159-1172.

Corfu, F., Andrews, A.J., 1986. A U-Pb age for mineralized Nipissing diabase, Gowganda, Ontario. Canadian Journal of Earth Sciences 23, 107-109

Cowan, E.J., 1996. Deformation of the Eastern Sudbury Basin. Ph.D. thesis, University of Toronto, Toronto, 366p.

Cowan, E.J., 1999. Magnetic fabric constraints on the initial geometry of the Sudbury Igneous Complex: a folded sheet or a basin-shaped igneous body? Tectonophysics 307, 135-162.

Cowan, E.J., Schwerdtner W.M. 1994. Fold origin in the Sudbury basin. In: Lightfoot, P.C., Naldrett, A.J. (Eds.), Proceedings of the Sudbury - Noril'sk Symposium, Special Volume 5. Ontario Geological Survey, 45-55.

Cowan, E.J., Riller, U., Schwerdtner, W.M., 1999. Emplacement geometry of the Sudbury Igneous Complex: Structural examination of a proposed impact melt-sheet. *In*: Dressler, B.O., Sharpton, V.L., Large Meteorite Impacts and Planetary Evolution II. GSA Special Paper 339. Geological Society of America, Boulder, 399–418.

Deutsch, A., Grieve, R.A.F., Avermann, M., Bischoff, L., Brockmeyer, P., Buhl, D., Lakomy, R., Müller-Mohr, V., Ostermann, M., Stöffler, D., 1995. The Sudbury Structure (Ontario, Canada): A tectonically deformed multi-ring impact basin. Geologische Rundschau 84, 697-709.

Dietz, R., 1964. Sudbury Structure as an Astrobleme. Journal of Geology 72, 412-434.

Dreuse, R., Doman, D., Santimano, T., Riller, U., 2010. Crater-floor topography and impact melt sheet geometry of the Sudbury impact structure, Canada. Terra Nova 22, 463-469.

Easton, R.M. 2000. Metamorphism of the Canadian Shield, Ontario, Canada. II. Proterozoic metamorphic history. Canadian Mineralogist 38, 319-344.

Fleet, M.E., Barnett, R.L., 1978. Al^{iv}/Al^{vi} partitioning in calciferous amphiboles from the Frood mine, Sudbury, Ontario. Canadian Mineralogist 16, 527-532.

Fleet, M.E., Barnett, R.L., Morris, W.A., 1987. Prograde metamorphism of the Sudbury igneous complex. Canadian Mineralogist 25, 499-514.

Fueten, F., Redmond, D.J., 1997. Documentation of a 1450 Ma contractional orogeny preserved

between the 1850 Ma Sudbury Impact Structure and the 1 Ga Grenville orogenic front, Ontario, Canada. Geological Society of America Bulletin 109, 268-279.

Gates, T.M., Hurley, P.M., 1973. Evaluation of Rb-Sr dating methods applied to the Matachewan, Abitibi, Mackenzie, and Sudbury dike swarms in Canada. Canadian Journal of Earth Sciences 10, 900-919.

Grieve, R., Stöffler, D., Deutsch, A., 1991. The Sudbury Structure - controversial or misunderstood. Journal of Geophysical Research 96, 22753-22764.

Grieve, R.A.F., Reimold, W.U., Morgan, J., Riller, U., Pilkington, M., 2008. Observations and interpretations at Vredefort, Sudbury and Chicxulub: Towards an empirical model of terrestrial impact basin formation. Meteoritics and Planetary Science 43, 855–882.

Grieve, R.A.F., Ames, D.E., Morgan, J.V., Artemieva, N., 2010. The evolution of the Onaping Formation at the Sudbury Impact Structure. Meteoritics and Planetary Science 45, 759-782.

Halls, H.C., 2009. A 100 km-long paleomagnetic traverse radial to the Sudbury Structure, Canada, and its bearing on Proterozoic deformation and metamorphism of the surrounding basement. Tectonophysics 474, 493-506.

Keays, R.R., Lightfoot, P.C., 2004. Formation of Ni-Cu-Platinum group element sulfide mineralization in the Sudbury Impact Melt Sheet. Mineralogy and Petrology 82, 217–258.

Klimczak, C., Wittek, A., Doman, D., Riller, U., 2007. Fold origin of the NE-lobe of the Sudbury Basin, Canada: Evidence from heterogeneous fabric development in the Onaping Formation and the Sudbury Igneous Complex. Journal of Structural Geology 29, 1744-1756.

Krogh T.E., Davis D.W., Corfu F., 1984. Precise U-Pb zircon and Baddeleyite Ages for the Sudbury Area. *In*: Pye, E.G., Naldrett, A.J., Giblin, P.E. (Eds.), The Geology and Ore Deposits of the Sudbury Structure. Special Publication 1, Ontario Geological Survey, Toronto, 431-446.

Kronenberg, A.K., Segall, P., Wolf, G.H., 1990. Hydrolytic weakening and penetrative deformation within a natural shear zone. Geophysical Monograph 56, 21-36.

Lightfoot, P.C., 2009. Mechanisms of Ni-Cu-PGE Sulphide Ore Formation in the Impact-generated Sudbury Melt Sheet. AGU Joint Assembly, abstract GA32B-04.

Means, W.D., 1989. Synkinematic microscopy of transparent polycrystals. Journal of Structural Geology 11, 163-174.

Milkereit, B., Green, A., Sudbury Working Group, 1992. Deep geometry of the Sudbury structure from seismic reflection profiling. Geology 20, 807-811.

Naldrett, A.J., Bray, J.G., Gasparrini, E L., Podolsky, T., Rucklidge, J C., 1970. Cryptic Variation and the Petrology of the Sudbury Nickel Irruptive. Economic Geology and the Bulletin of the

Society of Economic Geologists 65, 122-274.

Naldrett, A.J., Hewins, R.H., 1984. The Main Mass of the Sudbury Igneous Complex. *In*: Pye, E.G., Naldrett, A.J., Giblin, P.E. (Eds.), The Geology and Ore Deposits of the Sudbury Structure. Special Publication 1. Ontario Geological Survey, Toronto, 235-252.

Pennacchioni, G., 2005. Control of the geometry of precursor brittle structures on the type of ductile shear zone in the Adamello tonalites, Southern Alps (Italy). Journal of Structural Geology 27, 627-644.

Peredery, W.V., Morrison, G.G., 1984. Discussion of the Origin of the Sudbury Structure. *In*: Pye, E.G., Naldrett, A.J., Giblin, P.E. (Eds.), The Geology and Ore Deposits of the Sudbury Structure. Special Publication 1, Ontario Geological Survey, Toronto, 491-511.

Piercey, P., Schneider, D.A., Holm, D.K., 2007. Geochronology of Proterozoic metamorphism in the deformed Southern Province, northern Lake Huron region, Canada. Precambrian Research 157, 127-143.

Pye, E.G., Naldrett, A.J., Giblin, P.E. (Eds.), 1984. The Geology and Ore Deposits of the Sudbury Structure. Ontario Geological Survey, Special Volume 1, Toronto.

Riller, U., Schwerdtner, W., 1997. Mid-crustal deformation at the southern flank of the Sudbury Basin, central Ontario, Canada. Geological Society of America Bulletin 109, 841-854.

Riller, U., Schwerdtner, W. M., Robin, P.-Y. F., 1998. Low-temperature deformation mechanisms at a lithotectonic interface near the Sudbury Basin, Eastern Penokean Orogen, Canada. Tectonophysics 287, 59-75.

Riller, U., Schwerdtner, W., Halls, H., Card, K., 1999. Transpressive tectonism in the eastern Penokean orogen, Canada. Consequences for Proterozoic crustal kinematics and continental fragmentation. Precambrian Research 93, 51-70.

Riller, U., 2005. Structural characteristics of the Sudbury Impact Structure, Canada: impact-induced and orogenic deformation – a review. Meteoritics and Planetary Science 40, 1723-1740.

Riller, U., Boutelier, D., Schrank, C., Cruden, A.R., 2010. Role of kilometer-scale weak circular heterogeneities on upper crustal deformation patterns: evidence from scaled analogue modeling and the Sudbury Basin, Canada. Earth and Planetary Science Letters 297, 587-597.

Rousell, D.H., 1975. Origin of foliation and lineation in Onaping Formation and deformation of Sudbury Basin. Canadian Journal of Earth Sciences 12, 1379-1395.

Rousell, D.H., 1984. Structural Geology of the Sudbury Basin. *In*: Pye, E.G., Naldrett, A.J., Giblin, P.E. (Eds.), The Geology and Ore Deposits of the Sudbury Structure. Special Publication 1, Ontario Geological Survey, Toronto, 83-95.

Segall, P., Simpson, C., 1968. Nucleation of ductile shear zones on dilatant fractures. Geology 14, 56-59.

Shanks, W.S., Schwerdtner, W.M., 1991. Structural analysis of the central and southwestern Sudbury Structure, Southern Province, Canadian Shield. Canadian Journal of Earth Sciences 28, 411-430.

Spray, J.G., Butler, H.R., Thompson, L.M, 2004. Tectonic influences on the morphometry of the Sudbury impact structure: Implications for terrestrial cratering and modeling. Meteoritics and Planetary Science 39, 287-301.

Spang, J.H., 1972. Numerical method for dynamic analysis of calcite twin lamellae. Geological Society of America Bulletin 83, 467-471.

Thomson, M.L., R.L. Barnett, Fleet, M.E., Kerrich, R., 1985. Metamorphic assemblages in the South-Range Norite and the footwall mafic rocks near the Kirkwood Mine, Sudbury, Ontario. The Canadian Mineralogist 23, 173-186.

Tourigny, G., Tremblay, A., 1997. Origin and incremental evolution of brittle/ductile shear zones in granitic rocks: natural examples from the southern Abitibi Belt, Canada. Journal of Structural Geology 19, 15-27.

Watts, M., Williams, G.D., 1979. Fault rocks as indicators of progressive shear deformation in Guingamp region, Brittany. Journal of Structural Geology 1, 323-332.

Wu, J.J., Milkereit, B., Boerner, D., 1994. Timing constraints on deformation history of the Sudbury Impact Structure. Canadian Journal of Earth Sciences 31, 1654-1660.

4.   Effect of the SIC on the deformation geometry of its host rocks

4.1.   Introduction

Superimposed structures in deformed terranes are often attributed to distinct tectono-metamorphic events (e.g., Turner and Weiss, 1963). Specifically, different orientations and styles of tectono-metamorphic structures, notably planar mineral fabrics, shear zones and folds, are commonly attributed to distinct deformation phases (e.g., Cosgrove, 1980; Platt and Lister, 1985; Rosenbaum et al., 2002; Xypolias et al., 2003; Sayab, 2006; Forster and Lister, 2008). Unless precise ages of the structures are determined, their relative age is based on cross-cutting relationships or correlation of fabric orientation with regional shortening directions. However, the effects of mechanical heterogeneities on the spatial distribution and geometry of structures is often underestimated in structural interpretations (Tobisch and Paterson, 1988; Burg, 1999). In this chapter, I document the generation of centimetre- to kilometre-scale planar structures that differ in orientation and style, but can be explained by a single deformation regime that predates and postdates meteorite impact in the Sudbury area and which shaped the Sudbury Basin (Fig. 4.1).

Due to their geometry and mechanical properties particularly with respect to sedimentary host rocks, spherical and sheet-like igneous intrusions can profoundly influence the orientation of strain fabrics in the host rocks during post-emplacement deformation (e.g., Brun and Pons, 1981; Schofield and D'Lemos, 1998; Wilson and Grocott, 1999; Vigneresse et al., 1999; Chen et al., 2001). In particular, the orientations of metamorphic foliation surfaces near the margins of igneous sheets are influenced by contact strain effects and, thus, cannot readily be used as indicators of regional strain or kinematics of deformation (Burg, 1987; Wilson and Grocott, 1999). Similarly, distortion of mechanically less competent circular heterogeneities, such as collapse calderas (Holohan et al., 2005; Bosworth et al., 2003), impact craters (Pappalardo and Collins, 2005; Kenkmann et al., 2008; Riller et al., 2010) and sedimentary basins (Betts, 1999; Panien et al., 2006) can produce strain fabric geometries that deviate from those formed in mechanically homogeneous rock masses under uniform regional shortening.

Strain fabrics within metavolcanic and metasedimentary rocks of the Paleoproterozoic Huronian Supergroup, located in the periphery of the non-cylindrical Sudbury Basin (Fig. 4.1a), offer insights into the geometric variability of structures that formed under regional NW-SE shortening. The Sudbury Basin is defined by the Main Mass of the 1.85 Ga Sudbury Igneous Complex (SIC), the relic of a deformed impact melt sheet, impact-melt breccia of the Onaping Formation, and post-impact sedimentary rocks (Brocoum and Dalziel, 1974; Rousell et al., 1997). The style of deformation of the SIC and its wall rocks is not fully understood but is paramount for exploration of Cu-Ni- and related ore deposits of this world-class mining camp and unravelling orogenic events at the southern margin of the Archean Superior Province. Strain fabrics in the Sudbury area have been attributed to the (1) 2.4 to 2.2 Ga Blezardian orogenic event (Rousell et al., 1997; Riller and Schwerdtner, 1997; Riller et al., 1999), (2) deformation apparently active during crater formation and cooling of the SIC (Ivanov and Deutsch, 1999; Peredery and Morrison, 1984; Riller, 2005; Klimczak et al., 2007) and (3) deformation significantly post-dating the formation of the SIC (Card et al., 1984; Wu et al., 1994; Riller et al.,

1998). Due to the paucity of radiometric studies, it has not yet been possible to unequivocally discern individual orogenic events in terms of fabric development in the Sudbury area.

By analyzing the structure of the southern SIC and its wall rocks, this section of my study aims to elucidate the mechanical and kinematic response of an igneous sheet and its Paleoproterozoic supracrustal wall rocks to uniform regional shortening. In particular, my field data documents local perturbations of strain fabrics, notably NW-SE trending fold hinges and metamorphic foliations in wall rocks, which appear to be incompatible with regional NW-SE shortening. I provide a comprehensive interpretation of all fabric types in terms of the progressive shape change of the SIC. Specifically, my study addresses the structure of Huronian rocks at the southern flank of the Sudbury Basin and the variation of fabric orientations in relation to lithological contacts. Using impact melt breccias in Huronian rocks as a time marker, I am able to distinguish between fabrics formed prior to and after the impact event and determine the local shortening directions under which the fabrics formed. My analysis also shows that the presence of the SIC led to local perturbation of far-field stresses and, thus, significantly influenced the deformation kinematics of the Huronian rocks. This resulted in variable orientations of structures that can be explained by protracted deformation under a uniform deformation regime, but would traditionally be explained in terms of distinct deformation events.

Figure 4.1 (following page): Geological and structural overview of the Sudbury Basin. (a) Simplified structural map showing the Sudbury Basin and its Archean and Paleoproterozoic host rocks. Foliation trajectories and fold axes are from Riller (2005), dip angles of the SIC basal and upper contacts are from Rousell (1975) and Dreuse et al. (2010). Sections across the South Range of the Sudbury Basin illustrate the variation in dip of lithological contacts, metamorphic foliation and fold structure in the Huronian rocks. Stratigraphy of Huronian rocks is after Young et al. (2001). The v-signature indicates volcanic rocks, grey shades in increasing lightness indicate mud-, silt- and sandstone, and circular pattern denotes conglomerate. (b) Orientation of higher-order, brittle-ductile shear zones of prominent deformation zones, i.e., Whitewater Lake Fault Zone (WFZ), Mont Rouleau Shear Zone (MRSZ), Thayer Lindsley Shear Zone (TLSZ), Whitson Lake Shear Zone (WLSZ), Garson Fault (GF) and Falconbridge Fault (FF) in the southern Sudbury area. Diagrams are lower-hemisphere equal-area projections showing brittle-ductile shear zones (great circles) and respective striations (arrows). Arrows on great circles indicate sense of hanging wall displacement.
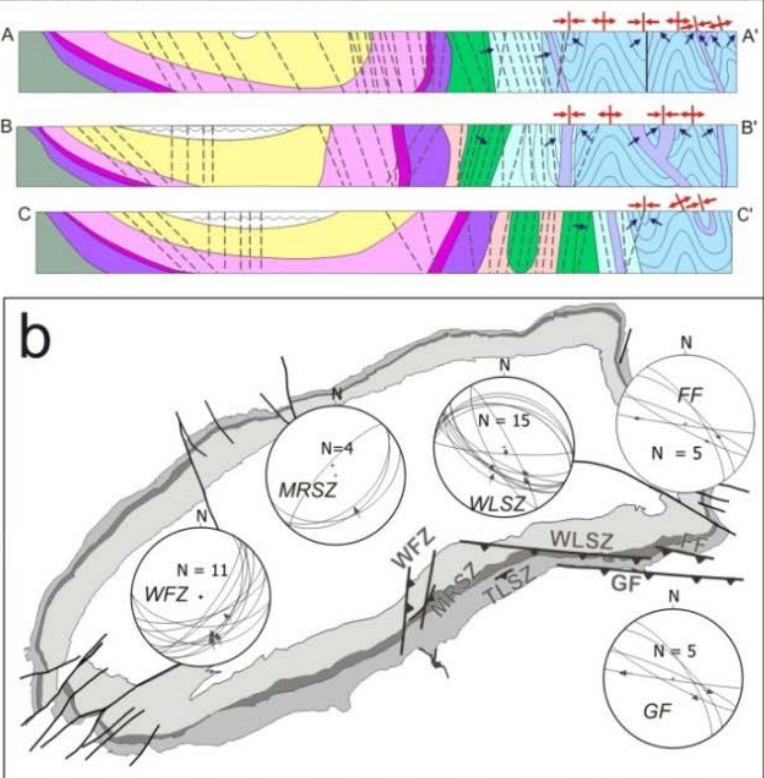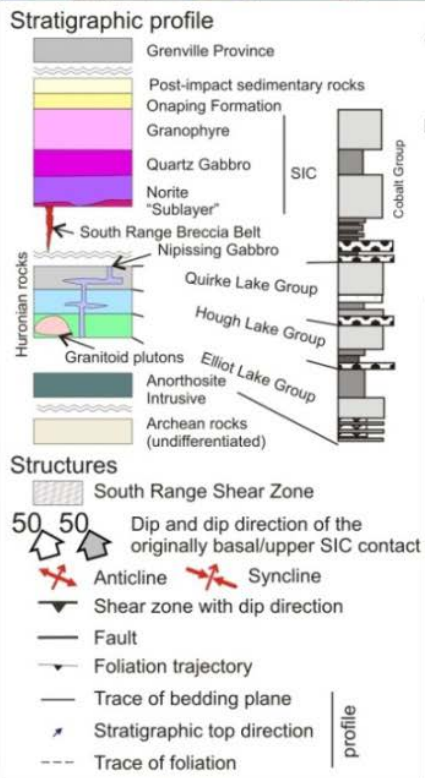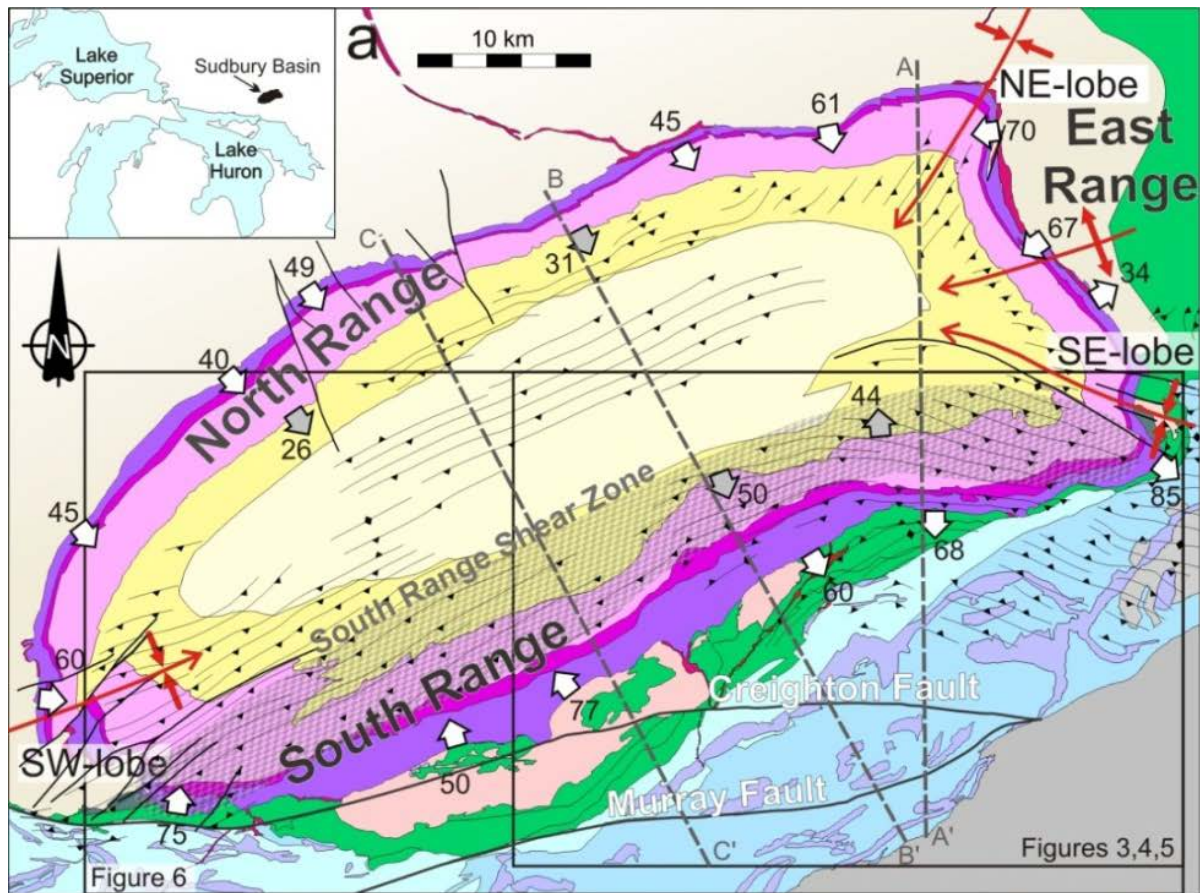
4.2.   Geological Setting

The Sudbury Basin straddles granitoid and gneissic rocks of the Archean Superior Province in the north and metavolcanic and metasedimentary rocks of the Paleoproterozoic Huronian Supergroup in the south (Fig. 4.1a). The Basin comprises the Sudbury Igneous Complex (SIC), impact melt-breccia of the Onaping Formation (Grieve et al., 2010), and pelagic sedimentary rocks of the Onwatin and Chelmsford Formations (Rousell, 1984a). The SIC is the relic of a 1.85 Ga impact melt sheet (Krogh et al., 1984) that differentiated into the Norite, Quartz Gabbro and Granophyre layers. The Sudbury Basin contains three higher-order synclines, the NE-lobe, the SE-lobe and the western fold closure (Fig. 4.1a). These synclines divide the SIC into weakly curved segments that are topographically elevated and known as the North Range, the East Range and the South Range (Fig. 4.1a). In the North Range, the SIC dips moderately south, i.e., toward the Basin centre, whereas in the South Range it dips steeply northwards or is overturned (Fig. 4.1a).

The Huronian Supergroup is made up of metasedimentary and metavolcanic rocks deposited unconformably onto the Archean craton between 2.45-2.22 Ga (Bennett et al., 1991). In the Sudbury region, the Supergroup is up to 10.5 km thick (Brocoum and Dalziel, 1974) and consists, from oldest to youngest, of four Groups: Elliot Lake, Hough Lake, Quirke Lake and Cobalt (Fig. 4.1a). The Elliot Lake Group comprises chiefly metabasalt flows of the Elsie Mountain and Stobie Formations, rhyolitic pyroclastic flows of the Copper Cliff Formation, arkose of the Matinenda Formation and wacke of the McKim Formation (Card, 1978; Card et al., 1984; Johns, 1996). The three younger Groups are each made up of a basal conglomerate overlain by mudstone, siltstone or carbonate, and capped by sandstone (Card et al., 1984). The Elsie Mountain and Stobie Formations are intruded by the granitoid Murray pluton dated at 2.48 (Krogh et al., 1984) and 2.38 Ga (Krogh et al., 1996) and the Creighton pluton dated at 2.33 Ga (Frarey et al., 1982) and 2.42 Ga (Smith and Heaman, 1999). Dikes and sills of the 2.2 Ga Nipissing suite (Corfu and Andrews, 1986; Buchan et al., 1989; Lightfoot et al., 1993) intrude all rock units of the Huronian Supergroup.

4.3.   Deformation and metamorphism in the Sudbury area

Paleoproterozoic rocks in the Sudbury area were metamorphosed under conditions reaching lower amphibolite facies (Card et al., 1972; Card, 1978; Easton, 2000). Peak metamorphic temperatures in rocks of the Huronian Supergroup in the Sudbury area decrease toward the southeast with the highest metamorphic grade preserved near the Murray and Creighton plutons (Dutch, 1979; Riller and Schwerdtner, 1997). Metamorphism and deformation of the Huronian Supergroup has been attributed to the ca. 2.45 to 2.22 Ga Blezardian Orogeny (Riller and Schwerdtner, 1997; Riller et al., 1999), the ca. 1.87 to 1.83 Ga Penokean Orogeny (Brocoum and Dalziel, 1974; Van Schmus, 1976; Riller, 2005; Klimczak et al., 2007), the ca. 1.7 to 1.6 Ga Mazatzal Orogeny (Bailey et al., 2004; Piercey et al., 2007) and the ca. 1.2 to 1 Ga Grenville Orogeny (Brocoum and Dalziel, 1974; Tschirhart and Morris, 2012). Except for the Mazatzal Orogeny, Proterozoic deformation pulses in the Sudbury area have not been dated radiometrically. The approximate duration and deformational effects of the orogenic events are chiefly based on structural relationships between dated igneous rocks and respective host rocks.

Apparently, all Paleoproterozoic deformation events contributed to the formation of the prominent NE-SW trending structural grain in the Sudbury area, evident mostly by inclined metamorphic foliation surfaces and fold-axial traces in pre-impact, impact-related and post-impact rocks (Card and Pattison, 1973; Brocoum and Dalziel, 1974; Rousell, 1975, 1984a). Thus, the structural characteristics of individual orogenic events in terms of mineral fabric geometry are not well constrained at Sudbury.

The meteorite impact had profound structural and thermal effects on the Archean and Paleoproterozoic rocks in the Sudbury area. Such effects include the formation of impact-melt breccias, notably the so-called Sudbury Breccia (Rousell et al., 2003), planar deformation features in quartz, shatter cones (Dressler, 1984a), shock-induced melting of rocks (Grieve et al., 1991; Ivanov, 2005) and tilting of Huronian strata (Riller, 2005). Planar deformation features in quartz and shatter cones have been documented to be present up to 10 km from the basal SIC contact in the North Range (Grieve and Therriault, 2000). Based on scaling of equivalent phenomena from other large terrestrial impact structures, the spatial extent of impact-induced shape change of Archean and Proterozoic rocks may extend 150 to 200 km from the Basin centre (Grieve et al., 2008).

The Sudbury Breccia is a heterolithic impact-melt breccia that forms irregular dike-like bodies in rocks close to the SIC (Peredery and Morrison, 1984; Dressler 1984a; Rousell et al., 2003). Breccia bodies decrease in size and occurrence with increasing distance from the SIC (Speers, 1957). The largest breccia body, the South Range Breccia Belt, is approximately 11 km long and strikes parallel to lithological boundaries of the Elliot Lake Group (Fig. 4.1a). Sudbury Breccia is generally composed of rounded and angular host rock fragments set in a dark aphanitic matrix (Speers, 1957; Fig. 4.2d). The matrix is described as originally glassy and devitrified (Dressler, 1984a). Formation of Breccia bodies has been attributed to shock loading (Lafrance et al., 2008; Lafrance and Kamber, 2010), decompression following shock loading (Rousell et al., 2003), friction-induced comminution (Scott and Spray, 2000) or drainage of impact melt into crater floor fractures (Riller et al., 2010). Regardless of its proposed origin, all authors agree that Sudbury Breccia bodies formed during cratering and, thus, constitute a time marker with respect to deformation preceding and postdating the impact event.

Post-impact deformation is evident in impact-induced rocks, notably the SIC and Sudbury Breccia bodies, and post-impact sedimentary rocks of the Sudbury Basin. Deformation of the SIC was mainly achieved by folding (Morris 1980, 1984; Cowan and Schwerdtner, 1994) and northwest-directed thrusting of the South Range on the South Range Shear Zone (Shanks and Schwerdtner, 1991; Milkereit et al., 1992). Both deformation mechanisms are portrayed by the orientation of metamorphic foliations in the SIC and the Onaping Formation as well as disjunctive cleavage and fold axes in the Onwatin Formation and the Chelmsford Formation (Rousell, 1975). Overall, the foliations strike NE-SW, formed under lower greenschist-facies metamorphism and are most pronounced in the South Range Shear Zone (Fig. 4.1a). Here, foliations dip moderately to steeply to the southwest and strike parallel to the long axis of the Sudbury Basin. Toward the east, the foliations diverge and are axial-planar to the NE-lobe, the SE-lobe and the anticline between the two lobes (Fig. 4.1a). The steeply north-dipping and locally overturned basal contact of the SIC in the South Range (Fig. 4.1a) indicates that the South Range is more strongly deformed than the moderately south-dipping SIC under the North

Range (Fig. 4.1a). This is corroborated by the pervasive presence of metamorphic foliations in the South Range SIC (Lenauer and Riller, 2012) compared to the North Range.

Strain fabrics in Sudbury Breccia bodies were recognized by Speers (1957) who noted that the breccia matrix is sporadically characterized by a metamorphic foliation that strikes overall NE-SW. Metamorphism in the breccia matrix is evident by poikilitic and porphyroblastic oligoclase, biotite and scapolite (Speers, 1957; Scott and Spray, 2000). Thompson and Spray (1996) attribute crystals overgrowing the matrix minerals and clasts to retrograde greenschist- and sub-greenschist-facies metamorphism during post-impact tectonothermal events. Similarly, Szabo et al. (2006) concluded that the metamorphic mineral assemblage of Sudbury Breccia in the South Range and the North Range indicates low to middle greenschist facies metamorphic conditions. Therefore, the formation of post-impact structures did not exceed middle greenschist-facies metamorphic conditions. Based on magnetic fabric analysis, Scott and Spray (1999) recorded subvertical magnetic foliations and lineations in the South Range Breccia Belt that are concordant to the NE-SW striking margins of this Breccia Belt and to the visible metamorphic mineral fabrics in the Sudbury Breccia matrix.

Besides pervasive strain fabrics, the South Range SIC and the adjacent Huronian rocks host a number of prominent faults and shear zones (Fig. 4.1). These are the Murray, Creighton and Garson Faults in Huronian rocks and the Falconbridge Fault, the Whitewater Lake Fault Zone, the Mont Rouleau Shear Zone, the Thayer Lindsley Shear Zone and Whitson Lake Shear Zone in the SIC (Fig. 4.1). The location of these fault zones are delimited by an increase in strain intensity, recognized by the spacing of individual shear faults. The kinematics of the deformation zones is evident from strike separations of lithological contacts, shear planes and striations, as well as the geometry and the increase in strain intensity of associated brittle-ductile, higher-order shear zones (Fig. 4.1b).

The E-W to ENE-WSW striking Murray and Creighton Faults (Fig. 4.1a) have a protracted history of activity that started with deposition of Huronian sediments (Card et al., 1972; Card, 1978). After meteorite impact the faults were mostly active as dextral strike-slip faults (Dressler, 1984b; Riller et al., 1999). Similarly, the Garson Fault shows dextral strike separations of Huronian lithological contacts (Ames et al., 2005), but has recently been identified as a steeply south-dipping reverse fault (Mukwakwami et al., 2012). The Whitson Lake Shear Zone, located just north of the Garson Fault, is evident by km-scale discontinuities and curvature of foliation surfaces in map view (Ames et al., 2005). The shear zone dips steeply SSW and, like other E-W striking deformation zones in this area, shows components of reverse and dextral sense-of-shear (Santimano and Riller, 2012; Fig. 4.1b). The Falconbridge Fault on the other hand has been described as an oblique sinistral reverse fault that dips steeply N at surface and steeply S at depth (Rousell, 1984b).

The Whitewater Lake Fault Zone, occupying the central South Range SIC, is a fairly wide N-S striking, brittle-ductile shear zone that displays cm- to dm-scale anastomosing foliation surfaces and accomplished bulk horizontal shortening (Lenauer and Riller, 2012). Its conjugate character with respect to the E-W striking dextral deformation zones is corroborated by sinistral strike separations of SIC layer contacts and SE-dipping, higher-order reverse faults that are oblique to the strike of the fault (Fig. 4.1b). The orientations of striations on the Whitewater Lake Fault

Zone indicate oblique reverse top-to-N sense-of-shear (Fig. 4.1b). The Mont Rouleau Shear Zone (Shanks and Schwerdtner, 1991) and the Thayer Lindsley Shear Zone (Bailey et al., 2004) are located between the Whitewater Lake Fault Zone and the E-W striking deformation zones. These shear zones dip moderately to the SE and show asymmetric mineral fabrics indicating reverse sense-of-shear (Fig. 4.1b). In summary, all deformation zones accomplished bulk NW-SE shortening.
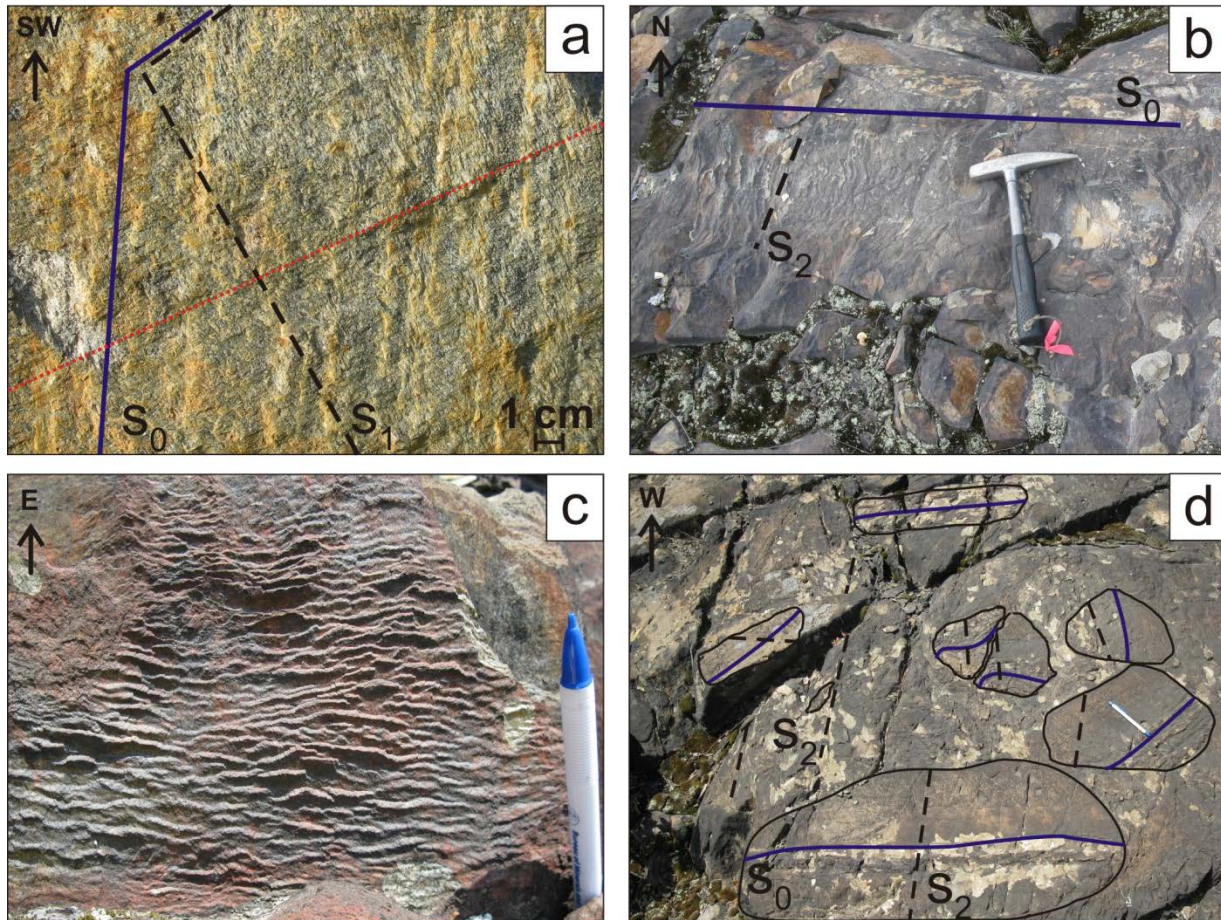
Figure 4.2: Outcrop images of structures in Huronian rocks of the study area. (a) Metamorphic foliation (s_1) and bedding (s_0) in meta-siltstone of the Elliot Lake Formation. Stippled line indicates striation on a brittle fault plane. (b) Localized cleavage (s_2) confined to a meta-siltstone layer at high angle to bedding plane (s_0). (c) Crenulation cleavage in meta-siltstone. (d) Sudbury Breccia with rotated fragments evident by the variation of bedding planes (s_0), overprinted by metamorphic foliation (s_2) in both matrix and fragments.

4.4.   Results

Structural data from the South Range SIC and adjacent Huronian rocks was collected in the field and compiled from published studies. In order to distinguish between post-impact deformation and earlier tectonic events, I compare the geometry of structures in Huronian rocks with that in the SIC and Sudbury Breccia bodies. Specifically, the orientation of bedding planes and stratigraphic top directions were used to constrain deformation by folding on the km-scale in Huronian strata. This data was complemented by orientation measurements of mesoscopic fold-axial planes, fold hinges, metamorphic foliations and brittle-ductile shear zones to identify the spatial variation in local shortening directions and increments of deformation. Analysis of brittle shear faults in the SIC and Huronian rocks and the orientation of metamorphic foliations in Sudbury Breccia bodies allowed me further to constrain post-impact deformation kinematics in Huronian rocks.

4.4.1. Folds in Huronian strata

Orientations of kilometre-scale folds in Huronian strata were inferred from bedding plane orientations at a total of 737 stations. In addition, bedding plane orientations at 350 and 218 stations were compiled respectively from Riller et al. (1999) and from Dressler (1984b) and Cowan (1996). Hand-drawn strike trajectories of inclined bedding planes for Huronian strata were constructed to facilitate visualization and analysis of this data set (Fig. 4.3a). Overall, Huronian strata dip steeply southeast, but in places they dip toward the northwest (Fig. 4.3a, b).

Sedimentary structures, such as dewatering structures, cross-bedding and conglomerate-filled erosion channels, were used to identify the stratigraphic top direction in meta-sandstone and meta-siltstone. In addition to bedding plane trajectories, top directions were used to constrain the location and attitude of km-scale folds in Huronian rocks (Fig. 4.3a). Stratigraphic top directions in meta-sandstone of the Elliot Lake Group indicate that these strata are mostly overturned toward the south (Fig. 4.3a). The folds in this Group are characterized by NNW- and SSE-plunging axes (Fig. 4.3d), which are most pronounced east of the Murray pluton, i.e., where the SIC is curved in map view (Fig. 4.3a). Rocks of the Hough Lake Group show a greater variation in the orientation of bedding planes and stratigraphic top directions. Sandstone strata of this Group form doubly-plunging anti- and synclines (Fig. 4.3a), the fold axes of which trend NE-SW (Figs. 4.1, 4.3a, e).

Folds of bedding planes on the centimetre- to metre scale were observed throughout the Huronian rocks, but are most evident by meta-siltstone laminations in the Elliot Lake Group. The interlimb angles of these folds range from 30° to 120°. Fold axes are commonly subvertical and fold-axial planes dip steeply to the NW or E (Fig. 4.3c), although poles to fold-axial planes show variable orientations. Cluster analysis of fold-axial plane orientations indicates the presence of two crudely defined maxima, one indicating steeply NW-dipping and the other steeply E-dipping planes (Fig. 4.3c). The orientations of fold-axial planes of small-scale folds match with the traces of kilometre-scale fold-axial planes.
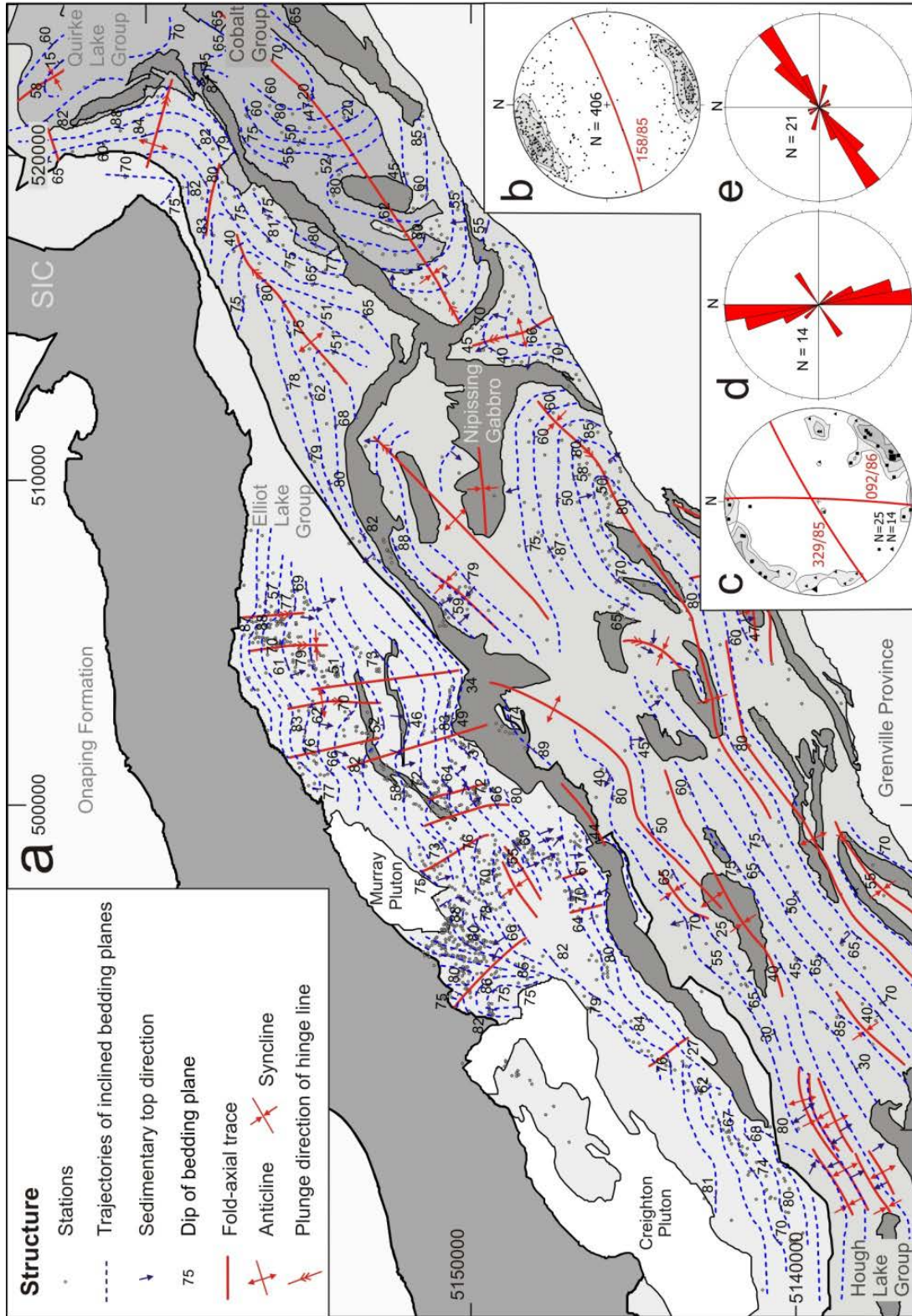
Figure 4.3: Structure of Huronian strata south of the SIC. (a) Map showing trajectories of inclined bedding planes, sedimentary top directions and traces of km-scale folds. (b) Lower-hemisphere, equal-area projection showing poles to bedding planes. The orientation of the mean bedding plane is indicated by a great circle. Coordinates are given in UTM NAD27 Zone 17N. (b) Lower-hemisphere, equal-area projection showing poles to bedding planes. The orientation of the mean bedding plane is indicated by a great circle. Contours are at 2, 3 and 5%. (c) Lower-hemisphere, equal-area projection of poles to fold-axial planes of small-scale folds of bedding planes. Triangles and squares indicate two clusters, derived by using a k-means algorithm via Fisher distribution. Great circles indicate mean fold-axial planes. (d) Rose diagram showing trends of fold-axial traces in the Elliot Lake Group at 10° intervals. (e) Rose diagram showing trends of fold-axial traces in the Hough Lake and Quirke Lake Groups at 10° intervals.

4.4.2. Metamorphic shape fabrics

The orientation of planar metamorphic mineral fabrics, i.e., foliation planes, was examined in the South Range SIC and adjacent Huronian rocks at a total of 2734 stations. New data was acquired at 955 stations from the Elliot Lake Group and Hough Lake Group. These measurements were complemented by data from Dressler (1984b), Riller et al. (1999) and Cowan et al. (1999). Foliation is not well developed in the Nipissing Gabbro and quartzite of the Hough Lake Group (Fig. 4.4a). Trajectories of mineral shape fabrics in granitoid rocks of the Murray and Creighton Plutons pertain mostly to magma strain during pluton emplacement (Riller and Schwerdtner, 1997) and, thus, are not discussed herein.

In Huronian rocks, two distinctly oriented sets of planar structures are evident, in places in the same outcrop. The first set, Set 1, consists of steeply NW-dipping structures (Fig. 4.4b) that are at low angles to bedding planes (Fig. 4.2a). Specifically, the planar structures are defined by the shape-preferred orientations of primary markers, such as elongate amygdules and conglomerate clasts, planar mineral fabrics characterized by biotite and amphibole, and brittle-ductile, chloritic shear zones. The second set of planar structures, Set 2, is defined by steeply NE- and SW-dipping, tightly spaced cleavage planes and micaceous foliation planes (Figs. 4.2c, 4.4c), which formed at high angles to bedding planes (Fig. 4.2b). As a result, hand-drawn strike trajectories of inclined planar structures in Huronian rocks consist of two sets (Fig. 4.4a). One set of trajectories strikes NE-SW and is mostly present in the Elliot Lake Group. The second set strikes NW-SE and is developed in the Elliot Lake, the Hough Lake and the Quirke Lake Groups (Fig. 4.4a).

Set 1 trajectories in the Huronian rocks are overall parallel to, and mimic the curvature of, the contact with the SIC (Fig. 4.4a). However, trajectories undulate on the hundred metre- to kilometre-scale in the Elliot Lake Group between the Murray and Creighton plutons and east of the Murray pluton (Fig. 4.4a). Foliation trajectories in the South Range SIC, notably in the South Range Shear Zone, are also variable in strike. Here, foliation trajectories curve from a NE-strike in the South Range into a WNW-strike in the SE-lobe (Fig. 4.4a). South of the South Range Shear Zone, foliations in the SIC are less pervasive and characterized by a conjugate set of SE- and NW-dipping planes (Fig. 4.4e). Set 1 structures are well apparent and ubiquitous in the Elliot Lake Group, decrease in abundance toward the SE and occur only sporadically in the Hough Lake Group (Fig. 4.4a).

Set 2 trajectories of planar structures in the Elliot Lake Group are perpendicular to the map-view trace of the basal SIC contact. Specifically, south of the Creighton pluton and the Murray pluton Set 2 trajectories trend NW, but trend N-S east of the Murray Pluton, i.e., where the basal SIC contact is curved in map view (Fig. 4.4a). Interestingly, Set 2 planar structures are axial-planar to map-scale open anticlines in strata of the Elliot Lake Group (Figs. 4.3a, 4.4a). East of the Murray pluton, Set 2 trajectories and fold-axial planes in the Elliot Lake Group diverge towards the contact with the SIC. Away from the contact of the Murray pluton with rocks of the Elliot Lake Group, trajectories in rocks of the Hough Lake and Quirke Lake Groups strike uniformly NW. Set 2 structures are ubiquitous in the Hough Lake Group, where they often are the only metamorphic shape fabric preserved in the rocks.

The occurrence of crenulation cleavage in Huronian rocks was first mentioned by Brocoum and Dalziel (1974), who did, however, not specify the location and orientation of these fabrics. We found that crenulation cleavage is well apparent in meta-siltstone of the Elliot Lake Group southeast of the Murray pluton. Here, this fabric is defined by symmetric microfolds of mica-rich foliation planes (Fig. 4.2c). Crenulation cleavage planes dip steeply toward the east and west and are orthogonal to crenulated foliation planes. It is important to note that crenulation cleavage and crenulated foliation surfaces seen in outcrop have the same orientation as Set 2 and Set 1 planar structures, respectively, on the map scale (Fig. 4.4b, c). Consequently, Set 2 structures overprint and, thus, postdate Set 1 structures.
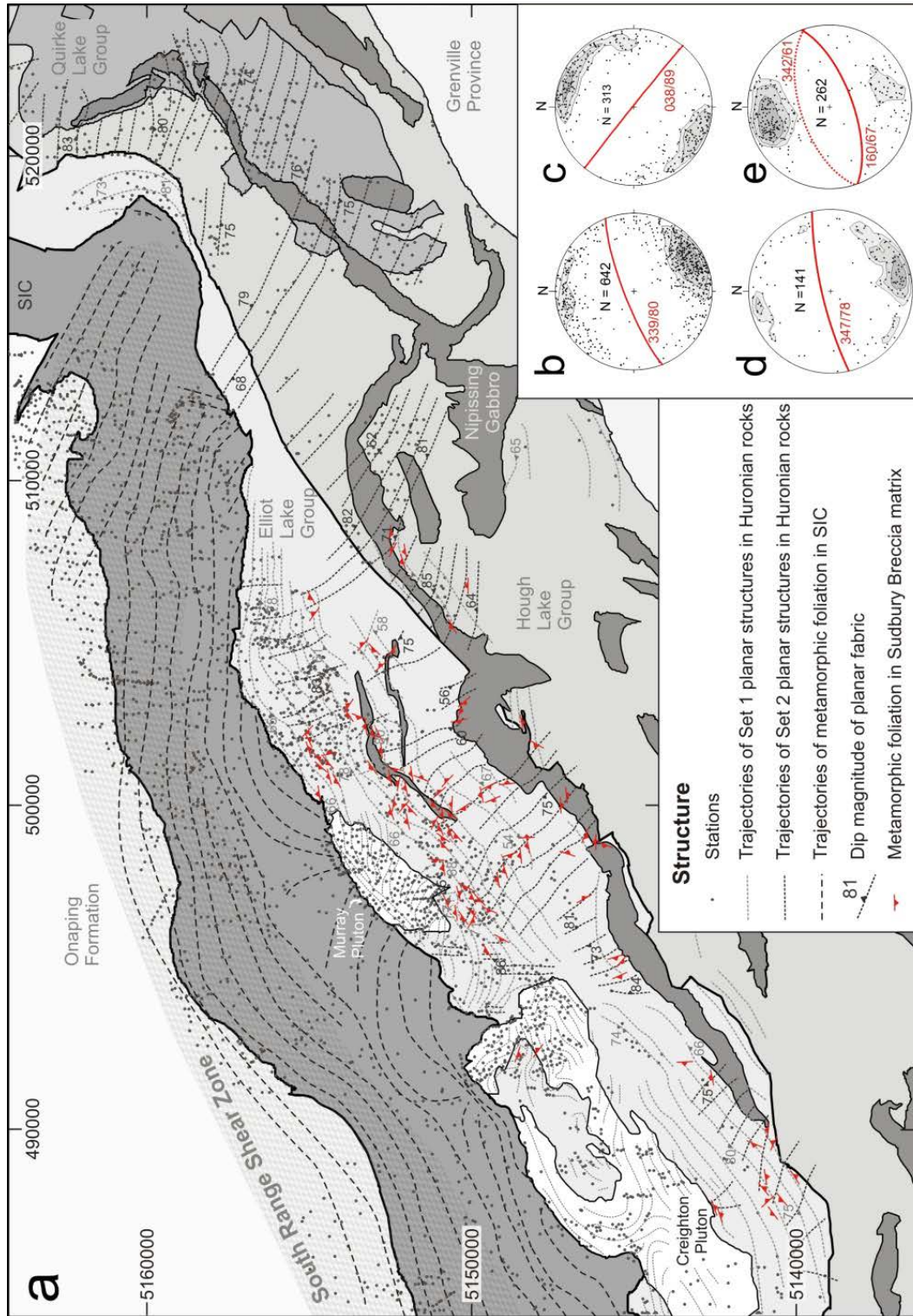
Figure 4.4: Orientation of planar structures in the Huronian rocks and the South Range SIC. (a) Trajectories of inclined planar structures in Huronian rocks and Sudbury Breccia matrix. Trajectories are drawn from new data, and data compiled from Riller and Schwerdtner (1997), Riller et al. (1998), Cowan and Schwerdtner (1994) and Dressler (1984b). Coordinates are given in UTM NAD 27 Zone 17N. (b) Lower-hemisphere, equal-area projection showing poles to Set 1 planar structures in Huronian rocks. (c) Lower-hemisphere, equal area projection of poles to Set 2 planar structures in Huronian rocks. (d) Lower-hemisphere, equal area projection of poles to metamorphic foliation in Sudbury Breccia matrix. (e) Lower-hemisphere, equal area projection of poles to metamorphic foliation in SIC. Great circles in (b)-(e) indicate mean orientations of planar structures.

4.4.3. Structures in Sudbury Breccia bodies

To better understand post-impact deformation, I studied the structure of Sudbury Breccia bodies at 56 locations (Fig. 4.5a). The analysis includes the orientations of bedding planes and metamorphic foliations in fragments, matrix and host rock of breccia bodies. Breccia fragments are mechanically more competent than the matrix. This is evident by foliations, which are more pronounced in the matrix than in fragments and by contact strain in the matrix at fragment margins. The intensity of metamorphic fabric development, evident by the spacing of foliation surfaces, varies on the metre-scale and depends on the distance to breccia fragments and host rock type. To avoid recording contact strain effects fabric orientations were measured at a distance of at least 10 cm from fragment boundaries on outcrop surfaces.

Metamorphic foliation characteristics in breccia fragments are identical to those observed in the host rocks. These include the shape-preferred orientation of primary markers, tightly spaced cleavage planes as well as biotite and amphibole mineral fabrics in metavolcanic rocks and muscovite mineral fabrics in meta-sandstone. Foliations in the breccia matrix are defined by chlorite and mica. Foliations in the breccia matrix of the Elliot Lake Group dip steeply to the NE and SW (Fig. 4.5b) and are locally concordant to planar fabrics in the host rock (Fig. 4.4a). Significant deviations from these orientations are observed in breccia matrices at lithological contacts, especially with Nipissing Gabbro bodies (Fig. 4.4a), and in the South Range Breccia Belt (Fig. 4.5a), in which foliations dip steeply toward the NW (Fig. 4.5c).

Two distinct geometric relationships between foliations and bedding planes in breccia fragments are recognized. One such relationship (Fig. 4.5d) is characterized by small angles between bedding planes (Fig. 4.5f) and foliations (Fig. 4.5g) in each breccia fragment. These angles are rather similar to equivalent ones in the host rock (Fig. 4.5h). Evidently, the angular relationship between foliations and bedding planes in the fragments was preserved during rotation of the respective fragments and indicates that the foliations predate brecciation. The other foliation-bedding relationship in breccia fragments (Fig. 4.5e) is characterized by random fragment orientation seen by the large variation in bedding planes in the fragments, but rather uniform orientation of foliations (Fig. 4.5j). This amounts to large angular variations between bedding and the foliations (Fig. 4.5k). This relationship denotes breccia bodies in which foliation development post-dates brecciation. Thus, Sudbury Breccia fragments record pre-brecciation and post-brecciation foliations.

The spatial distribution of the two foliation-bedding relationships is non-systematic and both variants are observed in breccia bodies regardless of host rock types. However, stations at which foliations overprint brecciation are more common (31 out of 56 stations) than stations at which brecciation overprints foliations (7 out of 56 stations). Except for the South Range Breccia Belt, the foliations overprinting Sudbury Breccia dip steeply toward the SSW and NE (Fig. 4.5a, b). These foliations correspond geometrically to Set 2 structures described in the previous section. Steeply NNW-dipping foliations, which form small angles to bedding planes, are concordant to Set 1 structures. As these foliations are mostly overprinted by breccia, Set 1 structures formed largely prior to brecciation. Set 1 structures are, however, also found in the breccia matrix, especially in the South Range Breccia Belt and were, thus, formed to some extent also after

brecciation. In summary, Set 1 structures formed prior and to some extent after brecciation, but Set 2 structures formed exclusively after brecciation.

Figure 4.5 (following page): Metamorphic foliations in Sudbury Breccia fragments and matrix. (a) Map showing distribution of two distinct geometric fabric relationships in Sudbury Breccia bodies. Orientations of foliations in breccia fragments are only shown from locations where these fabrics overprint the breccia. Location of Sudbury Breccia occurrences (cross-hatched areas) and South Range Breccia Belt (red cross-hatched area) are from Ames et al. (2005). N indicates the number of fragments used to determine breccia type. (b) Lower hemisphere, equal-area projection showing poles to foliations and respective plane of mean orientation in Sudbury Breccia bodies with overprinted fragments. (c) Lower hemisphere, equal-area projection showing poles to foliations and respective mean orientation of fragments of the South Range Breccia Belt. (d) Schematic diagram illustrating the scenario in which brecciation postdates the formation of foliations. (e) Schematic diagram illustrating the scenario in which foliations postdate brecciation. (f) Poles to bedding planes at Location (d). (g) Poles to planar structures at Location (d). (h) Rose diagram displaying angles between foliations and bedding planes in fragments from Location (d). (i) Poles to bedding planes at Location (e). (j) Poles to foliations at Location (e). (k) Rose diagram displaying angles between foliations and bedding planes in fragments from Location (e). Stippled line in rose diagrams show angles between foliations and bedding planes in host rock. Contours in lower-hemisphere, equal-area projections are at 2, 3 and 5%.
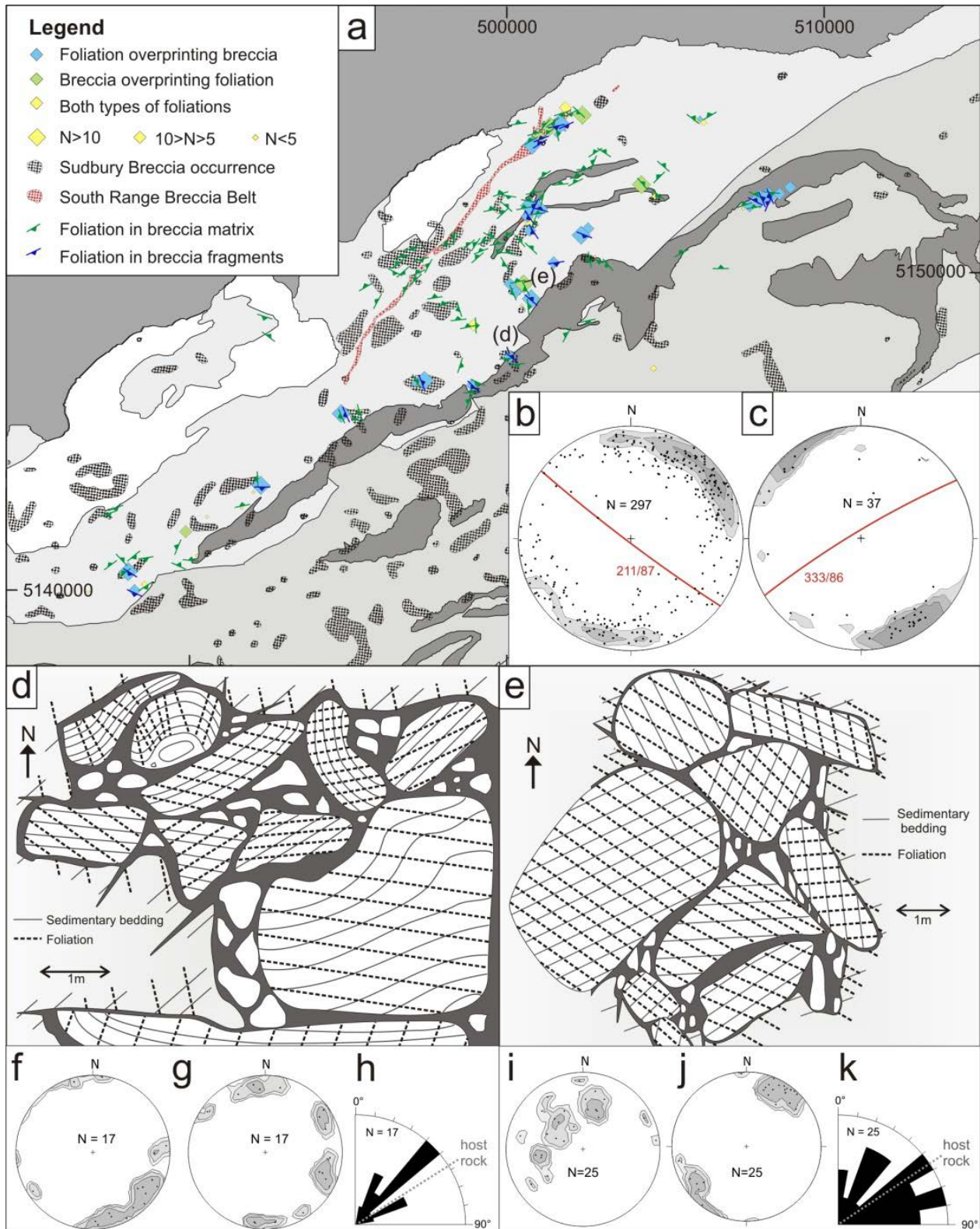
4.4.4. Brittle deformation

Small-scale brittle shear faults are useful to infer the kinematics of orogenic deformation and are ubiquitous in the Huronian rocks and the South Range SIC. Depending on the lithology, the fault planes are mostly decorated by fibrous chlorite, quartz and calcite. Using the orientation of fault surfaces, the orientation of mineral fibres and the inferred sense-of-slip on the faults (Angelier, 1979), principal axes of infinitesimal strain were obtained at a total of 139 stations (1835 faults). I acquired new fault-slip data at 64 stations (697 faults) to complemented data previously collected by Ulrich Riller at 75 stations (1138 faults), which are reported partly in Riller et al. (1999) and Cowan et al. (1999).

Slip senses on fault planes were obtained from the geometry of mineral fibres on a given fault surface and by the sense of displacement of passive markers, such as dikes and veins. For each fault population per station, the infinitesimal shortening and extension directions were calculated using the Numerical Dynamic Analysis (NDA: Spang, 1972). This method was used because of the pervasive presence of conjugate fault sets in the study area, which calls for an analytical method that considers the kinematics of each fault plane individually. NDA assigns a shear strain magnitude of 1 to each fault plane. Moreover, the angle between the maximum principal strain axes and the fault plane are the same for each fault population. For our analysis, we chose an angle of 30° between the maximum resolved shear strain and the maximal principal strain direction, which is in agreement with experimentally obtained values (Byerlee, 1968). By applying NDA we obtained the orientations of shortening (e_3), intermediate (e_2) and extension (e_1) axes, as well as the strain ratio (see supplementary material).

The orientation of infinitesimal principal strain axes, notably shortening directions, can be used to crudely identify individual deformation regimes in the South Range SIC and Huronian rocks (Fig. 4.6). Based on the orientation of the principal strain axes, the South Range and adjacent Huronian rocks were divided into three kinematic domains; the Western, the Central and the Eastern Domains (Fig. 4.6a). Uniform NW-SE shortening prevails in the Western Domain, which encompasses the South Range and Huronian rocks west of the Murray pluton (Fig. 4.6a, b). Here, intermediate and extension axes permutate around NE-SW and subvertical directions, thus forming a girdle distribution in the equal-area projection (Fig. 4.6b). In the Central Domain, i.e., south and immediately east of the Murray pluton, shortening directions are predominantly N-S to ENE-WSW and extension is either subvertical or trends E-W (Fig. 4.6a, c). It is noteworthy that the Central Domain shows also some subvertical shortening directions and corresponding NNW-SSE horizontal extension. In contrast to the Western and Central Domains, the infinitesimal principal strain axes in the Eastern Domain are oriented rather randomly (Fig. 4.6a, d).
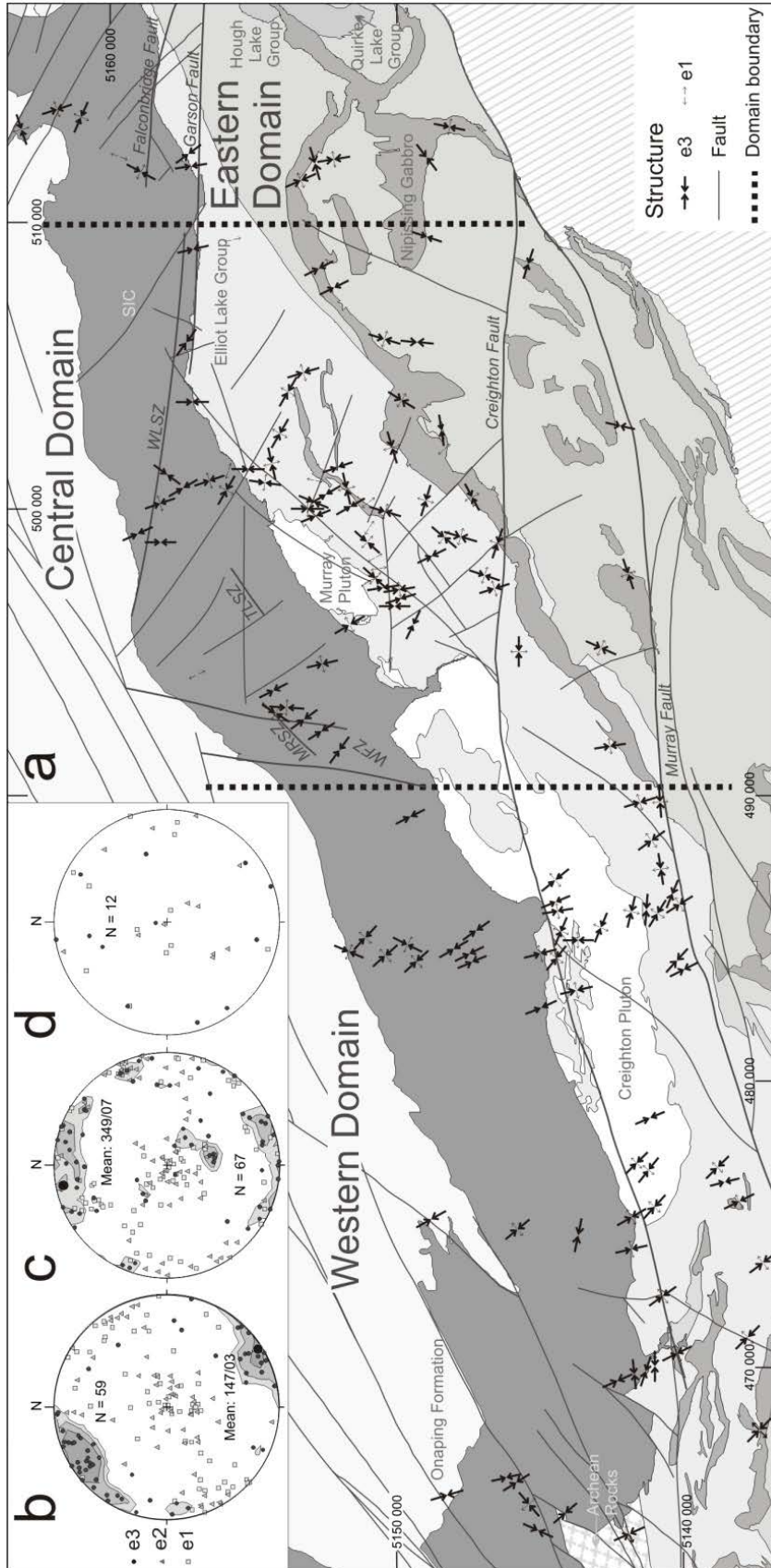
Figure 4.6: Orientation of infinitesimal strain axes in the South Range SIC and Huronian rocks. (a) Map showing major faults from Dressler (1984b) and own observations as well as principal shortening (e3) and extension (e1) directions calculated from brittle faults. (b)-(d) Lower-hemisphere, equal area projections of e1 ≥ e2 ≥ e3 axes of the Western, Central and Eastern Domvains, respectively. Contours of principal shortening direction (e3) are given in intervals of 2, 3 and 5%. WFZ = Whitewater Lake Fault Zone, WLSZ = Whitson Lake Shear Zone, MRSZ = Mont Rouleau Shear Zone, TLSZ = Thayer Lindsley Shear Zone.

4.4.5. Synthesis of results

Planar structures and fold axes in Huronian rocks near the South Range SIC are either concordant or orthogonal to the basal SIC contact. Concordant structures are referred to as Set 1, and orthogonal structures are labelled Set 2. The angular relationships between foliations and bedding planes in Sudbury Breccia bodies allowed us to distinguish between structures that predate and structures that postdate the brecciation, i.e., the impact event. Set 2 structures clearly postdate the impact event, whereas Set 1 structures largely predate but also postdate the impact event to some extent. The heterogeneity of deformation is well evident by the variation in the orientation of infinitesimal strain axes. Strain axis orientations correspond to the geometry of Set 1 and Set 2 structures in the Western and Central Domains, i.e., the shortening directions are normal to the respective structures in these domains. Along-strike changes in the orientations of structures in the Huronian rocks and orientations of infinitesimal strain axes correlate with the map-view curvature of the basal SIC contact.

4.5.   Discussion

4.5.1. Deformation kinematics in the South Range SIC and adjacent Huronian rocks

SE-dipping planar strain fabrics, notably at the Granophyre-Onaping Formation contact and in Huronian rocks, and NW-SE directed shortening directions have been attributed to thrusting on the South Range Shear Zone and large-scale folding of the South Range SIC and Huronian rocks (e.g., Shanks and Schwerdtner, 1991; Cowan and Schwerdtner, 1994; Cowan et al., 1999). However, many of the observed structural characteristics cannot be explained by these first-order deformation processes. These characteristics include: NW-trending fold axes in the Elliot Lake Group, steeply NE- and SW-dipping Set 2 planar structures in Huronian rocks and Sudbury Breccia matrix, as well as subvertical and ENE-WSW oriented shortening axes inferred from brittle fault data.

The structural characteristics unaccounted for by large-scale NW-directed thrusting and folding are most pronounced in the Central Domain between the Whitewater Lake Fault Zone (WFZ) and the Whitson Lake Shear Zone (WLSZ), but are also found as far west in Huronian Rocks just south of the Creighton Pluton and as far east as the SE-Lobe (Figs. 4.4, 4.7b). In the Central Domain, the Granophyre protrudes in map view into the Onaping Formation and the contact between these units dips steeply south (Fig. 4.1a), indicating that this contact segment is overturned. The WFZ and WLSZ (Fig. 4.7a) are characterized by local map-view thinning, reverse sense-of-shear and respective left-lateral and right-lateral strike separations of SIC units (Fig. 4.1b, see also Chapter 3). Toward the east, the WLSZ merges with the Garson Fault (Santimano and Riller, 2012), a steeply south-dipping ductile reverse fault, which displaces the basal contact of the SIC (Mukwakwami et al., 2012). Collectively, these fault zones constrain a triangular wedge in map view that consists of SIC and Huronian rocks (Fig. 4.7b). The wedge is characterized by structures that formed by both NW-SE and NE-SW shortening.
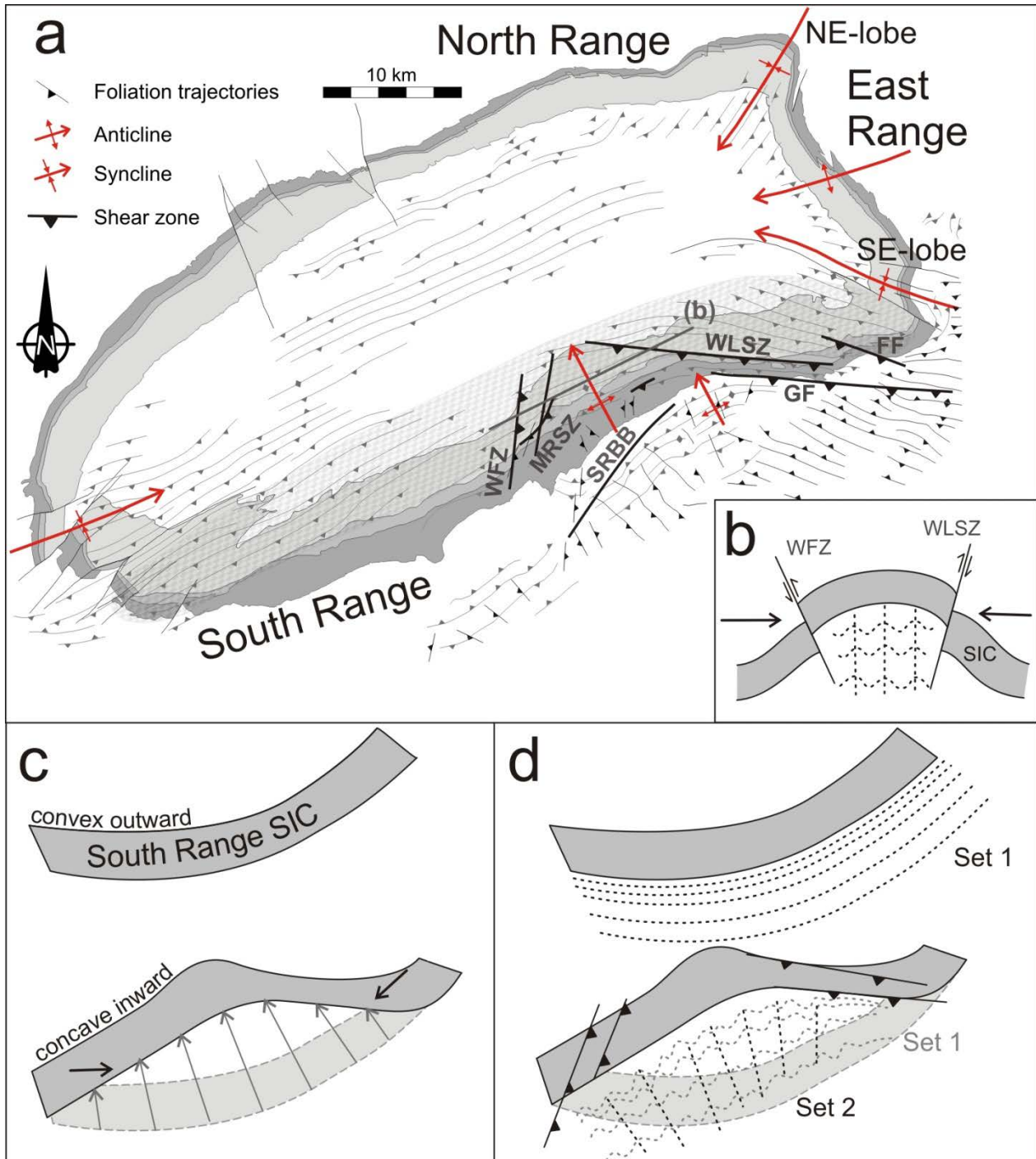
Figure 4.7: First-order structures of the Sudbury Basin and shape change of the South Range SIC and associated fabric development in Huronian rocks. (a) Structural map of the Sudbury Basin showing foliation trajectories, fold axes and major shear zones in the South Range. SRBB = South Range Breccia Belt, WFZ = Whitewater Lake Fault Zone, MRSZ = Mont Rouleau Shear Zone, WLSZ = Whitson Lake Shear Zone, GF = Garson Fault, FF = Falconbridge Fault. (b) NE-SW profile along line (b) indicated in (a). Arrows indicate local shortening direction. (c) Schematic diagrams showing proposed displacement gradient that may have affected the South Range. (d) Schematic diagrams showing the development of Set1 and Set 2 structures (dashed lines) as well as major shear zones (lines with barbs) as a consequence of shape change of the South Range.

4.5.2. Hypothesis on the shape change of the Southern SIC

Formation of the Sudbury Basin, notably rotation of the South Range SIC, may have been kinematically related to NW-directed thrusting on the South Range Shear Zone (Riller et al., 2010). Folding-induced activity of the Shear Zone is corroborated by the fact that the Shear Zone does not displace SIC contacts in the SE-lobe, into which the Shear Zone seems to merge (Fig. 4.1a). NW-directed thrusting on the central South Range Shear Zone is transferred to ductile transpressive deformation in the SE-lobe (Cowan, 1996; Cowan et al., 1999; Santimano and Riller, 2012). Alternatively, oblique thrusting on S-dipping surfaces, serving as lateral tips of the South Range Shear Zone in the SE-lobe, led to predominantly vertical rather than horizontal displacements. At any rate, displacement on the South Range Shear Zone decreases towards the SE-lobe. Such a displacement gradient on the South Range Shear Zone must have operated particularly at an early stage of Basin formation, i.e., when the shape of the South Range SIC was convex outward, similar to the present geometry of the less deformed North Range (Figs. 4.7c, 4.8a). Progressive NW-SE shortening and folding of the South Range SIC and associated thrusting on the South Range Shear Zone may have led to a change in the plan-view geometry of the South Range SIC from a convex outward to a concave inward geometry (Figs. 4.7c, 4.8b, c).

At an early stage of Basin formation, regional NW-SE shortening imparted NE-SW striking, post-impact Set 1 planar structures to Huronian rocks and to some extent to the Sudbury Breccia matrix. These fabrics formed mostly near the base of the SIC, possibly due to contact strain effects evident by the concentration and concordance of post-impact Set 1 planar structures at the basal SIC contact (Figs. 4.4a, 4.7d). With time, horizontal, layer-parallel shortening of the SIC may have gained locally in importance. This can account for the kilometre-scale corrugation of the SIC (Figs. 4.7c, d, 4.8b) as well as folding and crenulation of Set 1 planar structures in Huronian rocks (Figs. 4.4a, 4.7d). During this stage, the WFZ, WLSZ and the Garson Fault as well as Set 2 structures (Fig. 4.4a) and NW-SE striking fold-axial planes (Fig. 4.3a) formed in the Central Domain under local NE-SW shortening (Figs. 4.6, 4.7d, 4.8c). The relative increase in post-impact layer-parallel shortening over NW shortening can also account for the predominance of NE- and SW-dipping foliations over steeply NW-dipping fabrics in the Sudbury Breccia matrix (Fig. 4.5a).

Set 2 structures, including centimetre- to kilometre-scale folds, are most pervasive in the Elliot Lake Group east of the Murray Pluton. This area corresponds to a triangular wedge bound by the WFZ in the SW and the WLSZ and Garson Fault to the NE (Fig. 4.7a). This wedge also corresponds to the Central Domain showing highly variable shortening directions (Fig. 4.6a). Collectively, these structural relationships can be explained by the shape change of the SIC from the convex outward to the concave inward structural configuration accomplished by the formation of a wedge that is driven toward the NW along its bounding fault zones (Fig 4.7a). As these fault zones taper toward the NW, the wedge material is forced to converge toward the NW during regional NW-SE shortening, thus imparting constrictional strains to the wedge.

Northwest-ward convergence of wedge material possibly led to anticlinal buckling of the SIC around a NW-dipping hinge line (Fig. 4.7a, b). Thereby, Set 2 structures in layered rocks of the Elliot Lake Group and at the base of the SIC just north of the Murray pluton formed in the inner arc of, and are axial-planar to, the SIC buckle (Figs. 4.4a, 4.7a, b, d). Fanning of axial-planar

structures in the Elliot Lake Group toward the SIC as seen by the geometry of fold axes (Fig. 4.3a) and Set 2 trajectories (Fig. 4.4a) is typical for layered rocks occupying the inner arc of buckle folds (Dieterich, 1969). As the wedge was driven toward the NW, the tip of the buckled SIC steepened and rolled over toward the S as a consequence of shearing on the South Range Shear Zone. We propose that the wedge constitutes a hitherto unknown higher-order, anticlinal buckle of the SIC that is similar to the one between the NE- and SW-lobes in the East Range (Figs. 4.1, 4.7a).
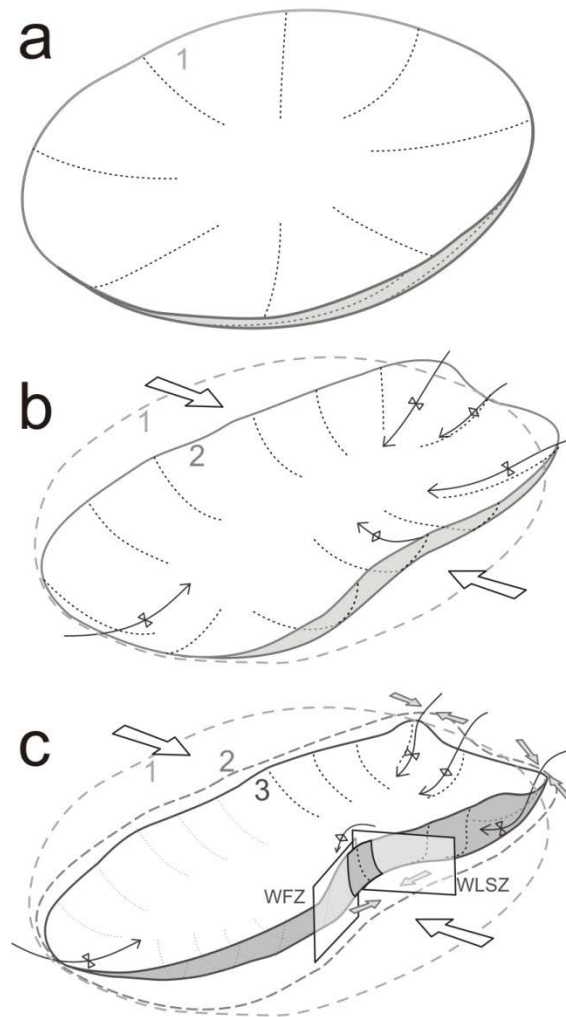
Figure 4.8: Major stages of shape change of the initially subhorizontal SIC to its present curvi-planar geometry. (a) Bowl-shaped SIC with shallowly dipping contacts after initial non-cylindrical buckling at stage 1. (b) Development of higher-order, radial folds (synclinal lobes and anticlinal buckle folds) and steepening of SIC contacts at stage 2. (c) Tightening of higher-order folds, steepening of SIC contacts and development of conjugate shear zones (WFZ = Whitewater Lake Fault Zone, WLSZ = Whitson Lake Shear Zone) as a consequence of enhanced concentric shortening (small arrows) under overall NW-SE shortening (large arrows) at stage 3. Stippled lines indicate perimeters of the SIC at stages 1 and 2.

4.5.3. Formation of higher-order folds and associated strain perturbations

The structural characteristics associated with the anticlinal buckle in the South Range SIC are similar to those of the synclinal NE- and SE-lobes and the anticlinal buckle in the East Range (Fig. 4.7a). Specifically, the characteristics are: (1) the hinge lines of the higher-order folds plunge moderately to steeply toward, and are radial with respect to, the Basin centre, (2) planar structures associated with each fold are axial-planar and (3) shortening directions inferred from fault-slip analysis are disposed at high angles to radial fold hinge lines, i.e., concentric with respect to the Basin centre (Cowan et al., 1999; Klimczak et al., 2007). Although not considered a lobe, the western terminus of the Sudbury Basin resembles a synclinal fold closure and also adheres to these structural characteristics (Riller et al., 1998).

The structure of the synclinal lobes and anticlinal buckles of the SIC are akin to those of higher-order structures associated with circular or spherical mechanical heterogeneities. Notably, concentric planar fabrics are observed at the contacts of spherical granitoid intrusive bodies (e.g., Brun and Pons, 1981; Vigneresse et al., 1999). Set 1 planar structures at the basal SIC contact (Figs. 4a, 7d) likely correspond to such concentric fabrics. Radial fabrics on the other hand are known from buoyancy-driven deformation associated with e.g., salt domes, diapirs and related extrusion structures (e.g., Talbot and Aftabi, 2004). In layered rocks, such deformation generates so-called curtain folds that are characterized by steep hinge lines plunging away from, and disposed radially to, the buoyant body as well as outward verging folds forming a rim syncline (Uken and Watkeys, 1997). The higher-order, synclinal lobes and anticlinal buckles of the Sudbury Basin as well as Set 2 planar structures adhere to the geometry of curtain folds and formed under concentric shortening.

The formation of higher-order folds in the SIC was unlikely driven by buoyancy forces. However, the folds and associated structures may well be due to a circular mechanical heterogeneity, i.e., the impact structure, from which the Sudbury Basin formed. More specifically, localisation of Basin formation was likely caused by the presence of a circular zone of mechanical weakness (Riller et al., 2010). Overall, distortion of the circular zone under NW-SE shortening induced concentric shortening in the periphery of the SIC. This strain perturbation led to layer-parallel buckling and ultimately radial folds with steep hinge zones (i.e., synclinal lobes and anticlinal buckles) of the SIC (Fig. 4.8b, c). The areas of buckling and lobe formation account for the observed variations in SIC thickness and geometry of the basal SIC contact. Primary thickness variations of the SIC (Dreuse et al., 2010) may have contributed to the localization of anticlinal buckle folds and synclinal lobes of the SIC.

Although the crust on the scale of the impact structure was mechanically weakened, the SIC was mechanically more competent than its adjacent layered rocks, the Onaping Formation and Huronian strata, after it solidified. As the North Range SIC is underlain by granulites and gneisses, this competency contrast to the SIC is lower than in the South Range, where the SIC is in contact with layered Huronian strata. This competency contrast is evident by the pervasive development of small-scale radial Set 2 structures in layered Huronian rocks that contrasts with the development of kilometre-scale folds and shear zones in the SIC. Thus, the more competent SIC controlled the geometry of higher-order structures in less competent rocks. As a consequence, local deviations in the orientations of planar structures and folds within and in the

periphery of the SIC from regional strain fabrics can be explained by local strain perturbations caused by the SIC. In such structural settings, the evolution of distinctly oriented structures may not be due to distinct tectonic events (e.g., Dieterich, 1969; Cowards and Potts, 1983).

4.6.   Conclusions

In this chapter I explored structures in the southern Sudbury Basin and adjacent Huronian rocks that cannot be accounted for by activity of the South Range Shear Zone and large-scale folding of the SIC around a NE-trending fold axis. In the periphery of the SIC, regional NW-SE shortening led to heterogeneous deformation, which includes concentric shortening and substantial strain perturbation. In Huronian rocks, this strain perturbation is evident by the initial formation of planar structures that are parallel to the contact with the SIC in map-view. At an advanced stage of Basin formation, the SIC likely changed from a convex outward to concave inward plan-view geometry. I suggest that during this deformation stage, concentric shortening became more important, and generated radial fabrics and kilometre-scale folds, which, collectively, overprinted contact-parallel structures. Concentric shortening of the SIC caused the formation of a hitherto unknown kilometre-scale buckle fold of the SIC and pervasive axial-planar fabrics in Huronian rocks. This buckle fold shares similar structural characteristics with the lobes of the SIC and the anticlinal buckle fold of the East Range. I propose that non-cylindrical buckling and associated fabric development accommodated the shape change of the SIC, which occupied a circular zone of mechanical heterogeneity, under protracted regional NW-SE shortening. This resulted in mutually perpendicular fabric orientations, which are compatible with overall NW-SE shortening. My structural analysis confirms previous studies in which highly discordant planar strain fabrics formed as a consequence of local strain perturbations near a folded sheet under a uniform deformation regime (e.g., Dieterich, 1969).

4.7. Summary

Deformation structures differing in style and orientation within a given terrane are often attributed to distinct tectono-metamorphic events. However, mechanical heterogeneities may locally cause strain perturbations that can have a profound effect on the geometry of such structures. My study documents highly variable orientations of planar structures, metre- to kilometre-scale folds and shortening directions inferred from brittle fault analysis within the synclinal and layered Sudbury Igneous Complex (SIC) and its Huronian host rocks. NW-SE shortening during Paleoproterozoic deformation led to the formation of planar structures in the host rocks that are parallel to the NE-SW striking contact of the southern SIC. During deformation, local contact-parallel shortening became more important than regional NW-SE shortening and generated contact-orthogonal planar mineral fabrics and folds. Local contact-parallel shortening is attributed to the shape change of the southern SIC from a convex outward to a concave inward curvi-planar geometry. Contact-parallel shortening accounts for the formation of a previously unidentified kilometre-scale buckle fold in the SIC and respective axial-planar mineral fabrics in Huronian host rocks. This buckle fold shares similar structural characteristics with known higher-order buckle folds of the eastern SIC. I suggest that non-cylindrical buckling and associated mineral fabric development accommodated the shape change of the SIC. This resulted in mutually perpendicular fabric orientations, which are compatible with overall NW-SE shortening. The original shape of the SIC seems to have had a profound influence particularly on the geometry of metamorphic foliations. My structural analysis supports earlier structural studies advocating that highly discordant planar strain fabrics can be generated by local strain perturbations near igneous sheets under uniform regional shortening.

References

Ames, D.E., Davidson, A., Buckle, J.L., Card, K.D., 2005. Geology, Sudbury bedrock compilation, Ontario. Geological Survey of Canada, Open File 4570, scale 1:50 000.

Angelier, J., 1979. Determination of the mean principal directions of stresses for a given fault population. Tectonophysics 56, T17-T26.

Bailey, J., Lafrance, B., McDonald, A.M., Fedorowich, J.S., Kamo, S., Archibald, D.A., 2004. Mazatzal–Labradorian-age (1.7–1.6 Ga) ductile deformation of the South Range Sudbury impact structure at the Thayer Lindsley mine, Ontario. Canadian Journal of Earth Sciences 41, 1491-1505.

Bennett, G., Dressler, B.O., Robertson, J.A., 1991. The Huronian Supergroup and associated intrusive rocks. *In:* Thurston, P.C., Williams, H.R., Sutcliffe, R.H., Scott, G.M. (Eds.), Geology of Ontario. Ontario Geological Survey, Special Volume 4, 549-591.

Betts, P.G., 1999. Paleoproterozoic mid-basin inversion in the northern Mt Isa terrane, Queensland. Australian Journal of Earth Sciences 46, 735-748.

Bosworth, W., Burke, K., Strecker, M., 2003. Effect of stress fields on magma chamber stability and the formation of collapse calderas. Tectonics 22, 16-1 - 16-21.

Brocoum, S., Dalziel, I., 1974. The Sudbury Basin, the Southern Province, the Grenville Front, and the Penokean Orogeny. Geological Society of America Bulletin 85, 1571-1580.

Brun, J.P., Pons, J., 1981. Strain patterns of pluton emplacement in a crust undergoing non-coaxial deformation, Sierra Morena, Southern Spain. Journal of Structural Geology 3, 219-229.

Buchan, K.L., Card, K.D., Chandler, F.W., 1989. Multiple ages of Nipissing Diabase intrusion: paleomagnetic evidence from the Englehart area, Ontario. Canadian Journal of Earth Sciences 26, 427-445.

Burg, J.P., 1987. Regional shear variation in relation to diapirism and folding. Journal of Structural Geology 9, 925-934.

Burg, J.P., 1999. Ductile structures and instabilities: their implication for Variscan tectonics in the Ardennes. Tectonophysics 309, 1-25.

Byerlee, J. D., 1968. Brittle ductile transition in rock. Journal of Geophysical Research 73, 4741-4750.

Card, K.D., 1978. Geology of the Sudbury-Manitoulin Area, District of Sudbury and Manitoulin; Ontario Geological Survey, Report 166, 238 p.

Card, K.D., Church, W.R., Franklin, J.M., Robertson, J.A., West, G.F., Young, G.M., 1972. The Southern Province. *In:* Price, R.A., Douglas, R.J.W. (Eds.), Variations in Tectonic Style in Canada. Geological Association of Canada Special Paper 8, 335-380.

Card, K.D., Pattison, E.F., 1973. Nipissing diabase of the Southern Province, Ontario. *In:* Young, G. M. (Ed.), Huronian stratigraphy and sedimentation. Geological Association of Canada, Special Paper 12, 7-30.

Card, K.D., Gupta, V.K., McGrath P H., Gant, F.S., 1984. The Sudbury structure: its regional geological and geophysical setting. *In:* Pye E. G., Naldrett A. J., Giblin P. E. (Eds.), The Geology and Ore Deposits of the Sudbury Structure. Ontario Geological Survey, Special Volume 1, 25-43.

Chen, S.F., Libby, J.W., Greenfield, J.E., Wyche, S., Riganti, A., 2001. Geometry and kinematics of large arcuate structures formed by impingement of rigid granitoids into greenstone belts during progressive shortening. Geology 29, 283-286.

Corfu, F., Andrews, A.J., 1986. A U-Pb age for mineralized Nipissing diabase. Gowganda, Ontario. Canadian Journal of Earth Sciences 27, 107-109.

Cosgrove, J.W., 1980 The tectonic implications of some small scale structures in the Mona Complex of Holy Isle, North Wales. Journal of Structural Geology 2, 383-396.

Cowan, E.J., 1996. Deformation of the Eastern Sudbury Basin. Ph.D. thesis, University of Toronto, Toronto, 366p.

Cowan, E.J., Schwerdtner, W.M., 1994. Fold Origin of the Sudbury Basin. *In:* Lightfoot, P.C., Naldrett, A.J. (Eds.), Proceedings of the Sudbury - Noril'sk symposium: Ontario Geological Survey Special Volume 5, 45-56.

Cowan, E.J., Riller, U., Schwerdtner, W.M., 1999. Emplacement geometry of the Sudbury Igneous Complex: Structural examination of a proposed impact melt sheet. *In:* Dressler, B.O., Sharpton, V.L. (Eds.), Large meteorite impacts and planetary evolution II. GSA Special Paper 339, Geological Society of America, Boulder, 399-418.

Coward, M.P., Potts, G.J., 1983. Complex strain patterns developed at the frontal and lateral tips to shear zones and thrust zones. Journal of Structural Geology 5, 383-399.

Dieterich, J.H., 1969. Origin of cleavage in folded rocks. American Journal of Science 267, 155-165.

Dressler, B.O., 1984a. The Effects of the Sudbury Event and the Intrusion of the Sudbury Igneous Complex on the Footwall Rocks of the Sudbury Structure. *In:* Pye, E.G., Naldrett, A.J., Giblin, P.E. (Eds.), The Geology and Ore Deposits of the Sudbury Structure. Special Publication 1. Ontario Geological Survey, Toronto, 97-136.

Dressler, B.O., 1984b. Sudbury Geological Compilation: Ontario Geological Survey Map 2491, Precambrian Geology Series, Scale 1:50 000.

Dreuse, R., Doman, D., Santimano, T., Riller, U., 2010. Crater floor topography and impact melt sheet geometry of the Sudbury impact structure, Canada. Terra Nova 22, 463-469.

Dutch, S. I., 1979. The Creighton pluton, Ontario: An unusual example of a forcefully emplaced intrusion. Canadian Journal of Earth Sciences 16, 333–349.

Easton, R.M., 2000. Metamorphism of the Canadian Shield, Ontario, Canada. II. Proterozoic metamorphic history. The Canadian Mineralogist 38, 319-344.

Forster, M., Lister, G., 2008. Tectonic sequence diagrams and structural evolution of schists and gneisses in multiply deformed terranes. Journal of the Geological Society 165, 923-939.

Frarey, M.J., Loverbridge, W.D., Sullivan, R.W., 1982. A U-Pb Zircon Age for the Creighton Granite, Ontario. *In:* Rb-Sr and U-Pb Isotopic Age Studies, Report 5, Current Research, Part C, Geological Survey of Canada, Paper 82-1C, 129-132

Grieve, R.A.F., Stöffler, D., Deutsch, A., 1991. The Sudbury Structure: Controversial or Misunderstood? Journal of Geophysical Research 96, 22753-22764.

Grieve, R.A.F., Therriault, A., 2000. Vredefort, Sudbury, Chicxulub: Three of a kind? Annual Reviews of Earth and Planetary Sciences 28, 305-338.

Grieve, R.A.F., Reimold, W.U., Morgan, J., Riller, U., Pilkington, M., 2008. Observations and interpretations at Vredefort, Sudbury and Chicxulub: Towards an empirical model of terrestrial impact basin formation. Meteoritics and Planetary Science 43, 855–882.

Grieve, R.A.F., Ames, D.E., Morgan, J.V., Artemieva, N., 2010. The evolution of the Onaping Formation at the Sudbury impact structure. Meteoritics and Planetary Science 45, 759-782.

Holohan, E.P., Troll, V.R., Walter, T.R., Münn, S., McDonnell, S., Shipton, Z.K., 2005. Elliptic calderas in active tectonic settings: an experimental approach. Journal of Volcanology and Geothermal Research 144, 119-136.

Ivanov, B. A., 2005. Numerical Modeling of the Largest Terrestrial Meteorite Craters. Solar System Research 39, 381-409.

Ivanov B. A., Deutsch A., 1999. Sudbury impact event: Cratering mechanics and thermal history. *In:* Dressler B. O., Sharpton V.L. (Eds.), Large meteorite impacts and planetary evolution II. GSA Special Paper 339, Geological Society of America, Boulder, 389–398.

Johns, G. W., 1996. Precambrian geology of the Garson and Blezard townships. Ontario Geological Survey, Open File Report, 5950, 47p.

Kenkmann, T., Kiebach, F., Rosenau, M., Raschke, U., Pigowske, A., Mittelhaus, K., Eue, D., 2008. Coupled effects of impact and orogeny: Is the marine Lockne crater, Sweden, pristine? Meteoritics and Planetary Science 42, 1995-2012.

Klimczak, C., Wittek, A., Doman, D., Riller, U., 2007. Fold origin of the NE-lobe of the Sudbury Basin, Canada: Evidence from heterogeneous fabric development in the Onaping Formation and the Sudbury Igneous Complex. Journal of Structural Geology 29, 1744-1756.

Krogh T.E., Davis D.W., Corfu F., 1984. Precise U-Pb Zircon and Baddeleyite Ages for the Sudbury Area. *In:* Pye, E.G., Naldrett, A.J., Giblin, P.E. (Eds.), The Geology and Ore Deposits of the Sudbury Structure. Special Publication 1. Ontario Geological Survey, Toronto, 431-446.

Krogh, T.E., Kamo, S.L., Bohor, B.F., 1996. Shocked metamorphosed zircons with correlated U-Pb discordance and melt rocks with concordant protolith ages indicate an impact origin for the Sudbury Structure. *In:* Basu, A., Hart, S. (Eds.), Earth processes: reading the isotopic code. American Geophysical Union, Monograph 95, 343-352.

Lafrance, B., Legault, D., Ames, D.E., 2008. The formation of the Sudbury breccia in the North Range of the Sudbury Impact Structure. Precambrian Research 165, 107-119.

Lafrance, B., Kamber, B.S., 2010. Geochemical and microstructural evidence for in situ formation of the pseudotachylitic Sudbury Breccia by shock-induced compression and cataclasis. Precambrian Research 180, 237-250.

Lightfoot, P.C., DeSouza, H., Doherty, W., 1993. Age and source of the Nipissing Diabase intrusions, Ontario, Canada. Canadian Journal of Earth Sciences 30, 1123-1140.

Milkereit, B., Green, A., and 21 others, 1992. Deep geometry of the Sudbury structure from seismic reflection profiling. Geology 20, 807-811.

Morris, W.A., 1980. Tectonic and Metamorphic History of the Sudbury Norite: The Evidence from Paleomagnetism. Economic Geology 76, 260-277.

Morris, W.A., 1984. Paleomagnetic Constraints on the Magmatic, Tectonic, and Metamorphic History of the Sudbury Basin Region *In:* Pye, E.G., Naldrett, A.J., Giblin, P.E. (Eds.), The Geology and Ore Deposits of the Sudbury Structure. Special Publication 1. Ontario Geological Survey, Toronto, 411-427.

Mukwakwami, J., Lafrance, B., Lesher, C.M., 2012. Back-Thrusting and Overturning of the Southern Margin of the 1.85 Ga Sudbury Igneous Complex at the Garson Mine, Sudbury, Ontario. Precambrian Research 196-197, 81-105.

Panien, M., Buiter, S.J.H., Schreurs, G., Pfiffner, O.A., 2006, Inversion of a symmetric basin: insights from a comparison between analogue and numerical experiments. *In:* Buiter, S.J.H., Schreurs, G. (Eds.), Analogue and Numerical Modelling of Crustal-Scale Processes, Geological Society, London, Special Publication 253, 253-270.

Pappalardo, R.T., Collins, G.C., 2005. Strained craters on Ganymede. Journal of Structural Geology 27, 827-838.

Peredery, W., Morrison, P., 1984. Discussion on the origin of the Sudbury Structure. *In:* Pye, E.G., Naldrett, A.J., Giblin, P.E. (Eds.), The Geology and Ore Deposits of the Sudbury Structure. Special Publication 1. Ontario Geological Survey, Toronto, 491-511.

Piercey, P., Schneider, D.A., Holm, D.K., 2007. Geochronology of Proterozoic metamorphism in the deformed Southern Province, northern Lake Huron region, Canada. Precambrian Research 157, 127-143.

Platt, T.P., Lister, G.S., 1985. Structural history of high-pressure metamorphic rocks in the southern Vanoise Massif, French Alps, and their relation to Alpine tectonic events. Journal of Structural Geology 7, 19-35.

Riller, U., 2005. Structural characteristics of the Sudbury Impact Structure, Canada: impact-induced and orogenic deformation – a review. Meteoritics and Planetary Science, 40 1723-1740.

Riller, U., Schwerdtner, W.M., 1997. Mid-crustal deformation at the southern flank of the Sudbury Basin, central Ontario, Canada. Geological Society of America Bulletin 109, 841-854.

Riller, U., Schwerdtner, W.M., Robin, P.-Y.F., 1998. Low-temperature deformation mechanisms at a lithotectonic interface near the Sudbury Basin, Eastern Penokean Orogen, Canada. Tectonophysics 287, 59-75.

Riller, U., Schwerdtner, W., Halls, H., Card, K., 1999. Transpressive tectonism in the Eastern Penokean Orogen, Canada. Consequences for Proterozoic crustal kinematics and continental fragmentation. Precambrian Research 93, 51-70.

Riller, U., Lieger, D., Gibson, R.L., Grieve, R.A.F., Stöffler, D., 2010. Origin of large-volume pseudotachylite in terrestrial impact structures. Geology 38, 619-622.

Rosenbaum, G., Avigad, D., Sánchez-Gómez, M., 2002. Coaxial flattening at deep levels of orogenic belts: evidence from blueschists and eclogites on Syros and Sifnos (Cyclades, Greece). Journal of Structural Geology 24, 1451-1462.

Rousell, D.H., 1975. The Origin of Foliation and Lineation in the Onaping Formation and the Deformation of the Sudbury Basin. Canadian Journal of Earth Sciences 12, 1379-1395.

Rousell, D.H., 1984a. Onwatin and Chelmsford Formations. *In:* Pye, E.G., Naldrett, A.J., Giblin, P.E. (Eds.), The Geology and Ore Deposits of the Sudbury Structure. Special Publication 1. Ontario Geological Survey, Toronto, 211-218.

Rousell, D.H., 1984b. Structural Geology of the Sudbury Basin. *In:* Pye, E.G, Naldrett, A.J., Giblin, P.E. (Eds.), The Geology and Ore Deposits of the Sudbury Structure. Special Publication 1. Ontario Geological Survey, Toronto, 83-96.

Rousell, D.H., Gibson, H.L., Jonasson, I.R., 1997. The tectonic, magmatic and mineralization history of the Sudbury Structure. Exploration and Mining Geology 6, 1-22.

Rousell, D.H., Fedorowich, J.S., Dressler, B.O., 2003. Sudbury Breccia (Canada): a product of the 1850 Ma Sudbury Event and host to footwall Cu-Ni-PGE deposits. Earth Science Reviews 60, 147-174.

Santimano, T., Riller, U., 2012. Revisiting thrusting, reverse faulting and transpression in the southern Sudbury Basin, Ontario. Precambrian Research 200-203, 74-81.

Sayab, M., 2006. Decompression through clockwise P-T path: implications for early N-S shortening orogenesis in the Mesoproterozoic Mt Isa Inlier (NE Australia). Journal of Metamorphic Geology 24, 89-105.

Schofield, D.I., D'Lemos, R.S., 1998. Relationships between syn-tectonic granite fabrics and regional PTtd paths: an example from the Gander-Avalon boundary of NE Newfoundland. Tectonophysics 20, 459-471.

Scott, R.G., Spray, J.G., 1999. Magnetic fabric constraints on friction melt flow regimes and ore emplacement direction within the South Range Breccia Belt, Sudbury Impact Structure. Tectonophysics 307, 163-189.

Scott, R.G., Spray, J.G., 2000. The South Range Breccia Belt of the Sudbury Impact Structure: A possible terrace collapse feature. Meteoritics and Planetary Science 35, 505-520.

Shanks, W.S., Schwerdtner, W.M., 1991. Structural analysis of the central and southwestern Sudbury Structure, Southern Province, Canadian Shield. Canadian Journal of Earth Sciences 28, 411-430.

Smith, M.D., Heaman, L.M., 1999. Constraints on the timing of felsic magmatism associated with Matachewan igneous events: preliminary results for the Creighton granite; Ontario. Geological Association of Canada – Mineralogical Association of Canada, Joint Annual Meeting, Abstract Volume 24, p. 119.

Spang, J.H., 1972. Numerical method for dynamic analysis of calcite twin lamellae. Geological Society of America Bulletin 83, 467-471.

Speers, E.C., 1957. The age relation and origin of common Sudbury Breccia. Journal of Geology 65, 497-514.

Talbot, C.J., Aftabi, P., 2004. Geology and models of salt extrusion at Qum Kuh, central Iran. Journal of the Geological Society 161, 321-334.

Tschirhart, P., Morris, W.A. 2012. Grenville age deformation of the Sudbury impact structure: evidence from magnetic modelling of the Sudbury diabase dyke swarm. Terra Nova 24, 213-220.

Thompson, L.M., Spray, J.G., 1996. Pseudotachylyte petrogenesis: constraints from the Sudbury impact structure. Contributions to Mineralogy and Petrology 125, 359-374.

Tobisch, O.T., Paterson, S.R., 1988. Analysis and interpretation of composite foliations in areas of progressive deformation. Journal of Structural Geology 10, 745754.

Turner, F.J., Weiss, L.E., 1963. Structural analysis of metamorphic tectonites. McGraw-Hill New York, 545p.

Uken, R., Watkeys, M.K., 1997. Diapirism initiated by the Bushveld Complex, South Africa. Geology 25, 723-726.

Van Schmus, W.R., 1976. Early and middle Proterozoic history of the Great Lakes area, North America. Royal Society of London Philosophical Transactions A280, 606-628.

Vigneresse, J.-L., Tikoff, B., Amélio, L., 1999. Modification of the regional stress field by magma intrusion and formation of tabular granitic plutons. Tectonophysics 302, 203-224.

Wilson, J., Grocott, J., 1999. The emplacement of the granitic Las Tazas complex, northern Chile: the relationship between local and regional strain. Journal of Structural Geology 21, 1513-1523.

Wu, J., Milkereit, B., Boerner, D., 1994. Timing constraints on deformation history of the Sudbury Impact Structure. Canadian Journal of Earth Sciences 31, 1654-1660.

Xypolias, P., Kokkalas, S., Skourlis, K., 2003. Upward extrusion and subsequent transpression as a possible mechanism for the exhumation of HP/LT rocks in Evia Island (Aegean Sea, Greece). Journal of Geodynamics 35, 303-332.

Young, G.M, Long, D.G.F., Fedo, C.M., Nesbitt, H.W., 2001. Paleoproterozoic Huronian basin: product of a Wilson cycle punctuated by glaciations and a meteorite impact. Sedimentary Geology 141-142, 233-254.

5.   A trishear model for the deformation of the southern Sudbury Basin

5.1.   Introduction

In areas of low topographic relief precise geological profiles based chiefly on structural data at surface are difficult to obtain. In these areas small-scale structural markers, such as primary layering and strain indicators, are most important for determining the mechanisms and kinematics of deformation. In contrast to sedimentary rocks, igneous rocks are characterized by low levels of primary planar fabric anisotropy, thus, hampering the assessment of rotational deformation components of these rocks in particular. The orientations of lithological contacts and deformation fabrics, such as mineral foliations and lineations at surface are often the only useful information to determine the magnitude and style of deformation in igneous rocks. Mineral fabrics provide information on the orientation of local shortening direction and the metamorphic grade of deformation. However, in order to quantify the rotation and translation components of deformation, additional information on magnitudes deformation parameters, such as displacement, is required.

Using the synformal and layered Sudbury Igneous Complex (SIC), Canada, as an example, I demonstrate in this chapter how structural data collected at surface in combination with geometric modelling of deformation can provide plausible solutions as to the progressive shape change of crystalline sheets. The SIC delimits the Sudbury Basin (Fig. 5.1) and provides an ideal geological unit for this task as its surface geometry and deformation structures are mapped in considerable detail (e.g., Rousell, 1975; Dressler, 1984; Shanks and Schwerdtner, 1991a; Cowan 1996, 1999; Chapter 3 of this thesis). Nonetheless, there is avid debate regarding the geometry and magnitude of deformation that affected the SIC (Rousell, 1984a; Cowan et al., 1999), which can be resolved by elucidating the mechanism and associated kinematics of deformation.

The Sudbury Basin is highly asymmetric, evident by variation in the dips of the SIC contacts and metamorphic foliation in the northern and the southern portions of the Sudbury Basin, i.e., the North Range and the South Range (Fig. 5.1a). In the North Range, the SIC dips moderately toward the Basin center and lacks pervasive metamorphic mineral fabrics. In the South Range, the SIC dips steeply and displays foliation planes that strike mostly parallel to the long axis of the Basin (Fig. 5.1a). The synformal shape of the SIC has previously been ascribed to melt sheet sagging during cooling (Peredery and Morrison, 1984) or is considered as primary (Cowan et al., 1999). Recent structural studies draw upon the pervasive presence of foliation surfaces in rocks of the SIC as evidence for post-impact, non-cylindrical folding (Cowan and Schwerdtner, 1994; Riller et al., 1998; Riller, 2005; Klimczak et al., 2007; Chapter 3 of this thesis). However, it is not yet understood how folding and thrusting on the South Range Shear Zone (Fig. 5.1a; Shanks and Schwerdtner, 1991a) accounts for the observed variation in orientations of layer contacts and foliations, notably in the South Range SIC.

To identify the mechanisms of shape change of the southern Sudbury Basin, I review the orientations of the SIC contacts, igneous layering and metamorphic foliations at surface. Then I generate forward kinematic models to constrain the geometry of SIC contacts in the South Range and to better understand which deformation parameters significantly influenced deformation to its present geometry. Based on these results, I attempt a three-dimensional (3-D) kinematic

restoration of the SIC by varying specific quantities of deformation, such as displacement magnitudes, fault angles and fault tip position. From a number of possible deformation parameter combinations, I choose combinations that result in an initially rather even geometry of SIC contacts. The deformation parameters that account best for the initial geometry for the SIC for each section are analyzed for variation along strike of the South Range. Finally, I address the effect of the modelling deformation on the geometric evolution of the SIC.

Figure 5.1 (following page): Structural maps of the Sudbury Basin. (a) Compilation of structural elements of the Sudbury Basin. Shape fabric trajectories are from Cowan et al. (1999), fold axes are from Chapter 1 and Clark et al. (2012), dip angles of the SIC basal and upper contacts are from Rousell (1975) and Dreuse et al. (2010). Foliation dip magnitudes are compiled from Dressler (1984), Cowan (1996) and own data. (b) Cleavage intensity (0 to II) in the Chelmsford Formation after Clendenen et al. (1988). 0: poorly developed or absent cleavage, I: weakly developed cleavage, II: strongly developed cleavage. Cleavage intensity in the Onaping Formation after Hirt et al. (1993). 0: no cleavage, 1: weakly developed cleavage, 2: pervasive cleavage, 3: mylonitic cleavage. Gridded k-values (Flinn, 1962) representing the prolateness factor of the fabric ellipsoid compiled from Shanks and Schwerdtner (1991a). (c) Orientation of shortening directions based on magnetic fabric anisotropy and shape-preferred orientation of concretions in sedimentary rocks of the Chelmsford Formation (grey bars; Clendenen et al., 1988) and kinematic analysis of brittle faults from the SIC and its Huronian host rocks (black bars; from Chapter 2).
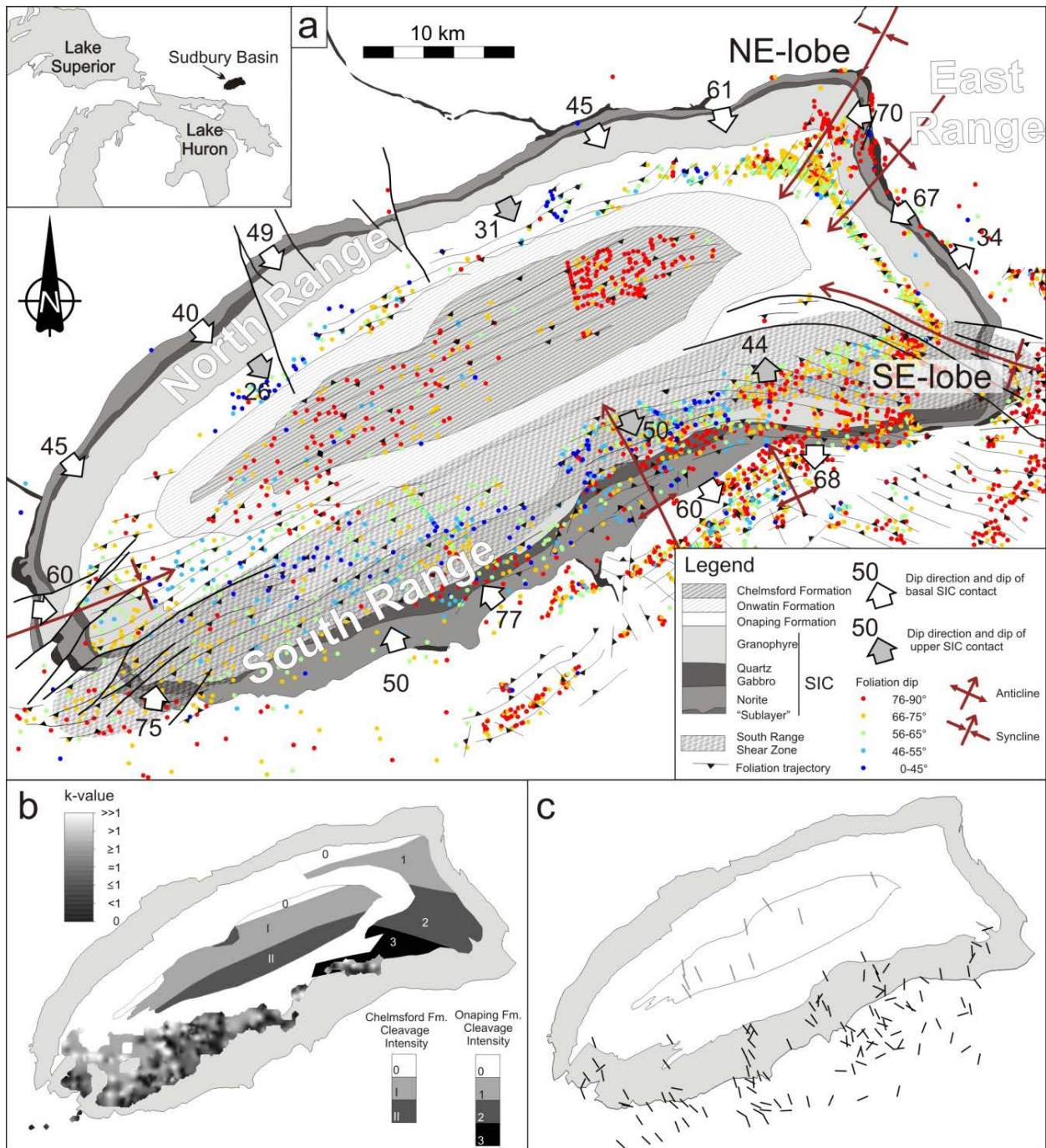
5.2. *Geological Setting*

The Sudbury Basin (Fig. 5.1a) straddles granitoid and gneissic rocks of the Archean Superior Province in the north and metavolcanic and metasedimentary rocks of the Paleoproterozoic Huronian Supergroup in the south. The Basin comprises the 1.85 Ga Main Mass of the SIC (Krogh et al., 1984), the relic of an impact melt sheet (Grieve et al., 1991; Deutsch et al., 1995), clast-melt breccias of the Onaping Formation (Peredery and Morrison, 1984; Grieve et al., 2010), and post-impact sedimentary rocks of the Chelmsford and Onwatin Formations (Rousell, 1984a, 1984b). At the time of deposition of these Formations, the SIC likely formed an open and shallow SW-plunging syncline (Cantin and Walker, 1972; Morris, 1980; Morris, 1984) in a foreland tectonic setting (McDaniel et al., 1994; Long, 2004; Young et al., 2001). The Main Mass of the SIC is made up of the Norite, Quartz Gabbro and Granophyre layers, which overlie gabbroic and noritic rocks of the Sublayer (Fig. 5.1a). The Sublayer hosts economically most important Cu-Ni-PGE sulphide deposits (e.g., Keays and Lightfoot, 2004; Ames and Farrow, 2007), making the Sudbury Basin a world-class mining camp.

Much of the Sudbury Basin and adjacent Huronian host rocks to the south of the Basin were affected by deformation, the metamorphic grade of which varies from greenschist-facies in the North Range to lower amphibolite-facies in the South Range (Card, 1978; Thomson et al., 1985; Fleet et al., 1987). Metamorphism and deformation of the Huronian rock has been attributed to the ca. 2.45 to 2.22 Ga Blezardian Orogeny (Riller and Schwerdtner, 1997; Riller et al., 1999), the ca. 1.87 to 1.83 Ga Penokean Orogeny (Brocoum and Dalziel, 1974; Van Schmus, 1976; Riller, 2005; Klimczak et al., 2007), the ca. 1.7 to 1.6 Ga Mazatzal Orogeny (Bailey et al., 2004; Piercey et al., 2007) and the ca. 1.2 to 1 Ga Grenville Orogeny (Brocoum and Dalziel, 1974; Tschirhart and Morris, 2012). Apparently, all Paleoproterozoic deformation events contributed to the formation of the prominent NE-SW trending structural grain in the Sudbury area, evident mostly by inclined metamorphic foliation surfaces and fold-axial traces in pre-impact, impact-related and post-impact rocks (Card and Pattison, 1973; Brocoum and Dalziel, 1974; Rousell, 1975, 1984a).

5.3. *Structure of the Sudbury Basin*

The Sudbury Basin contains three higher-order synclines, the NE-lobe, the SE-lobe and the western fold closure, and two anticlines (Fig. 5.1a). Collectively, these fold structures are disposed radially with respect to, and plunge toward, the center of the Basin. The geometry of the Sudbury Basin at depth is documented by the contact geometry of the Norite and Quartz Gabbro inferred from the Lithoprobe seismic profiles (Milkereit et al., 1992; Wu et al., 1995). The seismic profile intersecting the eastern portion of the North Range shows that the basal SIC and the base of the Quartz Gabbro dip south at 20 to 30° (Wu et al., 1995). The seismic profiles crossing the western portion of the South Range are interpreted to show that SIC layers dip north and are offset by south-dipping reflectors (Milkereit et al., 1992; Boerner et al., 2000), which correspond to faults exposed at surface (Wu et al., 1995). Offset of lithological contacts by these faults in map view, notably at the western fold closure, is on the order of 500 to 2000 meters (Fig. 5.1a).

In addition to the dip of SIC contacts, the orientation of planar igneous cumulate fabrics observed in the Norite of the South Range SIC provides further information on the post-emplacement deformation, specifically the rotational components, of this layer. Cumulate mineral fabrics of the South Range Norite dip toward the NW at approximately 50°, which is likely the result of both tilting and shear-induced rotation of an originally flat SIC (Lenauer and Riller, 2012a). In the SE-lobe, planar igneous fabrics in the SIC dip either steeply to the N or to the S (Lenauer and Riller, 2012a). Here, S-dipping igneous layering in the Norite corroborates the observation that the base of the SIC is overturned to the North.

Metamorphic foliations in the Sudbury Basin strike parallel to its long axis and are either subvertical or dip southward (Shanks and Schwerdtner, 1991a; Cowan, 1996; Fig. 5.1a). In the NE-lobe and SE-lobe, the foliations are axial-planar to the plan-view curvature of the SIC (Cowan, 1999; Klimczak et al., 2007), indicative of a fold origin of the two lobes (Cowan and Schwerdtner, 1994; Riller, 2005; Klimczak et al., 2007). In the South Range Norite, oppositely dipping foliations point to low levels of map-scale strain accomplished under co-axial deformation (Lenauer and Riller, 2012a). Strain intensity and non-coaxial deformation increase toward the South Range Shear Zone (SRSZ), where foliations dip rather uniformly southward (Shanks and Schwerdtner, 1991a; Lenauer and Riller, 2012a).

The SRSZ (Rousell, 1975; Shanks and Schwerdtner, 1991a) is a prominent SE-dipping ductile deformation zone that deformed the South Range SIC and Onaping Formation (Fig. 5.1a). Mineral fabrics of the deformation zone display L-S geometry and formed mostly at or near the contact of the Granophyre with the Onaping Formation (Fig. 5.1a). Variations in the prolateness factor of the fabric ellipsoid (Shanks and Schwerdtner, 1991a) are displayed in Figure 5.1b and show an increase of fabric prolateness from W to E and from N to S. Foliation dips approximately 60° toward the SE and associated asymmetric mineral fabrics characterize the SRSZ as a zone of non-coaxial deformation with top-to-NW sense of displacement (Shanks and Schwerdtner, 1991a; Santimano and Riller, 2012). However, the presence of anastomosing, subvertical foliation planes in the South Range Granophyre indicates that rocks in the SRSZ also underwent flattening strains (Lenauer and Riller, 2012a). Similarly, subvertical fold-axial planes associated with steeply dipping foliation planes in the Onwatin and Chelmsford Formations (Rousell, 1984b, Shanks and Schwerdtner, 1991a) and oppositely dipping foliations in the South Range Norite (Lenauer and Riller, 2012a) point to coaxial deformation on either side of the SRSZ.

Similar to the SIC, the Chelmsford and Onaping Formations are characterized by heterogeneous deformation. Clendenen et al. (1988) identified areas in the Chelmsford Formation in which cleavage is poorly, moderately and well developed (Fig. 5.1b). Likewise, Hirt et al. (1993) documented a map-scale strain gradient in the Onaping Formation of the eastern Sudbury Basin that is evident by areas in which cleavage is absent, weakly developed, pervasive and mylonitic (Fig. 5.1b). Collectively, the variation in cleavage development suggests an increase in strain from NW to SE in the Basin center, i.e., toward the SRSZ.

Shortening directions are an important basis for kinematic reconstructions. In the Sudbury Basin and adjacent Huronian rocks local shortening directions have been inferred from magnetic fabric anisotropy (Clendenen et al., 1988) and kinematic analysis of brittle shear faults (Chapter 4 of

this thesis). Magnetic fabrics in the Chelmsford Formation indicate uniform NNW-SSE shortening (Fig. 5.1c). In the South Range SIC and adjacent Huronian rocks, shortening directions are orthogonal to the strike of the SIC basal contact (Fig. 5.1c). Here, the shortening directions change from NW-SE in the central and western South Range to N-S in the eastern South Range (Chapter 4). In Huronian rocks, some shortening directions are also observed to be E-W due to local strain perturbation (Chapter 4). Overall, however, shortening directions in the Sudbury Basin and Huronian rocks are oriented NW-SE and are, thus, parallel to the minimum diameter of the Sudbury Basin (Fig. 1c).

Previous attempts at quantifying the magnitude of NW-SE shortening are based on shape fabric analysis using deformed sedimentary concretions of the Chelmsford Formation (Clendenen, 1986), transformation of the Basin circumference into a circle (Muir, 1984), planar fabrics in the Onaping Formation (Rousell, 1975) and metamorphic mineral fabrics in the SRSZ (Shanks and Schwerdtner, 1991b). In the Chelmsford Formation, bulk NW-SE layer-parallel shortening is estimated to be at least 38%, with only minor shortening parallel to the long axis of the Sudbury Basin (Clendenen et al., 1988). Restoration of deformation on the SRSZ result in a NW-SE basin diameter that is larger than the current diameter by at least a factor of 2 to 3 (Shanks and Schwerdtner, 1991b). Both reconstructions estimate the original NW-SE diameter of the exposed portion of the SIC at approximately 60 km (Clendenen et al., 1988; Shanks and Schwerdtner, 1991b). The restoration attempts are, however, based on the assumption that deformation is homogeneous and that changes in contact dips are exclusively the result of solid-body rotation. Shearing-induced rotation of material surfaces, such as lithological contacts, bedding planes and primary planar mineral fabrics, is not considered in these studies, but is likely of considerable importance in the deformation of the South Range and adjacent Huronian rocks (Chapter 3 of this thesis). Nonetheless, NW-SE shortening significantly reduced the NW-SE diameter of the SIC in plan-view and acted as the main driving force in transforming the SIC to its current non-cylindrical shape.

In summary, key structural characteristics of the Sudbury Basin are its plan-view elliptical shape, variations in contact dips and thickness of the SIC, and strain that increases in intensity toward the SRSZ, a broad southward-dipping zone of ductile deformation. Moreover, the South Range differs markedly from the North Range by its steeper dip of SIC contacts and pervasive foliation. Due to these structural characteristics, it is unlikely that the Sudbury Basin formed under pure horizontal shortening and simple folding. Prominent faults imaged in seismic profiles and the geometry of mineral fabrics associated with the SRSZ point to deformation associated with thrusting and differential rotation of the SIC in the South Range. A basal fault and distributed deformation near the fault tip are typical for fault-propagation folding, specifically trishear deformation. This deformation mechanism will be tested for the South Range by means of forward and backward kinematic modelling.

5.4. *Trishear deformation*

The trishear model, initially proposed by Erslev (1991), describes folding of upper-crustal layers in front of a propagating thrust fault cutting through mid-crustal basement rocks. A main characteristic of trishear deformation is the transfer of localized displacement on a basal thrust

fault to distributed deformation and associated displacements within a triangular zone, the trishear zone (Fig. 5.2). More specifically, distributed deformation in the trishear zone is caused by displacement on a deeper-seated thrust fault and propagation of the tip of this fault (Erslev, 1991; Hardy and Ford, 1997; Allmendinger, 1998; Cardozo et al., 2003; Cristallini et al., 2004). Within the trishear zone, the shear strain vector varies both in orientation and magnitude. The magnitude of strain decreases from the top of the trishear zone toward the fault tip and from the centre of the trishear zone to its boundaries (Hardy and Ford, 1997). At the top of the trishear zone, local displacement magnitude equals the hanging wall slip, whereas there is no slip at the base of the trishear zone (Hardy and Ford, 1997; Allmendinger, 1998). This gradient in shear direction and magnitude of the slip results in a change in layer thickness and layer dips during progressive deformation and depends on position within the trishear zone.

The final geometry of layers deformed by trishear is the product of a number of parameters controlling trishear deformation (Allmendinger, 1998; Fig. 5.2a). These are the dip of the basal thrust fault (ramp angle α), apical angle of the trishear zone (trishear angle φ), magnitude of displacement on the thrust fault (d), ratio of fault propagation to fault slip (p/s), the position of the fault tip, and the symmetry of the trishear zone relative to the fault (angular offset *ao*). The angular offset is the factor that describes the angular position of the trishear zone relative to the orientation of the basal thrust fault (edge of the trishear zone = α ± φ·*ao*). For example, an *ao* of 0.5 would represent a trishear zone in which the basal fault is the symmetry plane of the trishear zone. The p/s ratio controls the forelimb geometry (Hardy and Ford, 1997). Low p/s ratios result in forelimb thickening and tight folding, whereas large p/s ratios generate large interlimb angles and small layer thicknesses (Allmendinger, 1998).

Displacement varies across the trishear zone and results in strain gradients within the zone (Hardy and Ford, 1997; Zehnder and Allmendinger, 2000). The trishear zone delimits an area of distributed shear, outside of which the hanging wall is translated without internal distortion (Fig. 5.2a). The magnitude of shear decreases away from the fault tip (Fig. 5.2b). Thus, the trishear zone is recognized by an abrupt decrease in internal deformation towards the hanging wall.
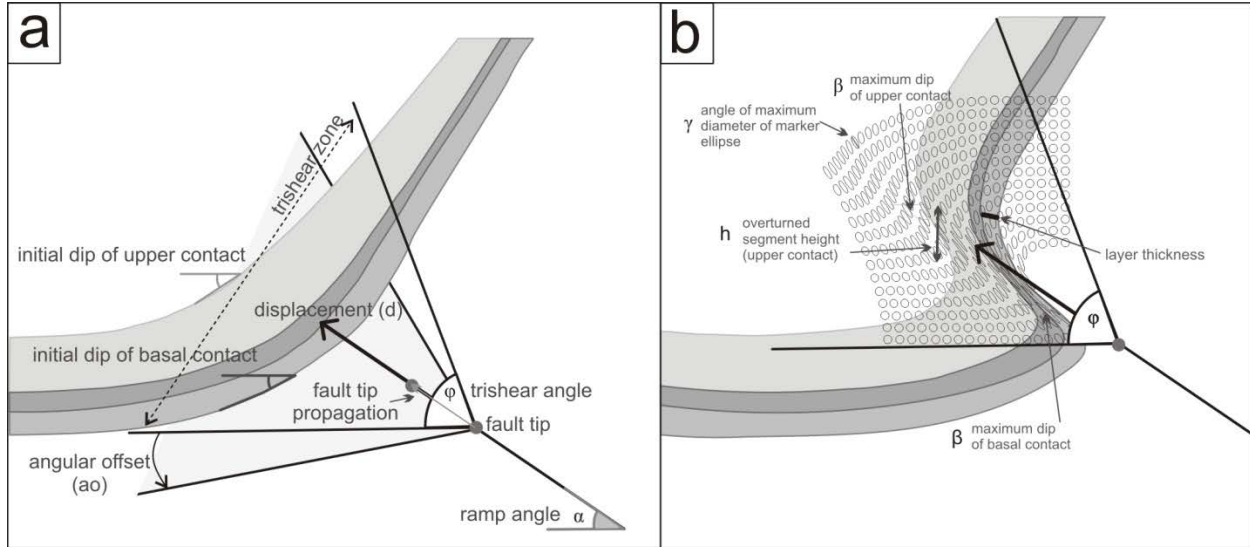
Figure 5.2: Characteristic elements of trishear deformation. (a) Key parameters that affect the outcome of trishear deformation are displacement magnitude d, trishear angle φ, ramp angle α, position of the fault tip, fault tip propagation, angular offset and the initial dips of material surfaces such as the lithological contacts. (b) Measured geometric parameters are the maximum dip β of lithological contacts after deformation, the height h of the overturned contact, orthogonal layer thickness and γ the orientation of maximum diameter in marker ellipses.

5.5. Methodology

In order to assess deformation quantities that influenced the geometry of the South Range SIC of the Sudbury Basin, we apply both forward and backward kinematic models of trishear deformation using the software *Move* (Midland Valley) and *FaultFoldForward* (Allmendinger, 1998; Zehnder and Allmendinger, 2000). In trishear deformation a number of models, based on different geometric parameters, can account for the geometry of a particular structure (Cardozo, 2005). Numerical search algorithms allow the calculation of specific deformation parameters using the deformed geometry of layers (Cardozo, 2005). We use foliation orientation and the dips of SIC contacts to constrain deformation geometry using a combination of forward and backward modeling.

For forward modeling, we assume an initial synclinal geometry of the Norite, Quartz Gabbro and Granophyre layers and analyze the effect of varying deformation parameters on the geometry of the deformed layers and strain distribution. The orthogonal thickness of each layer is derived from mean thicknesses of these layers in the North Range (Dreuse et al., 2010), as layer thicknesses in the North Range are more uniform than in the South Range (Fig. 5.1a). The initial dips of the layers vary, but paleomagnetic data from the Norite indicate a rather symmetric basin geometry of the SIC prior to (trishear) deformation, with basin margins dipping inward at approximately 20° (Morris, 1980).

For analysing the effects of trishear deformation in the forward models, we document geometric parameters that compare to structural data from the surface of the Sudbury Basin. Specifically, the boundary conditions from the SIC considered for the model include: the inclination of the

upper and basal contacts, the orientation of igneous layering and foliation, and thickness variations of the SIC layers (Table 5.1). Measured quantities from the forward models are the maximum amount of rotation of layer contacts, the height of an overturned layer segment, layer thickness and the orientation and geometry of marker ellipses (Fig. 5.2b). The maximum angle of a layer contact is characterised by a dip that deviates most from its original orientation, regardless of its location. The height of the overturned layer segment provides a marker for the vertical extent of distributed deformation and aids in the construction of profiles for backward modeling. Measurements of orthogonal thickness at different locations within the trishear zone document the thickness variation of layers. The inclination of long axes of initially circular markers provides a proxy for the orientation of sectional strain ellipses approximated by metamorphic foliations in nature. Altogether this procedure provides a test for the validity of trishear deformation for the southern SIC. It furnishes initial constraints on deformation magnitudes, the possible primary geometry of the SIC and its current shape at depth.

Backward kinematic modeling provides a tool for restoring of the current SIC geometry into a symmetrical basin with shallowly dipping layers. For this purpose, eight sections across the Sudbury Basin are constructed and restored to initially inward dipping contacts that are symmetrical to the North Range. In the sections, surface dips of the SIC contacts are extrapolated to depth and above the present erosion surface. To comply with trishear deformation geometry, hanging wall layers above the erosion surface in the South Range are assumed to have the same dip magnitude as layers in the North Range. The comparison of post-deformation angles of SIC contacts and the orientation of foliation show which areas were affected by specific combinations of rotation and strain geometry. Deformation quantities for best-fit SIC geometries are assembled to 3D models show the shape of the Basin prior to trishear deformation. Restoration of the South Range SIC aims at quantifying the along-strike variation in trishear deformation parameters.

5.6. Results

5.6.1. Forward modeling of geometric effects of trishear deformation

In the forward models I observe the change in geometry of markers in relation to the variation of deformation parameters. Parameters that are examined and which are of importance in the attempted geometric reconstruction of the South Range SIC are: the p/s ratio, trishear angle φ, magnitude of displacement d, angular offset of the trishear zone, ramp angle α and fault tip position (Fig. 5.2a). Collectively, these parameters affect the geometry of the layer contacts and the shear strain distribution. By examining each parameter individually, its general effect on the geometry of the deformed layers is assessed. The effects of the parameters on the deformed layers are quantified using geometric measurements that are observed in the Sudbury Basin, namely the dip of layer contacts and strain distribution (Fig. 5.2b).

First, I explore the effect of the original dip of the SIC layers on the orientation of the layers in the deformed state for different ramp angles (Fig. 5.3a, b). Layers in the models are initially of uniform dip, ranging from 5° to 50°, at which the layer dip is perpendicular to the thrust fault. Layers are rotated by varying amounts in the trishear zone and the maximum post-deformation dip of a layer contact is given by the angle β. Overturned layer contacts are indicated by β-values

greater than 90°. Fig. 5.3a shows that the deformed layer dip of the basal contact is rotated by up to 90° f the initial dip. The height of the contact segment that is overturned increases systematically with steeper initial dips (Fig. 5.3b). Interestingly, the initial layer dip has a more profound effect on the final geometry of the basal contact than on the upper contact, despite the fact that the upper contact is located further away from the fault tip than the basal contact (Fig. 5.3a, b). For example, the maximum dip of the upper contact does not change with varying initial layer dip (Fig. 5.3a). Finally, a reversal of the heights of the overturned contacts occurs for initial layer dips greater than 25° (Fig. 5.3b). For steep initial dips the height of the overturned contact segment is greater for the upper layer than the basal layer (Fig. 5.3b). This relationship reversed in initial low initial layer dips (Fig. 5.3b). Thus, trishear deformation of shallowly dipping layer contacts overturns a larger segment of the basal contact than of the upper contact.

The magnitude of displacement on the thrust fault has a profound influence on the orientation of layer contacts (Fig. 5.3c, d). The amount of rotation is indicated by the difference between the maximum and initial dip angles of a contact and increases with increasing displacement magnitudes (Fig. 5.3c). At larger displacement magnitudes, the rotation approximates a vertical orientation for the basal contact but is overturned by about 50° for the upper contact (Fig. 5.3d). The basal contact is not overturned under a small displacement magnitudes and the height of the overturned upper contact increases linearly with the displacement magnitude (Fig. 5.3d). The effect of displacement magnitude on the final contact orientation is also related to the location of the fault tip. Shifting the position of the fault tip away from the contacts significantly affects the height of the overturned segments (Fig. 5.3e).

Variations in the apical angle of the trishear zone have little effect on the geometry of the deformed layers (Fig. 5.3f). The height of the overturned contact segment is slightly higher for small φ values (Fig. 5.3f). The effect on the maximum contact dip by increasing in the p/s ratio matches the effect of increasing the initial layer dip: the dip of the basal contact increases systematically and the dip of the upper contact shows little variation (Fig. 5.3a, g). The height of the overturned contact segment, however, increases as p/s ratios increase towards 1 (Fig. 5.3h). Overall, the p/s ratio has little effect on the geometry of the upper contact and mainly influences the dip of the basal contact.

Changes in the dip of the ramp angle α result in a systematic shift in the observed layer geometries (Fig. 5.3). Shallow ramp angles are marked by a small height of overturned upper and basal layers (Fig. 5.3b, d, e, f, h). The effect of the fault dip on the magnitude of layer rotation is overall small (Fig. 5.3a, c, g). Interestingly, faults dipping at a shallow angle result in a greater difference of maximum rotation between the basal and the upper layer than moderately dipping faults (Fig. 5.3a, c, g). The varying dips of the thrust fault affect the basal and the upper layer contact to an equal degree.

In addition to the geometry of layer contacts, the effect of trishear deformation can be examined with respect to orthogonal layer thickness. This is inspected with an initially inclined stack of three layers, akin to the Main Mass of the SIC, that is subjected to relative thickness variations, which depend on the position of the layers within the trishear zone and the displacement magnitude (Fig. 5.4). In the trishear zone the maximum and minimum orthogonal layer thickness are documented and placed in relation to the original thickness, providing a measure for

thickening and thinning of layers. The basal layer that is closest to the fault tip shows the largest thickness variation (Fig. 5.4a). Large amounts of thickening occur at low ramp angles (Fig. 5.4a), and layers are characterized by the least thickness at large ramp angles (Fig. 5.4a). The intermediate and upper layers increase in thickness as displacement on the fault becomes maximal (Fig. 5.4b, c). For the upper layer, the thickness variation is less pronounced than in the lower layers that are closer to the fault tip and thickening appears independent of the ramp angle (Fig. 5.4c). Overall, the effect of trishear deformation on the layer thickness decreases with distance to the fault tip.

Sectional strain of trishear deformation is documented along selected profiles and visualized by the long axis orientation of initially circular markers (Fig. 5.5). As metamorphic foliations are concordant to the XY-planes of strain ellipsoids (Passchier and Trouw, 2006), the long axes of marker ellipses γ portray the dips of foliation surfaces. This allows us to study the effects of the deformation parameters d, φ, p/s, and α and initial layer dips on the distortion of layers using marker ellipses as proxies along a given profile. In the forward models we document marker ellipse geometries at varying horizontal distances and at one structural level, located at a constant height above the fault tip (Fig. 5.5a). Across the trishear zone the maximum diameter of the marker ellipse is inclined both in the direction of ($\gamma < 90°$) and away from ($\gamma > 90°$) the direction of the thrust fault (Fig. 5.5a).

Large displacement magnitudes result in a narrow zone of rotated marker ellipses, characterized by steeply inclined maximum diameters (Fig. 5.5b) and steeper ramp angles result in steeper maximum diameters (Fig. 5.5c). The trishear angle directly affects the width of the deformed zone of rocks (Fig. 5.5d) and high p/s-ratios cause maximum diameters to be steeper and confined to narrower zones (Fig. 5.5e). Models with initially low layer dips show a more distributed area of deformation (Fig. 5.5f), i.e., a wider area marked by small amounts of rotation of elliptical markers. The largest variations in orientation of the elliptical markers are observed in models with high p/s-ratios and steep ramp angles (Fig. 5.5c, e).

In summary, the effects of trishear deformation are described by combinations of trishear parameters. This means that a change in layer geometry is not the result of a unique set of parameters and can be accounted for by a number of solutions. Nonetheless, the following key results are evident from forward modelling of an initially synformal SIC. Steepening and overturning of layer contacts are accompanied by low dips of foliation planes, i.e., higher shear strains, evident by the orientation of the maximum diameter of elliptical markers. Furthermore, shear strains increase towards the hanging wall and layers affected by high shear strains display lower orthogonal thicknesses. The results of the forward models can, thus, crudely constrain the magnitude and geometry of post-impact deformation of the SIC.
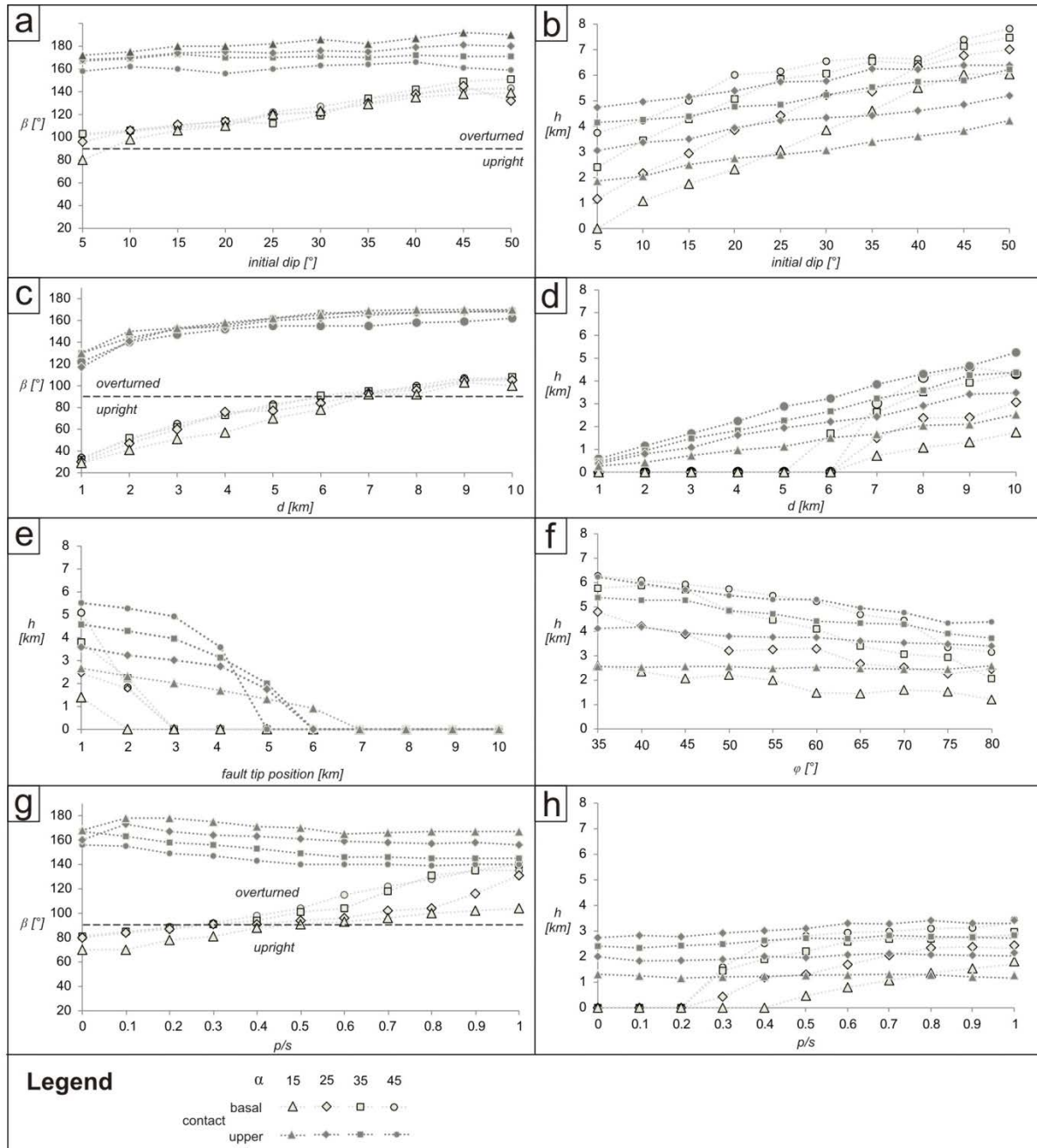
Figure 5.3: Effect of trishear parameters on the geometry of the deformed layers. The diagrams show the progressive variation of specific combinations of deformation parameters for the basal and upper contacts of a marker layer at four different ramp angles α. Note that the basal contact of the marker layer is closer to the fault tip than the upper contact. Unless specified otherwise, model parameter are 10 km displacement, 0.5 angular offset, 70° trishear angle, a propagation-to-slip ratio of 0, a fault tip position of 0. (a) Initial dip of a contact versus the height h of the overturned contact and (b) the maximum dip β of layer contacts. Magnitude of displacement d is displayed in relation to (c) the height h of overturned contact and (d) the maximum dip β of layer contact. (e) Fault tip position versus the height h of overturned contact. (f) Magnitude of trishear angle φ versus height h of overturned contact. Propagation-to-slip (p/s) ratio is displayed against (g) the height h of overturned contact and (h) the maximum dip β of layer contact.
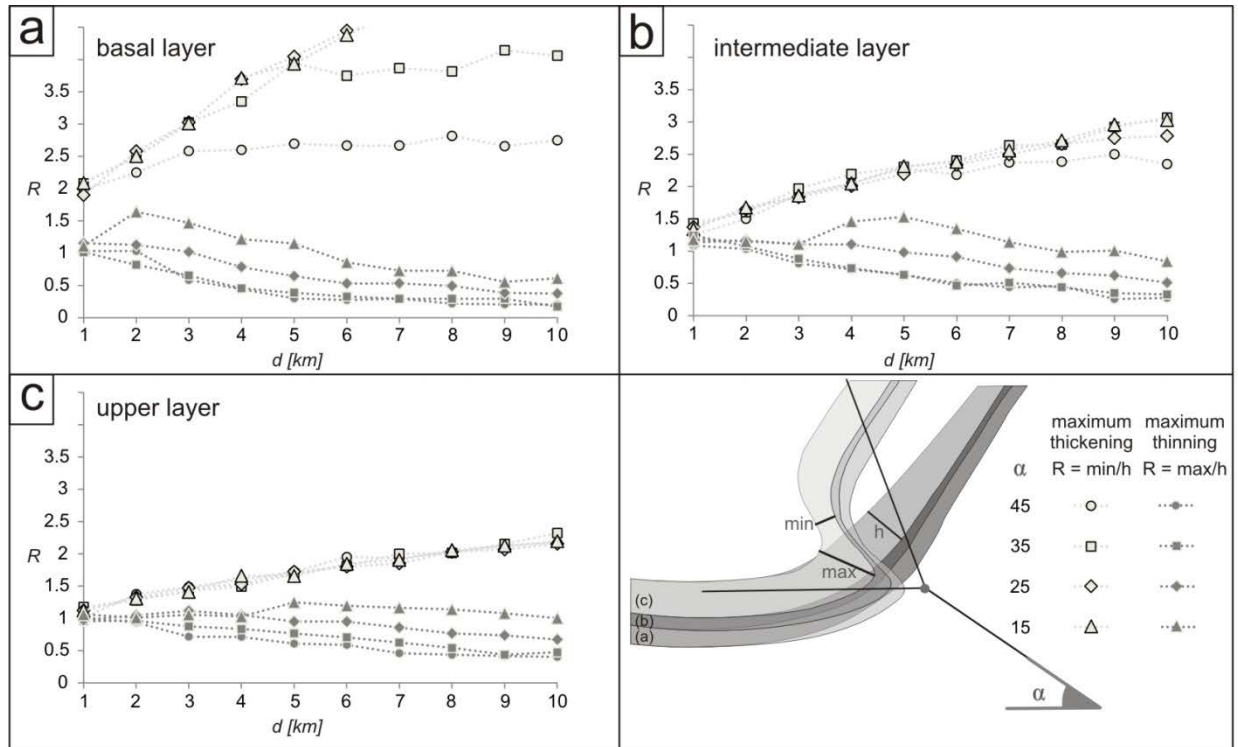
Figure 5.4: Thickness variations in a three-tiered layer stratigraphy after trishear deformation. Maximum and minimum thinning are recorded for (a) a basal layer, (b) an intermediate layer and (c) an upper layer. Thickness variations are from a forward model with d = 4 km, α = 35°, φ = 70°, p/s = 0.5, angular offset = 0.5, and a fault tip = 0 km. R represents the ratio of the layer thickness after and prior to deformation. It is calculated by the relation of the minimum orthogonal thickness min and maximum orthogonal thickness max, respectively, to the original layer thickness h.
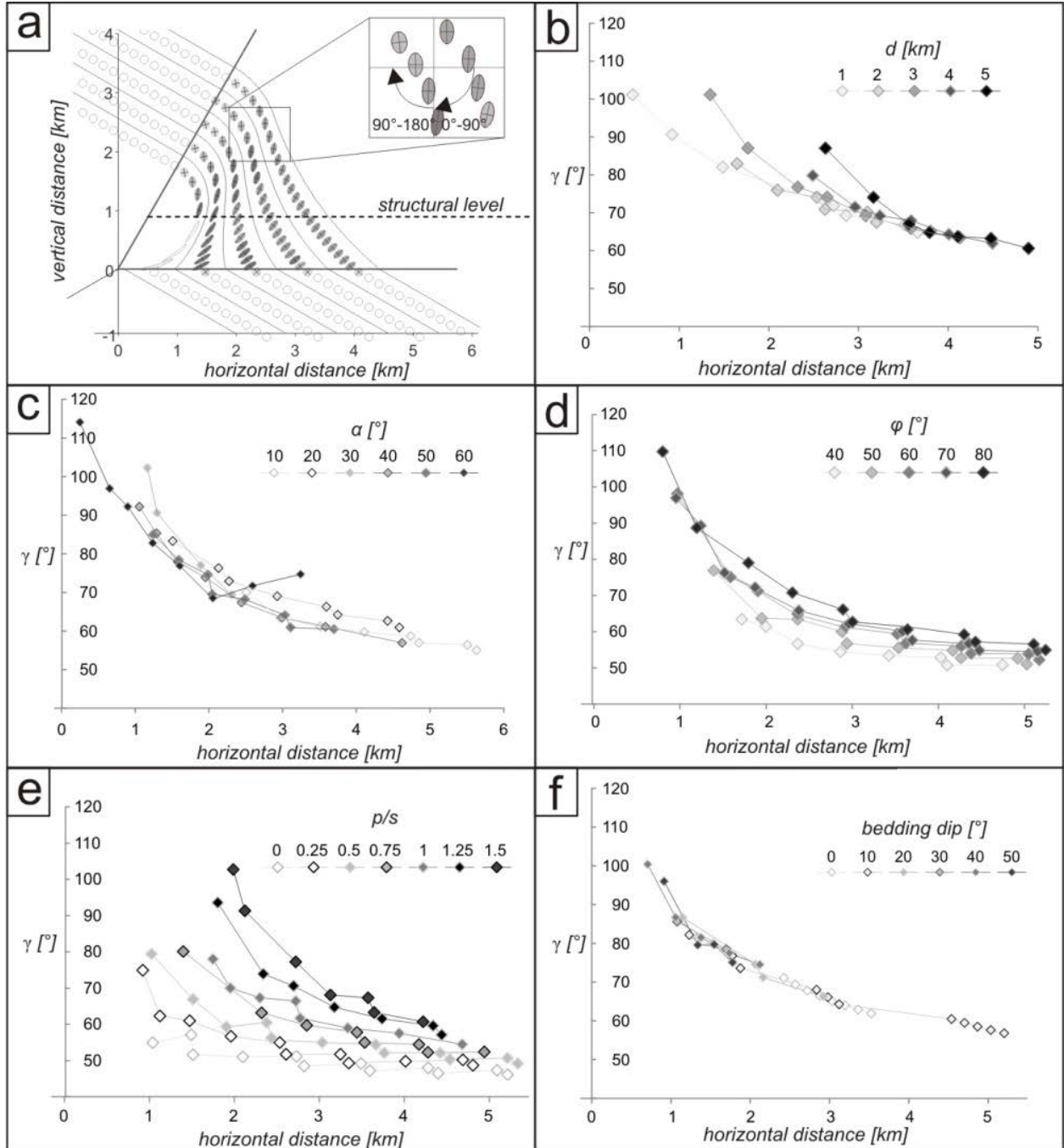
Figure 5.5: Forward models of trishear deformation showing the effects of selected parameters on the inclination of marker ellipse diameters (γ). (a) Reference frame for measurements of γ. The origin for the horizontal distance coincides with the position of the fault tip. Angles of maximum diameters are measured across one observation level (inset). The deformation parameters are: (b) displacement d, (c) ramp angle α, (d) trishear angle φ, (e) p/s ratio, and (f) initial bedding dip. Unless otherwise specified, the deformation parameters are d = 2 km, α = 30°, φ = 60°, p/s = 0.5, angular offset = 0.5 and an initial bedding dip of 30°.

5.6.2. Attempted restoration of the South Range SIC using the trishear deformation model

In section 5.6.1 I showed that a number of deformation parameters have significant effects on the geometry of the deformed layers and strain profiles. Understanding these effects aids in kinematically restoring the Sudbury Basin using the trishear deformation model. In order to satisfy the along-strike variations in deformation parameters of the South Range SIC, seven NE-SW striking profiles and one N-S striking profile (Fig. 5.6a, b) are constructed. The NE-SW striking profiles are parallel to the overall shortening direction (Fig. 5.1c) and at a high angle to the basal SIC contact (Fig. 5.6a). The N-S striking profile (profile VII in Fig. 5.6a) is positioned orthogonal to the strike of SIC in the eastern South Range (Fig. 5.6b). The orientation of basal faults, dipping approximately 30° to the SE, is based on the discontinuities imaged in the seismic profiles.

The North Range SIC does not feature structures induced by pervasive strain and, therefore, likely retained its primary orientation and thickness. For this reason, the northwestern profile portions, representing the North Range, are spatially pinned in all models. The layer contacts in the South Range are extrapolated upwards beyond the current erosion surface and, based on the geometry of the North Range SIC, the contacts are assumed to be gently dipping northward. This contact geometry is also justified by the forward models, which affected only the layer portions located close to the fault tip and which do not cause substantial rotation outside the trishear zone.

The sections across the SIC are restored by backward modeling, using a ramp angle of 30° and varying the quantities of d, p/s, φ, fault tip position and angular offset. For each profile, the selection of the model is based on the combination of deformation parameters that results in a restored geometry that shows the most plausible match with an initially gently inward dipping syncline. The restored layer contacts of four models for each section are displayed in Fig. 5.6a. Multiple models are displayed for each section to indicate that restoration solutions are non-unique and different combinations of deformation parameters can lead to similar geometries of restored layers. Values of displacement, p/s ratio, trishear angle, fault tip position, and angular offset are similar for different iterations on each section. Magnitudes of displacement on the basal fault are between 2.5 and 9 km (Fig. 5.6c), the p/s ratio varies from 0 to 0.8 (Fig. 5.6d), the trishear angle ranges from 45° to 72° (Fig. 5.6e), the position of the fault tip lies between 3 and 6 km from the intersection of the basal SIC with the fault (Fig. 5.6f; excluding profile VIII) and the angular offset values lie within 0.4 and 0.6 (Fig. 5.6g). These values show significant variations among the sections.

Along-strike variations in deformation are especially apparent in the p/s ratio, trishear angle and the displacement. From W to E, the displacement on the SE-dipping thrust faults first increases in profiles I to IV, then decreases in profiles V and VI, and finally increases again in profiles VII and VIII (Fig. 5.6c). The p/s ratio is at its maximum in the central South Range (profiles IV and V), the position of which coincides with an inward concave geometry of the upper SIC contact (Fig. 5.6b, d). Similarly, the trishear angle increases towards the central South Range and decreases toward the eastern South Range (Fig. 5.6e). The position of the fault tip decreases in distance towards the central South Range and is farthest from the base of the SIC in the SE-lobe (Fig. 5.6f). The symmetry of the trishear zone is depicted by the angular offset of the trishear zone in relation to the thrust fault, and shows little variation from W to E (Fig. 5.6g). In

summary, the rocks in the eastern South Range are most likely affected by a narrower zone of deformation, lower p/s ratios, and higher displacement magnitudes than those of the western South Range. Deformation in the central South Range is marked by the highest p/s ratios, large displacement magnitude and a wide shear zone.

Figure 5.6 (following page): Backward models of selected sections across the Sudbury Basin. (a) NW-SE striking sections show current geometry and four restored shapes of SIC contacts. The geometry of SIC layers is extrapolated over the erosion level and is based on the dip magnitudes of the SIC in the North Range and the assumption that only a portion of the South Range is affected by rotation of SIC contacts. (b) Sections I-VI and VIII strike parallel to the minimum plan-view diameter of the Basin, section VII strikes orthogonal to the basal SIC contact. Variations of deformation parameters in each of the restored sections: (c) displacement d, (d) p/s ratio, (e) trishear angle φ, (f) distance of fault tip from intersection between fault and base of the SIC, and (g) angular offset of trishear zone. Deformation parameters used in constructing the restored sections are listed in Table 6.2.
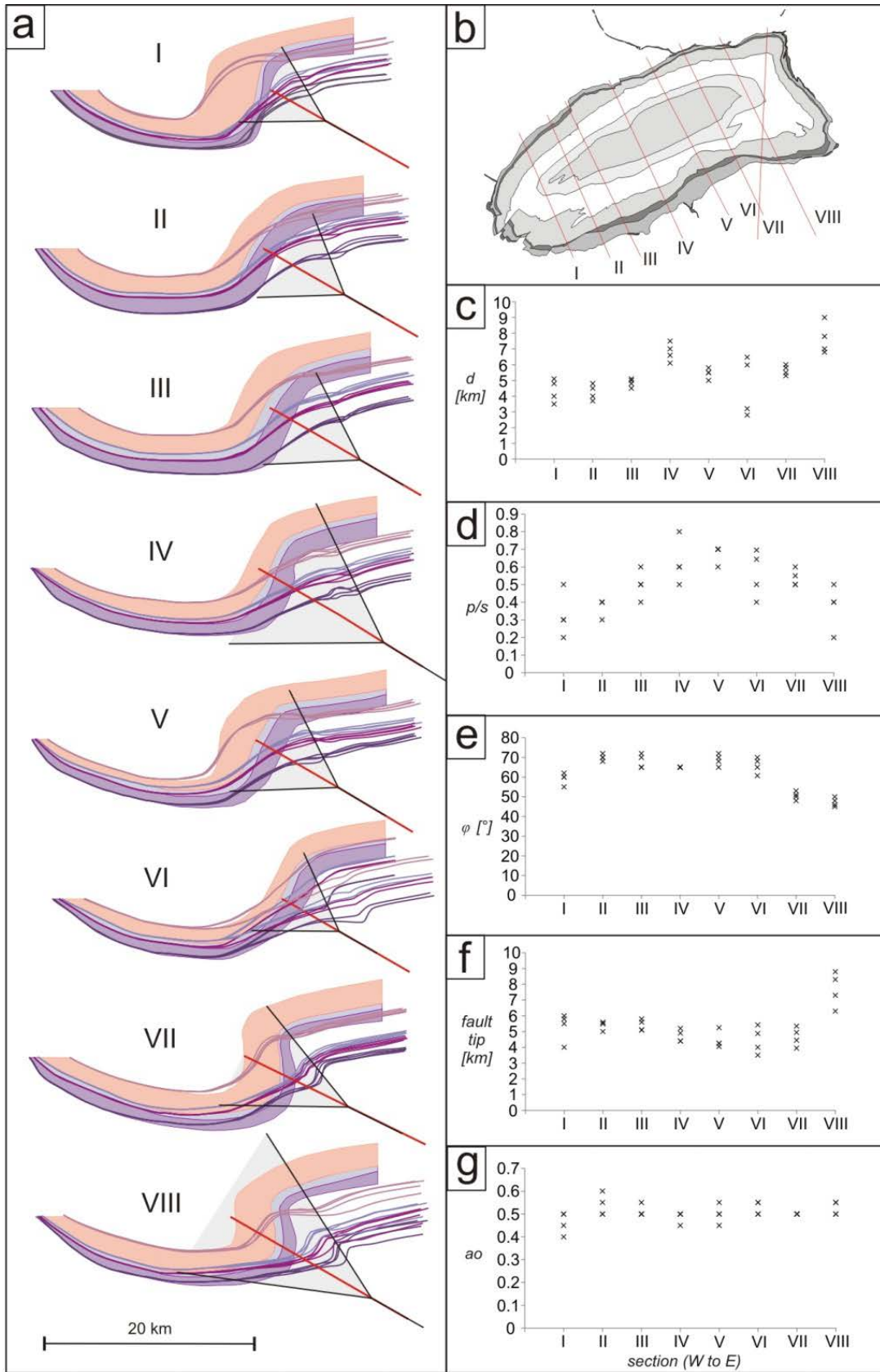
The three-dimensional geometry of the restored Sudbury Basin is characterized by the synclinal shape of the backward models. Based on the restoration, deformation is compatible with displacement on a thrust fault dipping approximately 30° to the SE. Large displacement magnitudes and p/s ratios in the central South Range lead to a restored shape of the SIC that is convex outward rather than concave inwards as it is today (Fig. 5.7). The length of the NW-SE diameter of the restored Basin, i.e., presently exposed perimeter of the SIC, at the current erosion surface amounts to 35 km. Backward modelling of the Basin shows that the SIC most likely had a synclinal shape (Fig. 5.7) caused by some non-cylindrical folding prior to trishear deformation.

Section*	North Range** contact dip [°]			South Range*** contact dip [°]			dip of igneous layering [°]	average foliation dip [°]			
	Base SIC	Base GP	Base OF	Base SIC	Base GP	Base OF		Norite	QG	GP	OF
I	44	53	47	75	n/a	10	n/a	115	106	110	121
II	50	54	26	50	17	9	n/a	89	105	117	117
III	49	54	24	50	18	12	45	125 & 65	102	125	125
IV	40	n/a	n/a	77	41	n/a	68	77	86	120	117
V	37	68	31	45	35	123	70	n/a	75	114	111
VI	35	45	20	120	45	48	70	69	91	135	131
VII	48	45	37	96	n/a	112	110	100	106	101	103
VIII	38	41	37	96	138	113	110	79	95	106	107

GP = Granophyre, OF = Onaping Formation, QG = Quartz Gabbro

* Locations of sections are displayed in Figure 6a.

** Contact dips to the SE.

*** Contact dips to the NW, values >90° are overturned to the SE.

Table 5.1: Inclination of planar elements of the SIC.

Section	Displace- ment	Trishear Angle	Angle Offset	Propaga- tion/Slip Ratio	Fault Tip Position	Ramp Angle
#	d [m]	φ [°]	ao	p/s	t [m]	α [°]
I	4000	60	0.5	0.5	4000	30
	3500	60	0.5	0.3	5500	30
	5100	62	0.4	0.2	6000	30
	4800	55	0.45	0.3	5800	30
II	4000	70	0.55	0.4	7000	30
	4500	70	0.6	0.4	7000	30
	4800	72	0.5	0.4	7100	30
	3700	68	0.5	0.3	6500	30
III	4500	65	0.5	0.6	7500	30
	5000	70	0.5	0.5	8000	30
	5100	72	0.55	0.4	8200	30
	4800	65	0.5	0.5	7500	30
IV	7000	65	0.5	0.8	8000	30
	7500	65	0.5	0.6	8000	30
	6100	65	0.5	0.6	8500	30
	6600	65	0.45	0.5	8800	30
V	5000	65	0.5	0.7	7000	30
	5500	70	0.5	0.7	8000	30
	5500	72	0.45	0.6	6800	30
	5800	68	0.55	0.7	7000	30
VI	6500	60	0.5	0.7	7000	30
	6000	65	0.5	0.65	7500	30
	3200	68	0.55	0.5	5000	30
	2800	70	0.55	0.4	5500	30
VII	6000	50	0.5	0.5	10000	30
	5300	53	0.5	0.5	9000	30
	5800	51	0.5	0.6	9500	30
	5500	48	0.5	0.55	10400	30
VII	9000	50	0.55	0.2	15000	30
	6800	45	0.55	0.5	13000	30
	7000	48	0.5	0.4	14000	30
	7800	46	0.5	0.4	15500	30

Table 5.2: Deformation parameters used for section restoration in Figure 5.6.
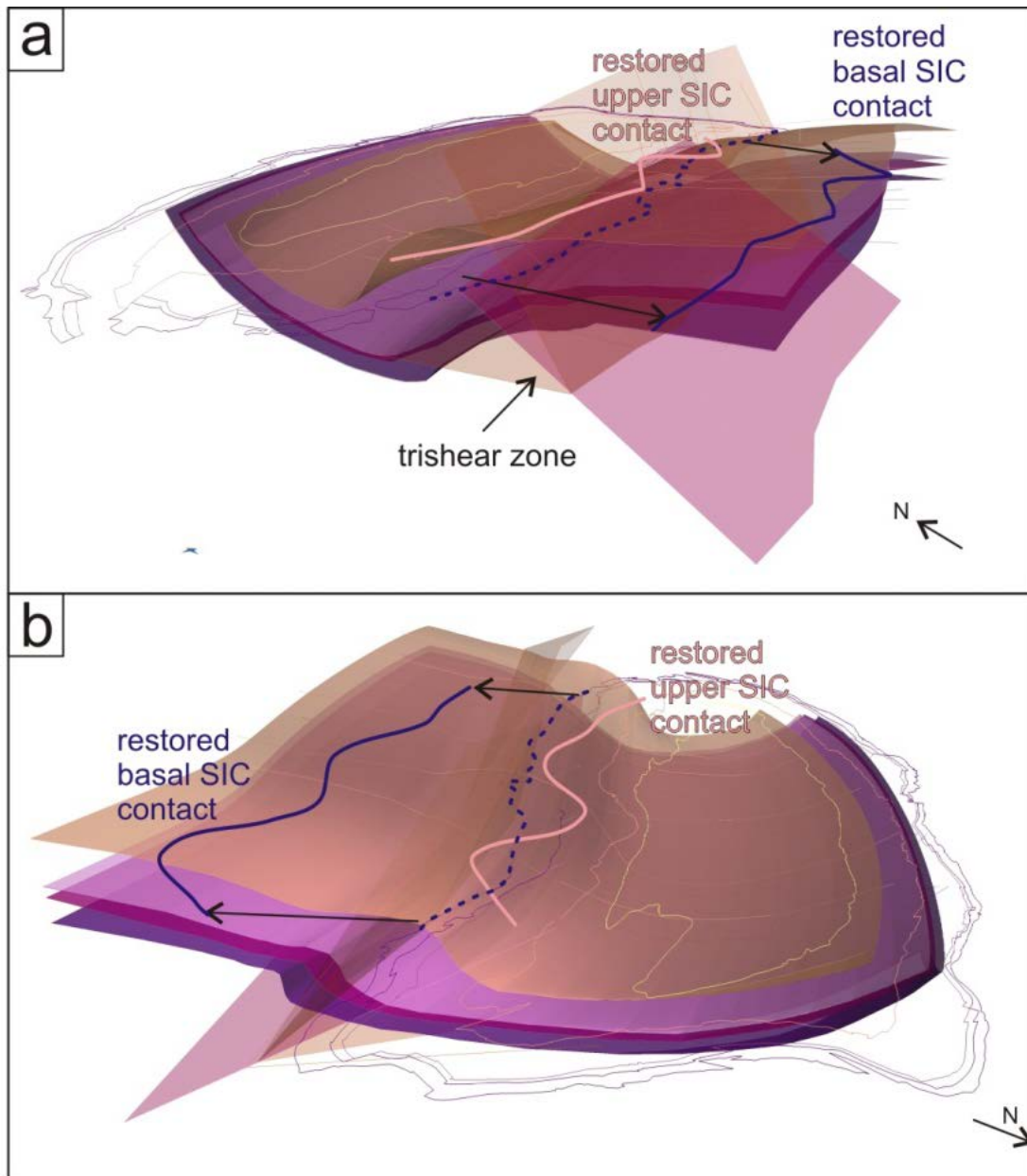
Figure 5.7: 3D geometry of the restored SIC based on backward kinematic modelling. The trishear zone is delimited by red surfaces. The restored SIC shows the original convex outward geometry and the change in length NW-SE diameter of the Basin. Lines indicate the location of the restored basal and upper SIC contact at the erosion level of the current SIC.

5.7.   Discussion

5.7.1. Comparison of forward models with observed structural characteristics of the SIC

To investigate whether the modeled layer geometries adequately represent the deformed SIC, I compared structural data acquired at surface to modelled geometries. In particular, the orientation of foliation planes and SIC contacts indicate principal strain directions and rotational components, respectively. To document the relationship between rotation and strain quantities, I analyze stations from the South Range SIC at which both contact dip and foliation orientation are known (Fig. 8a). From a trishear forward model I record the orientations of deformed layer contacts and the orientations of the maximum diameter of marker ellipses at that location (Fig. 8b). This allows me to correlate the rotation of material planes and strain orientation in the trishear deformation models and the South Range SIC.

At locations in the South Range SIC where both foliation and contact orientations are known, these quantities show a positive correlation (Fig. 5.8a). Specifically, in places where SIC layers dip chiefly towards the SE, foliation planes also dip to the SE (Fig. 5.8a). Notably the foliation in the Onaping Formation and its basal contact dip predominantly to the SE (Fig. 5.8a). In the forward models, the inclination of marker ellipses and layer contacts are marked by a relationship that is strikingly similar to that observed in the SIC (Fig. 5.8b). Evidently, a change in contact orientation corresponds to a change in the strain geometry, represented by the maximum diameter of the marker ellipses. Interestingly, dips of both maximum ellipse diameter and layer contacts in the forward model and foliation and layer dips in the SIC cover a similar range of magnitude (Fig. 8). The similarity in the orientation of planar elements and strain supports the initial assumption that trishear deformation can account for a number of observed structural characteristics of the South Range SIC.

The changes in dip of foliation and SIC contacts at a given profile across the southern Sudbury Basin also provide a test for the validity of the trishear deformation model for the SIC. Shear strain in the forward models is estimated from initially circular markers and changes in the inclination of marker ellipses γ are affected by variations in the deformation parameters, such as *d*, p/s, φ, *ao* and α (Fig. 5.5). In each of the forward models, maximum ellipse diameters are inclined steeply adjacent to the undeformed hanging wall (Fig. 5.5). The inclination of γ decreases gradually across the trishear zone toward the undeformed footwall. In the Sudbury Basin, the dip of foliations at selected profiles shows a similar pattern from the Basin centre toward the SIC (Figs. 5.1, 5.9a). Towards the Basin centre, and thus at a large distance from the basal SIC contact, foliations dip mostly at 80° to the SE (Figs. 5.1, 5.9a). Towards the upper contacts of the SIC, i.e., the left margin of the stippled box in Fig. 5.9a, and in an area marked by the SRSZ the foliation dips decrease to an average of 60° to the SE (Fig. 5.9a). At the base of the SIC, i.e., the right margin of stippled box in Fig. 5.9a, foliation planes are rather steep and are sporadically dipping toward the NW (Fig. 5.9a). This gradual decrease in dip of foliation and maximum diameters of marker ellipses, and the sharp reversal of dip direction is observed both in the forward models and in nature. High amounts of rotation of the marker ellipses in the trishear zone match the orientation of foliation in the SRSZ (Fig. 5.9). Shear strain profiles in forward deformation models and from the SIC indicates that both show gradual increases and

abrupt decreases in the orientation of strain markers. Therefore, trishear deformation accounts well for the fabric orientations observed in the South Range SIC.
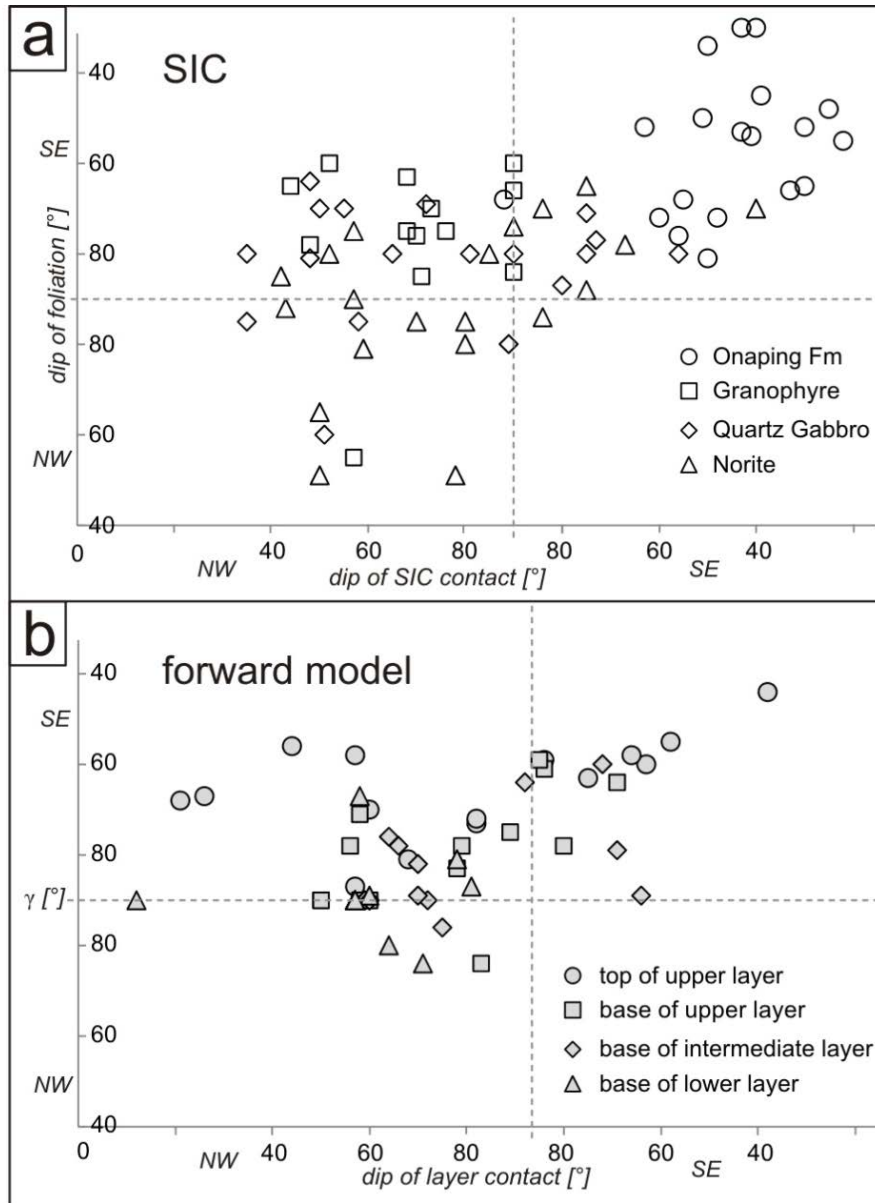
Figure 5.8: Comparison of surface data from the SIC with forward modeled quantities. (a) Dip of SIC contacts versus dip of foliations at the same location from sections across the South Range SIC. (b) Dip of layer contacts versus dip of maximum of elliptical marker γ at the same location in trishear forward model.
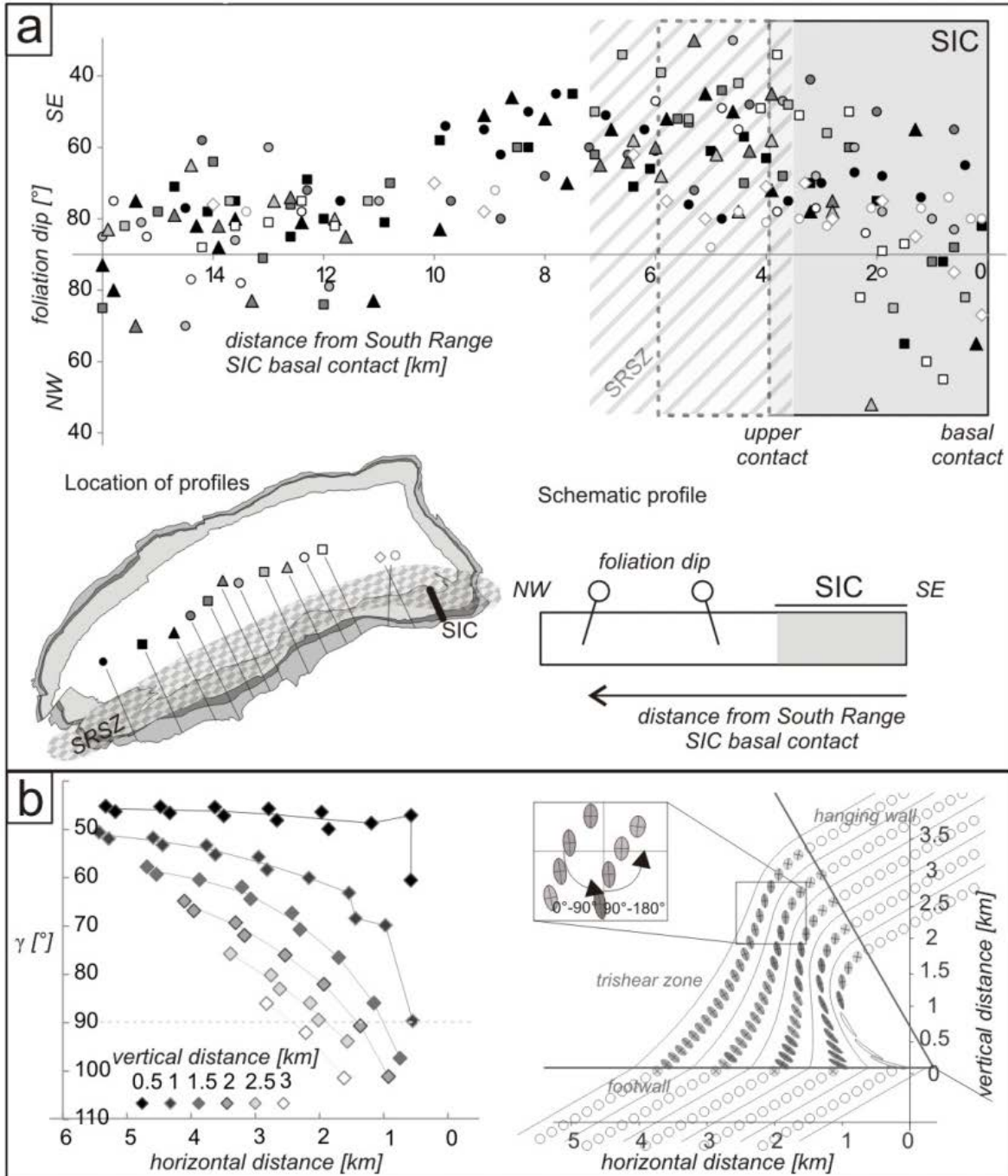
Figure 5.9: Geometric correlation of foliation dips of the SIC with marker ellipses of trishear forward models. (a) Variation of foliation dips with distance to basal SIC contact on selected profiles across the SIC. The horizontal axis marks the distance from the basal SIC contact towards the NW. Data points are values derived from the profiles. The shaded box indicates the plan-view extent of the SIC, the size of which varies according to thickness variations of the SIC along strike of the South Range. Striped area denotes location of SRSZ. (b) Dips of maximum diameters of marker ellipses at specific structural levels of the trishear zone. The dip of maximum diameters γ is plotted according to horizontal distance for each structural level. Schematic diagram of trishear zone shows location of deformed ellipses. Parameters used for forward model are d = 1, φ = 60, α = 30, p/s = 0.5.

5.7.2. Correlation of current erosion surface with level within trishear zone

In order to determine which structural level in the trishear zone corresponds to the current erosion surface of the South Range SIC, I compare the orientations of elliptical markers and contacts in forward models with the orientations of foliations (Fig. 5.9) and contacts (Fig. 5.10) of the SIC. A correlation of the observed structures of the South Range SIC with a particular structural level of the trishear zone is further achieved by analyzing the changes in the marker ellipse orientations at selected structural levels (Fig. 5.9). In general, the variation in the orientation of marker ellipses is minimal near the fault tip but increases with distance from the tip (Fig. 5.9b).

Examination of the changes in foliation and contact dips in the SIC provides information on the geometry of its individual layers, namely the Norite, Quartz Gabbro and Granophyre. This is achieved by plotting contact dips versus their along-strike position, which highlights the changes in dip magnitudes of the SIC layers along the South Range (Fig. 5.10b). Similarly, means of foliation dips acquired from the same locations as the contact dips show respective along-strike variations of the South Range (Fig. 5.10c). Based on the patterns of contact and foliation dips the South Range can be divided into three zones, Zones 1, 2 and 3, of similar dips of these planar elements (Fig. 5.10a).

In the western South Range (Zone 2 in Fig. 5.10a, b), dips of the Quartz Gabbro and Granophyre bases are rather shallow, the Norite base dips steeply and the base of the Onaping Formation is overturned to the SE. The central South Range (Zone 1 in Fig. 5.10a, b) is marked by shallow NW-dips of the base of the Norite, steep dips of the base of the Granophyre and shallow SE-dips of the base of the Onaping Formation (Fig. 5.10b). This zone shows moderately to steeply NW-dipping foliations in the Norite, subvertical foliations in the Quartz Gabbro and Granophyre and SE-dipping foliations in the Onaping Formation (Fig. 5.10c). In the westernmost South Range (Zone 3 in Fig. 5.10c), foliations dip at 60° to 80° toward the SE and, thus, show little variation in orientation. Overall SIC contacts are rarely concordant to each other in the South Range, unlike SIC contacts in the North Range. This indicates that material planes in the South Range SIC were affected by heterogeneous deformation, notably rotation. This is corroborated by the systematic variation in foliation dips across SIC layers.

In the forward models, the observed change in contact dip from the upper to the basal layer differs systematically with regard to the structural level in the trishear zone (Fig. 5.10a). Layer contacts are overturned at low levels in the trishear zone and steepen towards the hanging wall (Fig. 5.10d), where layers maintain their original dip. The footwall of the trishear zone is also characterized by little rotation of the upper layer contact and steepening of the basal layer, without affecting the upper layer (Fig. 5.10d). This pattern in layer contact dip is observed in the western South Range, i.e., Zone 2, in which the base of the Norite is steeply dipping and the other SIC layers dip gently inward (Fig. 5.10a, b, d). Steep dips of the basal layer and overturned upper layers are found at the erosion level of the central portion of the trishear zone (Fig. 5.10a, d). This pattern in contact dips is evident from the central South Range, i.e., Zone 1, where the base of the Onaping Formation is overturned to the S and the base of the Norite dips steeply NW (Figs. 5.1a, 5.10b).

Across the trishear zone the maximum diameters of marker ellipses dip shallower in the basal layer than in the upper layers (Fig. 5.10e). In Zone 1, maximum diameters dip shallowly in the upper layers and are steep in the basal layer (Fig. 5.10e). This matches the observed foliation dip pattern in the SIC, in which foliations are shallower in the Onaping Formation and Granophyre than in the Quartz Gabbro and Norite (Figs. 5.1a; 5.10c). The geometry of the SIC contacts and the orientations of principal strain axes, thus, vary significantly with structural level evident in the forward models (Fig. 5.10).

The dips of the SIC contacts and foliation vary considerably along strike in the South Range. However, not all combinations of contact and foliation dips can be accounted for by trishear deformation. For example, the western South Range shows SIC contact dips that are typical for the lower levels of the trishear zone (Box 2 in Fig. 5.10b, d). However, the foliation dips in this area do not match with the marker ellipse orientations observed at the respective level in the trishear zone (Fig. 5.10c, e). Likewise, in the SE-lobe of the Sudbury Basin (Zone 3 in Fig. 5.10) the foliation geometry deviates from all marker ellipse orientations of forward models. This calls for a different deformation mechanism for the SE-lobe. The axial-planar geometry of the foliations with respect to the curvature of SIC contacts is similar to that of the NE-lobe (Klimczak et al., 2007) and points to a fold origin of the SE-lobe.

The central South Range matches the structural characteristics of upper structural levels of Zone 1 in the trishear forward models (Fig. 5.10). Here the upper layer, represented by the contact between the Granophyre and the Onaping Formation, dips to the SE but the basal layers dip toward the NW (Fig. 5.10a, c). Foliations dip shallowly to the SE in the Granophyre and steepen towards the underlying Quartz Gabbro and Norite (Fig. 5.10b, d). Therefore, deformation in the center of the South Range is best described by trishear fault propagation folding and the lateral tips of the South Range are more likely to be influenced by other deformation mechanisms, such as folding strain.

Foliations in the South Range are most pervasive in the upper layers of the SIC, namely in the South Range Shear Zone (Fig. 5.1a). The SRSZ is characterized by uniformly SE-dipping foliation planes and pervasive metamorphic mineral fabrics (Fig. 5.1a, 9a). Similarly, the orientation of marker ellipses in the upper layers of the forward models (Fig. 5.10e) dip at a shallow angle in the direction of the fault. I propose that pattern observed in the SRSZ represents the central part of the trishear zone and that pervasive development of foliation surfaces in the SRSZ is a consequence of trishear fault propagation folding (Fig. 5.12).
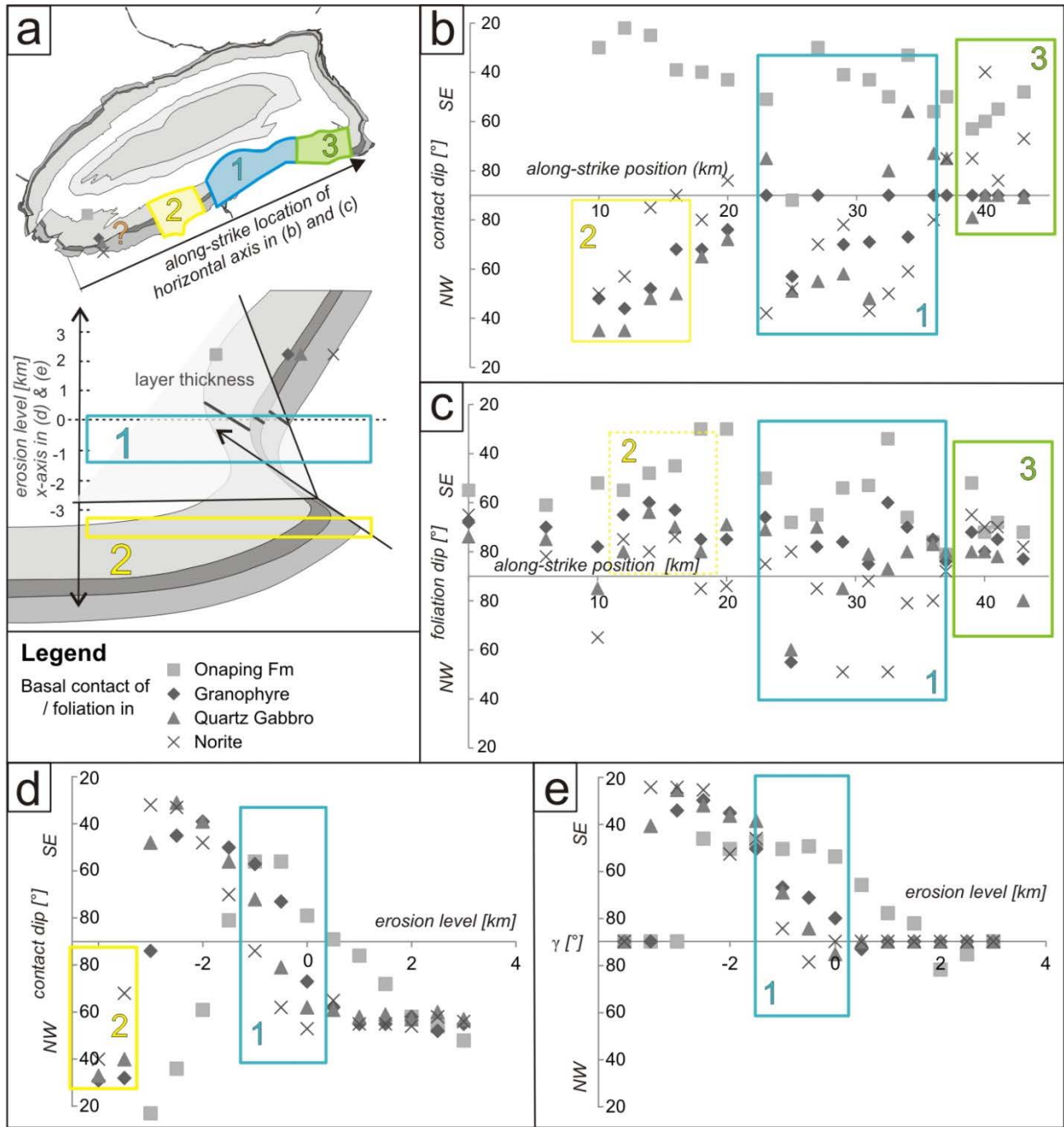
Figure 5.10: Comparison of variation in layer and foliation dip between upper and basal layers in the SIC and in forward models. (a) Location of the Zones 1, 2 and 3 characterized by similar dip magnitudes in relation to the trishear zone and in the Sudbury Basin. Orientations of layer dips and strain fabrics at several structural levels in the forward models, (b) and (c), and in the SIC, (c) and (d). Layers in the forward models are labelled with the units of the SIC for easier comparison. Strain fabric orientation is given by foliation dip for the SIC and by the dip of the maximum diameter of marker ellipses γ in the forward models. The horizontal axis in (b) and (c) marks the position of each data point respective to the southeastern-most point of the SIC basal contact as shown in (a).
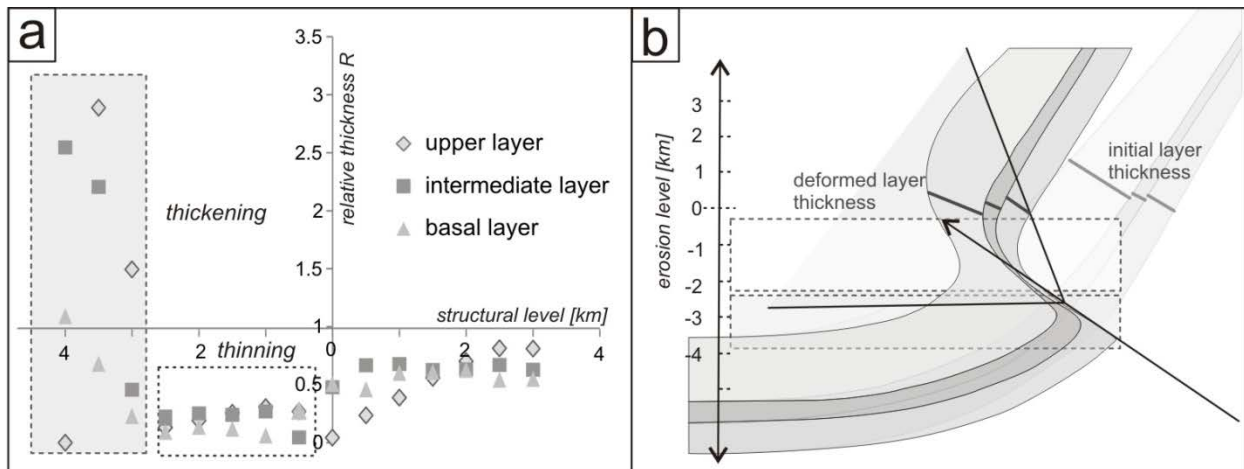
Figure 5.11: Variations in orthogonal thickness of a deformed layer at different structural levels of the trishear zone. (a) R is the orthogonal layer thickness after deformation with respect to its original thickness. Horizontal axis crosses at R=1, which denotes no thickness change. Grey box denotes area in which layers are thickened. The white box marks an area of maximum thinning. (b) Location of measured parameters and areas of thickening and thinning relative to the trishear zone.
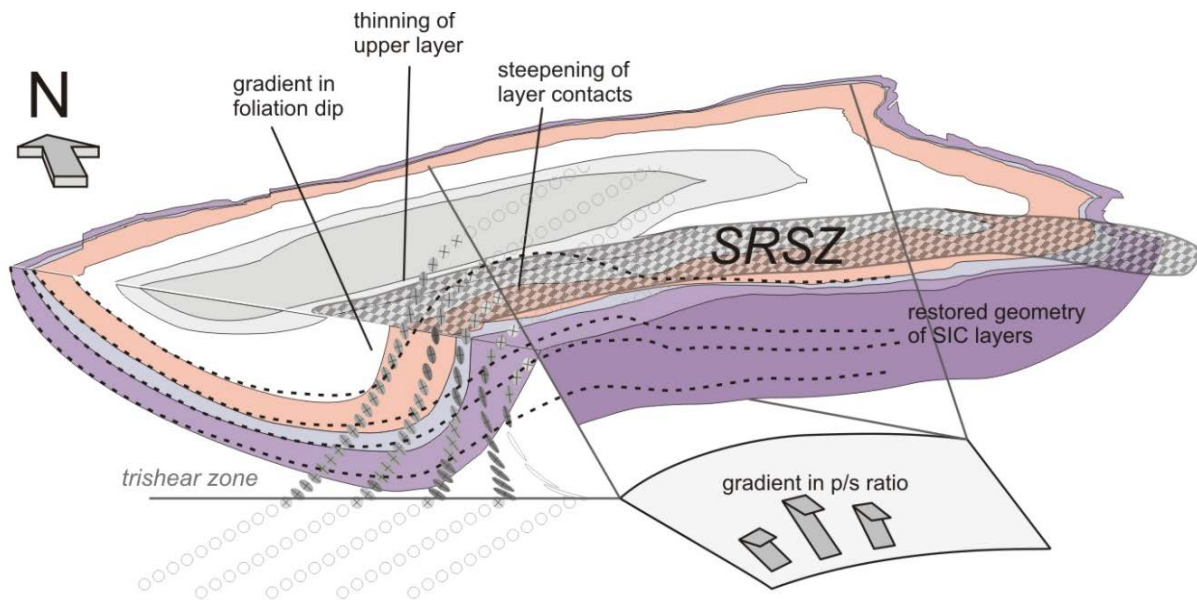
Figure 5.12: Schematic block model of the SIC with location of the trishear deformation zone. Major effects of trishear deformation on the geometry of the SIC are explained in the text.

5.7.3. Structural uplift and estimates on the height of the eroded SIC

Erosion levels in the Sudbury Basin, especially the South Range, are not well known. Estimates on the amount of structural uplift lie between 8 and 15 km (Shanks and Schwerdtner, 1991a; Golightly, 1994; Grieve and Therriault, 2000), with larger magnitudes of uplift in the South Range than in the North Range (Shanks and Schwerdtner, 1991a). The amount of eroded SIC and the geometry of the eroded sections have important ramifications on the original size of the impact melt sheet. As discussed in section 3, the height of the undeformed hanging wall is determined by the position of the trishear zone relative to the SIC and by the displacement magnitude on the thrust fault. I estimate the likely position of the eroded hanging wall based on the structural level in the trishear zone that best matches the geometry of the SIC contacts and foliation dips at the current erosion surface.

Deformation parameter important for estimating quantities of structural uplift of the hanging wall are d, α, and the p/s ratio. The distance u of the eroded SIC above the current erosion surface is a direct function of the amount of displacement on the thrust faults and its ramp angle ($u = \cos\alpha\, d$). In our backward models (Fig. 5.6), the thrust fault α dips SE at approximately 30° and displacement magnitudes range from $d = 3$ to 8 km. These numbers result in a height of the eroded SIC base that ranges from 2.6 to 6.9 km above the erosion surface. However, the p/s ratio influences the actual amount of hanging wall uplift due to fault tip propagation, whereby high p/s ratios increase the magnitude of hanging wall uplift. For example, a p/s ratio of 1 doubles the displacement d of the hanging wall on the thrust fault. In the restored section, p/s ratios vary from 0.2 to 0.8, which corresponds to height of the eroded SIC base between 3.1 and 12.5 km above the erosion surface.

To estimate the position of the eroded hanging wall, the amount of uplift u is put in relation to the position of the trishear zone with respect to the SIC. The central South Range is best represented by a structural level of the trishear zone that is located approximately 1.5 to 2.5 km above the fault tip based on the geometry of layer dips, (Fig. 5.10a) and 0.5 to 2 km above the fault tip based on thickness changes of SIC layers (Fig. 5.11b). In the forward models, the transition from the trishear zone to the hanging wall is characterized by non-rotated layer contacts, a shallow dip of layer contacts to the NW, undeformed marker ellipses and no variations in thickness (Figs. 5.10, 5.11). In forward models the basal layer is translated in the hanging wall to a height of 2 km above the current erosion level (Fig. 5.10d). Based on thickness variations, all marker layers are translated to a position between 2 and 4 km above the structural level that best matches the current erosion level (Fig. 5.11). Thereby, the base of the SIC not affected by trishear deformation likely begins at approximately 2 km above the current erosion level. As the transition between trishear zone and hanging wall is located at an increasingly lower level in the direction of the basal layer the Huronian rocks likely constitute the translated hanging wall (Fig. 5.12).

5.7.4. Effect of trishear deformation on thickness of SIC layers

Significant thickness variations of the SIC are evident by changes in (1) overall plan-view thickness, (2) the relative thicknesses of the Norite, Quartz, Gabbro and Granophyre layers, and (3) the geometry of SIC contacts (Fig. 5.1a). The causes of plan-view thickness variations in the

SIC are not yet fully understood. In general, SIC layers, especially the Norite, are thicker in the South Range than in the North Range (Fig. 5.1a). Although a petrographically distinct portion of the Norite, known as the felsic Norite, rarely exceeds 500 m plan-view thickness in the North Range, its thicknesses in the South Range generally exceed 500 m and locally even 1000 m (Keays and Lightfoot, 2004). The correlation between the thickness of the felsic Norite and the accumulation of ore deposits may indicate that the thickness variation in the Norite is primary rather than tectonically induced (Keays and Lightfoot, 2004). Consequently, the thickness variations of the entire Norite may be primary in origin. Similarly, the correspondence of plan-view SIC thickness with the metamorphic aureole in host rocks of the North Range suggests that the thickness variation of the North Range SIC is primary (Dreuse et al., 2010). In the South Range, however, the Granophyre is thinner in plan-view than in the North Range, despite the larger width of the SIC in the South Range. This supports structural studies indicating that the thickness of Granophyre in the South Range was significantly modified by deformation (Lenauer and Riller 2012a, 2012b). I investigate the effect of trishear deformation on the thickness variations of the South Range SIC.

Depending on the position of a layer in the trishear deformation zone, trishear fault propagation folding can have the effect of both thickening and thinning the layers (Fig. 5.4). Layer thinning is generally observed in the limbs and thickening in the hinge zone of the folded layers. When comparing changes in orthogonal layer thickness, it is important to note that maximum thickening of the basal layer is achieved at the base of the trishear zone (Fig. 5.11). At the base of the trishear zone the orientations of layer dips are, however, incompatible with orientations of SIC contacts (Fig. 5.10d). As the trishear zone at a structural level close to the fault tip cannot account for the geometries of lithological contacts, we surmise that layers were not thickened by trishear deformation at that level. Therefore, the increased thickness of the Norite in the South Range is likely not due to tectonic thickening.

A more likely cause for the change in proportional layer thicknesses in the South Range SIC is tectonic thinning of the Granophyre. This requires the entire SIC in the South Range to have had a larger initial thickness than in the North Range in order to maintain similar proportional widths of SIC layers. This scenario is supported by the distinct compositional difference between the SIC in the South and the North Ranges (Naldrett and Hewins, 1984). A thicker South Range SIC seems to be also evident in the Lithoprobe seismic lines and is required for gravity and magnetic models of the Sudbury Basin (Boerner et al., 2000). The sum of these pieces of evidence points to modification of proportional layer thicknesses in the South Range SIC by post-impact deformation.

True layer thicknesses were calculated for the North Range and are on average 0.5 km for the Norite and Quartz Gabbro, and 1.7 km for the Granophyre (Dreuse et al., 2010). The Norite and Quartz Gabbro constitute 28% of the total thickness of the SIC, and the Granophyre 72 %. In the South Range, the relative proportions of each of these layers are remarkably different from those of the North Range, as is well apparent from the map-view thickness of each layer (Fig. 5.1a). Based on the forward modelling profiles (Fig. 5.6), the changes in the true thicknesses of SIC layers in the South Range can be estimated. The Norite and Quartz Gabbro of the South Range SIC contribute on average 37 % and the Granophyre to 63 % of the total SIC thickness. The calculations are based on two assumptions: (1) relative proportions of the Norite and Quartz

Gabbro compared to the Granophyre were initially identical in the North and South Ranges, and (2) the Norite and Quartz Gabbro did not significantly change in thickness during deformation. The first assumption is supported by the processes of differentiation and gravitational settling of mineral phases that formed the SIC. The second assumption is corroborated by the observation that the South Range Norite is less affected by ductile deformation than the South Range Granophyre (Lenauer and Riller, 2012a). With an average combined true thickness of the Norite and Quartz Gabbro of 1.4 km, based on their proportions in the North Range, the total SIC thickness in the South Range would have amounted to 5.2 km prior to deformation. The Granophyre layer would have been approximately 3.8 km thick and, compared to its current thickness in the South Range, would have been shortened by approximately 40 %. This shortening magnitude is slightly higher than previous estimates on basin-wide shortening (Clendenen et al., 1988; Shanks and Schwerdtner, 1991b), but may actually amount to less if the Quartz Gabbro layer was also affected by tectonic thinning. In summary, areas of maximal thickness reductions correspond to areas replete with ductile deformation structures, i.e., the SRSZ.

5.8.   *Conclusions*

In this chapter I explored the combination of forward and backward modeling of deformation as a procedure to overcome insufficient depth information on planar structural elements such as lithological contacts and foliations. This procedure proved to be useful in using structural data collected at surface to infer layer geometries below and above the current erosion surface of the SIC. Dips of lithological contacts, foliation dips and thickness variations of layers are matched with layer and marker ellipse geometries in forward models. Coincidence of layer geometries of the SIC and the forward models determine the position of the trishear zone relative to the SIC at its current erosion level.

To date, the possibility of trishear fault propagation folding has not been considered for explaining the formation of the Sudbury Basin. Furthermore, few attempts have been made so far to quantify the shape change and rotation of the South Range SIC. To remedy these deficits, I applied the trishear deformation model to the SIC. Trishear deformation may serve as a plausible mechanism for the formation of the South Range SIC as the Sudbury Basin shows the following structural characteristics: (1) presence of a few thrust faults imaged in seismic lines accomplishing localized deformation (Wu et al., 1995), whereas deformation at surface is mostly distributed, (2) large angular discordance between upper and basal SIC contacts, (3) gradient in foliation dip and strain, (4) along-strike thickness variations of the SIC, (5) variable thicknesses among individual SIC layers, (6) uplifted and S-facing Huronian rocks rocks south of the SIC (Brocoum and Dalziel, 1974), and (7) correspondence of the SRSZ to high strain in the central portion of the trishear zone (Fig. 5.12). Collectively, these characteristics are not fully explained by previously invoked deformation models such as folding of the SIC followed by thrusting on SE-dipping faults (Wu et al., 1994), pure folding of the SIC (Cowan and Schwerdtner, 1994; Cowan et al., 1999), or pure translation and shearing of the South Range SIC on the SRSZ (Shanks and Schwerdtner, 1991a).

The geometry and magnitude of deformation inferred from the kinematic modeling provide the basis for a restoration of the Sudbury Basin prior to trishear deformation. The modeling allowed

us to quantify a number of deformation parameters such as displacement, p/s ratio, trishear angle, and ramp angle. The SE- and SW-termini of the South Range do not display variations in foliation dip and variations in contact dips of the SIC layers. The foliation in the SE- and SW-South Range are axial-planar to the synformal lobes and thus the metamorphic fabrics possibly formed as a consequence of folding. For the central portion of the South Range, however, trishear deformation represents a viable explanation for the deformation of the SIC and its host rocks.

Furthermore trishear deformation at Sudbury indicates that steep dips of basal SIC contact segments are spatially confined to the trishear zone and that the SIC layers dips shallowly in the footwall and in the hanging wall above the current erosion level. The hanging wall which is made up by Huronian rocks and the SIC Norite are mainly translated and show little internal deformation by shearing or rotation. As predicted by the trishear model, the highest shear strain magnitudes are present in rocks of the Granophyre and adjacent Onaping Formation, subjected to maximal tectonic thinning in the South Range. Thereby the South Range Shear Zone may be the surface manifestation of a trishear deformation zone.

5.9.   Summary

The Sudbury Igneous Complex (SIC), Canada, is an impact-induced layered sheet of crystalline rocks that deformed into an asymmetrical basin, the Sudbury Basin. The Basin geometry at depth is largely unknown. Few attempts have so far been made to quantify displacement and rotation of layer contacts and to restore the pre-deformation geometry of the SIC. Previous deformation models are based on simple folding and reverse faulting. However, variations in contact dips and layer thicknesses as well as observed gradients in foliation dip and strain of the southern SIC demand a mode complex deformation model. In this study I propose that the geometry of layers and orientations of foliation in the southern SIC can be adequately represented by trishear fault propagation folding. Trishear deformation of the central South Range SIC accounts for: (1) angular discordances between the upper and basal contact of the SIC, (2) local overturning of South Range SIC, (3) steepening of foliation planes from NW to SE, (4) strain gradient in the sedimentary rocks of the Sudbury Basin, and (5) thickness variations in the layers of South Range SIC. The South Range Shear Zone, a zone of elevated metamorphic fabric intensity, coincides with the surface manifestation of the proposed trishear zone.

My study demonstrates the use of structural data, namely dip of foliation planes, igneous layering and lithological contacts, in combination with forward kinematic modeling to determine deformation parameters such as displacement, propagation-to-slip ratio, fault angle and initial layer dip. Backward kinematic modelling of trishear deformation is used to restore the shape of igneous sheet and provides information on the geometry of and the strain distribution in the SIC.

References

Allmendinger, R., 1998. Inverse and forward numerical modeling of trishear fault-propagation folds. Tectonics 17, 640-656.

Ames, D.E., Golightly, J.P., Lightfoot, P.C., Gibson, H.L., 2002. Vitric Compositions in the Onaping Formation and Their Relationship to the Sudbury Igneous Complex, Sudbury Structure. Economic Geology 97, 1541-1562.

Ames, D.E., Farrow, C.E.G., 2007. Metallogeny of the Sudbury Mining Camp, Ontario. *In*: Goodfellow, W.D. (Ed.), Mineral deposits of Canada- A synthesis of Major Deposit types, District Metallogeny, the Evolution of Geological Provinces and Exploration Methods, Geological Association of Canada Special Publication 5, 329-350.

Bailey, J., Lafrance, B., McDonald, A.M., Fedorowich, J.S., Kamo, S., Archibald, D.A., 2004. Mazatzal–Labradorian-age (1.7–1.6 Ga) ductile deformation of the South Range Sudbury impact structure at the Thayer Lindsley mine, Ontario. Canadian Journal of Earth Sciences 41, 1491-1505.

Boerner, D.E., Milkereit, B., Wu, J., Salisbury, M., 2000. Seismic images and three-dimensional architecture of a Proterozoic shear zone in the Sudbury Structure (Superior Province, Canada). Tectonics 19, 397-405.

Brocoum, S., Dalziel, I., 1974. The Sudbury Basin, the Southern Province, the Grenville Front, and the Penokean Orogeny. Geological Society of America Bulletin 85, 1571-1580.

Cantin, R., Walker, R.G., 1972. Was the Sudbury Basin Circular During the Deposition of the Chelmsford Formation? Geological Association of Canada, Special Paper Number 10, 93-101.

Card, K.D., 1978. Geology of the Sudbury-Manitoulin Area, District of Sudbury and Manitoulin; Ontario Geological Survey, Report 166, 238 p.

Card, K.D., Church, W.R., Franklin, J.M., Robertson, J.A., West, G.F., Young, G.M., 1972. The Southern Province. *In*: Price, R.A., Douglas, R.J.W. (Eds.), Variations in Tectonic Style in Canada. Geological Association of Canada Special Paper 8, 335-380.

Card, K.D., Hutchinson, R.W., 1972. The Sudbury Structure: Its Regional Setting. Geological Association of Canada, Special Paper Number 10, 67-78.

Card, K.D., Pattison, E.F., 1973. Nipissing diabase of the Southern Province, Ontario. *In:* Young, G.M. (Ed.), Huronian Stratigraphy and Sedimentation. Geological Association of Canada, Special Paper 12, 7-30.

Cardozo, N., 2005. Trishear modeling of fold bedding data along a topographic profile. Journal of Structural Geology 27, 495-502.

Cardozo, N., Bhalla, K., Zehnder, A., Allmendinger, R., 2003. Mechanical models of fault propagation folds and comparison to the trishear kinematic model. Journal of Structural Geology 23, 1883-1899.

Clark, M.D., Riller, U., Morris, W.A., 2012. Upper-crustal, basement-involved folding in the East Range of the Sudbury Basin, Ontario, inferred from paleomagnetic data and spatial analysis of mafic dykes. Canadian Journal of Earth Science (in press).

Clendenen, W.S., 1986. Finite strain study of the Sudbury Basin, Ontario. M.Sc. thesis, University of Colorado, Boulder, 253 pp.

Clendenen, W.S., Kligfield, R., Hirt, A.M., Lowrie, W., 1988. Strain studies of cleavage development in the Chelmsford Formation, Sudbury Basin, Ontario. Tectonophysics, 145, 191-211.

Cowan, E.J., 1996. Deformation of the Eastern Sudbury Basin. Ph.D. thesis, University of Toronto, Toronto, 366p.

Cowan, J., 1999. Magnetic fabric constraints on the initial geometry of the Sudbury Igneous Complex: a folded sheet or a basin-shaped igneous body? Tectonophysics 307, 135-162.

Cowan, E.J., Schwerdtner W.M., 1994. Fold origin in the Sudbury basin. *In*: Lightfoot, P.C., Naldrett, A.J. (Eds.), Proceedings of the Sudbury - Noril'sk Symposium. Special Volume 5, Ontario Geological Survey, 45-55.

Cowan, E.J., Riller, U., Schwerdtner, W.M., 1999. Emplacement geometry of the Sudbury Igneous Complex: Structural examination of a proposed impact melt-sheet. *In*: Dressler, B.O., Sharpton, V.L., Large Meteorite Impacts and Planetary Evolution II. GSA Special Paper 339, Geological Society of America, Boulder, 399–418.

Cristallini, E.O., Giambiagi, L., Allmendinger, R.W., 2004. True three-dimensional trishear: A kinematic model for strike-slip and oblique-slip deformation. Geological Society of America Bulletin 116, 938-952.

Deutsch, A., Grieve, R.A.F., Avermann, M., Bischoff, L., Brockmeyer, P., Buhl, D., Lakomy, R., Müller-Mohr, V., Ostermann, M., Stöffler, D., 1995. The Sudbury Structure (Ontario, Canada): A tectonically deformed multi-ring impact basin. Geologische Rundschau 84, 697-709.

Dressler, B.O., 1984. Sudbury Geological Compilation: Ontario Geological Survey Map 2491, Precambrian Geology Series, Scale 1:50 000.

Dreuse, R., Doman, D., Santimano, T., Riller, U., 2010. Crater floor topography and impact melt sheet geometry of the Sudbury impact structure. Terra Nova, 22, 463-469.

Easton, R.M. 2000. Metamorphism of the Canadian Shield, Ontario, Canada. II. Proterozoic metamorphic history. Canadian Mineralogist 38, 319-344.

Erslev, E.A., 1991.Trishear fault-propagation folding. Geology 19, 617-620.

Fleet, M.E., Barnett, R.L., Morris, W.A., 1987. Prograde metamorphism of the Sudbury igneous complex. Canadian Mineralogist 25, 499-514.

Flinn, D., 1962. On Folding during Three-dimensional Progressive Deformation. Quarterly Journal of the Geological Society 118, 385-433.

Golightly, J.P., 1994. The Sudbury Igneous Complex as an Impact Melt: Evolution and Ore Genesis. *In:* Lightfoot, P.C., Naldrett, A.J. (Eds.), Proceedings of the Sudbury-Noril'sk Symposium. OGS Special Volume 5, 105-118.

Grieve, R., Stöffler, D., Deutsch, A., 1991. The Sudbury Structure - controversial or misunderstood. Journal of Geophysical Research 96, 22753-22764.

Grieve, R., Therriault, A., 2000. Vredeford, Sudbury, Chicxulub: Three of a kind? Annual Reviews of Earth and Planetary Sciences 28, 305-338.

Grieve, R.A.F., Ames, D.E., Morgan, J.V., Artemieva, N., 2010. The evolution of the Onaping Formation at the Sudbury Impact Structure. Meteoritics and Planetary Science 45, 759-782.

Hardy, S., Ford, M., 1997. Numerical modeling of trishear fault propagation folding. Tectonics 16, 841-854.

Hirt, A.M., Lowrie, W., Clendenen, W.S., Kligfield, R., 1993. Correlation of strain and the anisotropy of magnetic susceptibility in the Onaping Formation: evidence for a near-circular origin of the Sudbury Basin. Tectonophysics 225, 231-254.

Keays, R.R., Lightfoot, P.C., 2004. Formation of Ni-Cu-Platinum Group Element sulfide mineralization in the Sudbury Impact Melt Sheet. Mineralogy and Petrology 82, 217-258.

Kligfield, R., Lowrie, W., Dalziel, I.W.D., 1977.Magnetic susceptibility anisotropy as a strain indicator in the Sudbury Basin, Ontario. Tectonophysics, 40, 287-308.

Klimczak, C., Wittek, A., Doman, D., Riller, U., 2007. Fold origin of the NE-lobe of the Sudbury Basin, Canada: Evidence from heterogeneous fabric development in the Onaping Formation and the Sudbury Igneous Complex. Journal of Structural Geology 29, 1744-1756.

Krogh T.E., Davis D.W., Corfu F., 1984. Precise U-Pb zircon and Baddeleyite Ages for the Sudbury Area. *In*: Pye, E.G., Naldrett, A.J., Giblin, P.E. (Eds.), The Geology and Ore Deposits of the Sudbury Structure. Special Publication 1, Ontario Geological Survey, Toronto, 431-446.

Long, D.G.F., 2004. The tectonostratigraphic evolution of the Huronian basement and the subsequent basin fill: geological constraints on impact models of the Sudbury event Precambrian Research 129, 203-223.

McDaniel, D.K., Hemming, S.R., McLennan, S.M., Hanson, 1994. Petrographic, geochemical, and isotopic constraints on the provenance of the early Proterozoic Chelmsford Formation, Sudbury Basin, Ontario. Journal of Sedimentary Research 64, 362-372.

Milkereit, V., Green, A., Sudbury Working Group, 1992. Deep geometry of the Sudbury Structure from seismic reflection profiling. Geology 20, 807-811.

Morris, W.A., 1980. Tectonic and Metamorphic History of the Sudbury Norite: The Evidence from Paleomagnetism. Economic Geology 75, 260-277.

Morris, W.A., 1984. Paleomagnetic constraints on the magmatic, tectonic, and metamorphic evolution of the Sudbury Basin region. *In:* Pye, E.G., Naldrett, A.J., Giblin, P.E. (Eds.), The Geology and Ore Deposits of the Sudbury Structure. Special Publication 1. Ontario Geological Survey, Toronto, 411-427.

Naldrett, A.J., Hewins, H.R., 1984. The Main Mass of the Sudbury Igneous Complex. *In:* Pye, E.G., Naldrett, A.J., Giblin, P.E. (Eds.), The Geology and Ore Deposits of the Sudbury Structure. Special Publication 1. Ontario Geological Survey, Toronto, 235-252.

Peredery, W.V., Morrison, G.G., 1984. Discussion of the Origin of the Sudbury Structure. *In* Pye, E.G., Naldrett, A.J., Giblin, P.E. (Eds.), The Geology and Ore Deposits of the Sudbury Structure. Special Publication 1. Ontario Geological Survey, Toronto, 491-511.

Piercey, P., Schneider, D.A., Holm, D.K., 2007. Geochronology of Proterozoic metamorphism in the deformed Southern Province, northern Lake Huron region, Canada. Precambrian Research 157, 127-143.

Riller, 2005. Structural characteristics of the Sudbury impact structure, Canada: Impact-induced versus orogenic deformation – A review. Meteoritics and Planetary Science, 40, 1723-1740.

Riller, U., Schwerdtner, W.M., 1997. Mid-crustal deformation at the southern flank of the Sudbury Basin, central Ontario, Canada. Geological Society of America Bulletin 109, 841-854.

Riller, U., Schwerdtner, W. M., Robin, P.-Y. F., 1998. Low-temperature deformation mechanisms at a lithotectonic interface near the Sudbury Basin, Eastern Penokean Orogen, Canada. Tectonophysics 287, 59-75.

Riller, U., Schwerdtner, W., Halls, H., Card, K., 1999. Transpressive tectonism in the Eastern Penokean Orogen, Canada. Consequences for Proterozoic crustal kinematics and continental fragmentation. Precambrian Research 93, 51-70.

Rousell, D.H., 1975. The Origin of Foliation and Lineation in the Onaping Formation and the Deformation of the Sudbury Basin. Canadian Journal of Earth Sciences, 12, 1379-1395.

Rousell, D.H., 1984a. Structural Geology of the Sudbury Basin. *In* Pye, E.G., Naldrett, A.J., Giblin, P.E. (Eds.), The Geology and Ore Deposits of the Sudbury Structure. Special Publication 1. Ontario Geological Survey, Toronto, 83-96.

Rousell, D.H., 1984b. Onwatin and Chelmsford Formations. *In* Pye, E.G., Naldrett, A.J., Giblin, P.E. (Eds.), The Geology and Ore Deposits of the Sudbury Structure. Special Publication 1. Ontario Geological Survey, Toronto, 211-218.

Santimano, T., Riller, U., 2012. Revisiting thrusting, reverse faulting and transpression in the southern Sudbury Basin, Ontario. Precambrian Research 200-203, 74-81.

Shanks, W.S., Schwerdtner, W.M., 1991a. Structural analysis of the central and southwestern Sudbury Structure, Southern Province, Canadian Shield. Canadian Journal of Earth Sciences 28, 411-430.

Shanks, W.S., Schwerdtner, W.M., 1991b. Crude quantitative estimates of the original northwest-southeast dimension of the Sudbury Structure, southcentral Canadian Shield. Canadian Journal of Earth Sciences 28, 1677-1686.

Thomson, M.L., R.L. Barnett, Fleet, M.E., Kerrich, R., 1985. Metamorphic assemblages in the South-Range Norite and the footwall mafic rocks near the Kirkwood Mine, Sudbury, Ontario. The Canadian Mineralogist 23, 173-186.

Tschirhart, P., Morris, W.A. 2012. Grenville age deformation of the Sudbury impact structure: evidence from magnetic modelling of the Sudbury diabase dyke swarm. Terra Nova 24, 213-220.

Van Schmus, W.R., 1976. Early and middle Proterozoic history of the Great Lakes area, North America. Royal Society of London Philosophical Transactions A280, 606-628.

Wu, J., Milkereit, B., Boerner, D., 1995. Seismic imaging of the enigmatic Sudbury Structure. Journal of Geophysical Research, 100, 4117-4130.

Young, G.M., Long, D.G.F., Fedo, C.M., Nesbitt, H.W., 2001. Paleoproterozoic Huronian basin: product of a Wilson cycle punctuated by glaciations and meteorite impact. Sedimentary Geology 141-142, 233-254.

Zehnder, A.T., Allmendinger, R.W., 2000. Velocity field for the trishear model. Journal of Structural Geology 22, 1009-1014.

Zieg, M.J., Marsh, B.D., 2005. The Sudbury Igneous Complex: Viscous emulsion differentiation of a superheated melt sheet. Geological Society of America Bulletin 117, 1427-1450.

6.   Conclusions and future outlook

6.1.   *Key results*

In Chapter 3, I presented my analysis of igneous and metamorphic mineral fabrics to determine possible deformation mechanisms of the South Range SIC. The orientation of inclined igneous cumulate fabrics provided insight into the deforming SIC, specifically the amount of rotation of the South Range SIC. Chapter 3 focussed further on small-scale brittle to ductile shear faults and their relevance for the formation of a pervasive planar fabric. I found that brittle shear faults in the Norite coalesce and form a network of conjugate faults, and with increasing levels of deformation form a pervasive fabric. The process of fabric development with increasing deformation is observed on the scale of several meters, and is evident on map scale by a transition of a conjugate fabric in the Norite to uniformly dipping foliation in the Granophyre. The fabric is compatible with coaxial shortening, a process which contributed to the rotation of material planes, i.e., the igneous layering and the basal contact of the SIC.

My structural analyses in Chapter 4 explored the distribution and orientation of fold structures and mineral fabrics in the Huronian rocks south of the Sudbury Basin. Using the Sudbury Breccia as a marker, it was possible to distinguish between pre- and post-impact foliations. Post-impact foliations formed both orthogonal and parallel to the map-view trace of the basal SIC contact, although orthogonal fabrics generally overprint contact-parallel fabrics. Foliations at a high angle to the basal SIC contact are found most commonly in the central South Range, and, thus, are reminiscent of axial-planar cleavage of a buckle fold localized at the concave inward shape of the upper SIC contact. Radially disposed buckle folds form as a consequence of the shortening of circular mechanical heterogeneities and are proposed to accommodate the shape change of the SIC from a convex outward to a concave inward geometry. Due to the association of changes in fabric orientation with changes in strike of SIC contacts, it is suggested that the shape of the SIC itself had a significant influence of fabric formation in the adjacent rocks.

In Chapter 5, I assessed deformation mechanisms of the South Range SIC using structural modeling techniques. Specifically, I tested the applicability of trishear fault propagation folding to incorporate observations of SE-dipping thrust planes and distributed deformation with a strain gradient from NW to SE at surface. Initial experiments using forward modeling explored the effects of variable deformation parameters such as displacement, trishear angle, ramp angle and propagation-to-slip ratio on the geometry and strain on the deformed rocks. Restoration of sections across the Sudbury Basin showed that variable deformation parameters are required to restore deformation along strike of the South Range. To achieve a smooth initial geometry of the SIC, the central South Range requires propagation-to-slip ratios and displacements greater than in the eastern and western South Range. The trishear model accounts for the angular discordance of lithological contacts between the SIC layers, the gradient in foliation dip, and increased strain in the South Range Shear Zone associated with thinning of the South Range Granophyre, and subvertical orientation of Offset Dikes, i.e. non-rotation of Huronian rocks after the emplacement of the SIC.

In summary, the key results from my study specifically for the Sudbury Basin are: (1) brittle deformation significantly influenced the shape change of the South Range SIC, especially the

Norite, (2) non-cylindrical radially-disposed buckling and associated mineral fabric development accommodated the shape change of the SIC, resulting in mutually perpendicular fabric orientations compatible with overall NW-SE shortening, (3) the original shape of the SIC directly influenced the geometry of metamorphic foliations, (4) differential rotation affected the SIC layers and the Huronian host rocks, and (5) there is a gradational strain increase from the NW to the SW in the South Range. The major components of deformation of the southern Sudbury Basin and its host rocks are NW-SE horizontal shortening leading to steepening of the SIC layers and igneous fabrics, trishear fault-propagation folding at the tip of a SE-dipping thrust fault, and concentric layer-parallel shortening leading to buckling and formation of NW-SE striking axial-planar cleavage in the basal SIC and Huronian rocks.

This study has significant implications for understanding the response of a mafic crystalline sheet to tectonic strain. Shear faults and their spatial distribution in the igneous complex accommodated shortening by coalescing to form pervasive ductile fabrics. This mechanism leads to the rotation of material planes, such as igneous layering. Furthermore, I document the effect of mechanical heterogeneities on the geometry of deformation fabrics by illustrating the relationship between the orientation of lithological contacts and the orientation of mineral fabrics. As a consequence, highly discordant planar strain fabrics can be generated by local strain perturbations near igneous sheets under uniform regional shortening. Local shortening directions were successfully inferred from the inversion of brittle fault planes and striations. The methodology commonly applied for neotectonic settings proved equally effective for the determination of local shortening directions in Paleoproterozoic rocks. Finally, a compilation of surface data, i.e. shortening directions, foliation surfaces and igneous layering, provided the basis for kinematic modeling and restoration. I matched the geometry of deformed layers and markers in a forward model to the observed contact dips and foliation orientations in the study area. Thereby, it was possible to estimate the magnitude of deformation parameters such as displacement magnitude, fault angle and fault tip propagation. The combination of forward and backward modeling provided insight into the geometry of layers where depth information is scarce.

6.2.   Outlook for further research

6.2.1. <u>Documentation of metamorphic mineral fabrics</u>

The majority of my analyses are based on outcrop-scale observations of foliation surfaces, shear planes and the minerals decorating these faults. Data obtained at surface is compiled into plan-view deformation patterns, which allow the correlation of mineral fabrics and the interpretation of structures over a wide area. Structural field observations greatly benefit from the study of mineral composition and interactions on a grain-scale in foliated and sheared rocks. This would allow a better assessment of the pressure and temperature conditions under which metamorphic fabrics formed. Fleet et al. (1984) document prograde metamorphic mineral assemblages formed at lower amphibolite-facies metamorphic conditions in the South Range Norite. Their observations, which complement data from Card et al. (1978), indicate that the highest metamorphic grade occurs in the Offset Dikes near the South Range and that metamorphic grade decreases to the NW (Fleet et al., 1984). The zonation in metamorphic grade, however, differs from the intensity of ductile deformation, which is greatest in the Granophyre and decreases to the SE. In order to address this issue, the mineral composition of foliations and shear faults need to be places in context with map-scale deformation patterns.

Determination of pressure and temperature conditions of deformation at the time of tectonometamorphic overprint may further allow the deformation of the SIC to be correlated with the cooling of the melt sheet and with regional orogenic events. Such correlations are greatly facilitated by radiometric age dating of metamorphic minerals. To date the only radiometric age of deformation is obtained from $^{40}Ar/^{39}Ar$ analysis of syntectonic titanites (Bailey et al., 2004). The obtained 1.7 to 1.6 Ga age correlates with the Mazatzal-Labradorian orogeny. However, other studies attribute deformation of the SIC to 1.89 to 1.83 Ga Penokean age deformation (e.g. Riller, 2005), specifically during cooling of the melt sheet (e.g., Morris, 1981; Riller et al., 1996; Rosenberg and Riller, 2000; Klimczak et al., 2004). Radiometric dates of syntectonic minerals in the foliations observed in the Sudbury Breccia could provide additional constraints on the age of metamorphic fabric formation.

6.2.2. <u>South Range deformation in the context of the shape change of the Sudbury Basin</u>

This study focusses on the magnitude and orientation of deformation in the South Range of the Sudbury Basin, as the southern part of the Basin displays pervasive foliation and steepest dips of its lithological contacts. However, deformation of the SIC is not limited to the South Range, as is evident from the plan-view geometry of the Sudbury Basin. The Basin locally deviates from its overall elliptical shape and second-order syn- and anticlines are evidence that deformation affected various parts of the SIC. Metamorphic foliation crosscuts the East Range and the second-order folds of the SIC. Fault displacement is observed throughout the Basin.

For one, the North Range is dissected by NW-SE striking faults of the Onaping Fault System that displace the SIC (Buchan and Ernst, 1994). The North Range SIC dips approximately 30° SE (Dressler, 1984; Dreuse et al., 2010), a dip magnitude which had been attributed to 1) the original emplacement angle of the SIC (Cowan et al., 1999; Morris, 1980; Dreuse et al., 2010), 2) wholesale tilt of the Sudbury area to the SE (Ivanov, 2005; Halls, 2009), and 3) folding of the SIC during formation of the Sudbury Basin (Cowan and Schwerdtner, 1994). Secondly, the SIC

basal contact dips at a high angle to the W and is locally overturned in the East Range. Additionally to the rotation of the SIC contacts, the NE-lobe was formed due to folding (Klimczak et al., 2007; Clark et al., 2012). The relationship of steeply inclined lithological contacts with the fold geometry is, however, not yet resolved in detail. For the East Range the geometry and magnitude of deformation are largely unresolved.

In Chapter 4 the formation of the syn- and anticlines in the Sudbury Basin is described as the result of concentric shortening. The East Range and its bounding lobes may provide a suitable location for testing this scenario and for comparing deformation at different locations in the Sudbury Basin. Effectively, an analysis of foliations and brittle faults in the East Range SIC, its Huronian host rocks and Sudbury Breccia will provide more information on the folding mechanisms that accommodated the shape change of the SIC. Metamorphic mineral fabric analysis focussed on post-impact foliation in the footwall rocks of the North and East Ranges may provide additional insight into the mechanisms of the formation of higher-order folds. Furthermore, shear faults associated with buckle folds in the East and North Ranges may indicate that the consequences of concentric shortening are similar at various positions in the Sudbury Basin.

The results of my study describe mutually independent deformation mechanisms that affected the shape change of the Sudbury Basin. These are the formation of second-order buckle folds in the SIC, strain gradients, and uplift of a largely undeformed hanging wall, and rotation of material planes, i.e. the basal SIC contact, as a consequence of bulk thinning. However, the relative timing of deformation of the South Range and the formation of the synclinal lobes has not yet been resolved. One approach could involve the search for cross-cutting fabrics in the SE-lobe thus determining the transition of folding strain induced by the lobes and strain as a result of thrust faulting. Even though all components of deformation have been discussed separately, assembling the separate components into one quantitative model is a future project that needs to be tackled. This can be achieved by the creation of a Basin-wide model of the three-dimensional geometry and deformation.

6.2.3. The extent of post-impact deformation beyond the Sudbury Basin

The rocks surrounding the SIC are heterogeneous in composition, ranging from granulites and gneisses in the North Range, to metavolcanic and metasedimentary rocks in the South Range. This inhibits the Basin-wide correlation of deformation fabrics, as each rock type responds differently to strain and stress fields. The Sudbury Breccia, however, is likely mechanically similar independent of its host rock. In this study, the Breccia proved as a valuable marker in separating pre- from post-impact deformation. Outcrops of Sudbury Breccia are abundant and are present in each of the host rocks of the SIC and occur up to 80 km away from the basal SIC contact (Dressler, 1984). By tracking deformation fabrics in the breccia at various locations surrounding the Sudbury Basin, the tectonic effects on these rocks can be systematically documented and correlated over a large area.

Detailed studies of the fabric geometry and mineral composition of the deformed matrix of the Sudbury Breccia can provide a proxy for the deformation of the host rocks of the SIC. Specifically, in the South Range the documentation of fabrics in the Sudbury Breccia matrix

could be used to track a possible gradient of deformation intensity in relation to the SIC, or with distance to the Grenville Front Tectonic Zone. In the North Range, the fabric of the Sudbury Breccia allows tracking of local post-impact strain. For example, according to Kellett and Rivard (1997), Sudbury Breccia exposed in the Benny Deformation Zone, an E-W striking shear zone approximately 15 km north of the Sudbury Basin (Fig. 2.2), is deformed along with its country rocks. In areas where the recognition of post-impact structures is obscured by the presence of pre-impact fabrics, deformation-induced mineral fabrics in Sudbury Breccia allow identification of structures related to the deformation of the SIC itself. Thereby these rocks act as a key marker unit for assessing the extent of post-impact deformation.

The nature of the mineralogical changes through metamorphism in the Sudbury Breccia can lead to a clearer description of post-impact deformation. Additionally to the Sudbury Breccia, quartz diorite offset dikes can aid in constraining post-impact deformation. By constraining the magnitudes of fault offset, rotational components and internal shearing of breccia material, these dikes provide an additional marker for quantification of post-impact deformation. The offset dikes represent an ideal marker for deformation as they are disposed radially around the Sudbury Basin and are oriented both orthogonal and parallel to the SIC basal contact. The comparison of the orientation and possible rotation of the offset dikes at various positions might allow deformation magnitude to be traced around the Sudbury Basin.

References

Bailey, J., Lafrance, B., McDonald, A., Fedorowich, J., Kamo, S., Archibald, D., 2004. Mazatzal-Labradorian-age (1.7-1.6 Ga) ductile deformation of the South Range Sudbury impact structure at the Thayer Lindsley mine, Ontario. Canadian Journal of Earth Sciences 41, 1491-1505.

Buchan, K.L., Ernst, R.E., 1994. Onaping fault system: age constraints on deformation of the Kapuskasing structural zone and units underlying the Sudbury Structure. Canadian Journal of Earth Sciences 31, 1197-1205.

Clark, M.D., Riller, U., Morris, W.A., 2012. Upper-crustal, basement-involved folding in the East Range of the Sudbury Basin, Ontario, inferred from paleomagnetic data and spatial analysis of mafic dykes. Canadian Journal of Earth Sciences. (in press)

Card, K.D. 1978. Metamorphism of Middle Precambrian (Aphebian) rocks of the eastern Southern Province. *In*: Fraser, J.A., Heywood, W.W. (Eds.), Metamorphism in the Canadian Shield. Geological Survey of Canada, Paper 78-10, 269-282.

Cowan, E.J., Schwerdtner W.M., 1994. Fold origin in the Sudbury basin. *In*: Lightfoot, P.C., Naldrett, A.J. (Eds.), Proceedings of the Sudbury - Noril'sk Symposium. Special Volume 5, Ontario Geological Survey, 45-55.

Cowan, J., Riller, U., Schwerdtner, W., 1999. Emplacement geometry of the Sudbury Igneous Complex: Structural examination of a proposed impact melt sheet. *In:* Dressler, B. O., Sharpton, V. L. (Eds.), Large Meteorite Impacts and Planetary Evolution II. The Geological Society of America, Washington, D.C., 399-418.

Dressler, B.O., 1984. Sudbury Geological Compilation: Ontario Geological Survey Map 2491, Precambrian Geology Series, Scale 1:50 000.

Dreuse, R., Doman, D., Santimano, T., Riller, U., 2010. Crater floor topography and impact melt sheet geometry of the Sudbury impact structure. Terra Nova, 22, 463-469.

Fleet, M.E., Barnett, R.L., Morris, W.A., 1987. Prograde metamorphism of the Sudbury igneous complex. Canadian Mineralogist 25, 499-514.

Halls, H.C., 2009. A 100 km-long paleomagnetic traverse radial to the Sudbury Structure, Canada and its bearing on Proterozoic deformation and metamorphism of the surrounding basement. Tectonophysics 474, 493-506.

Ivanov, B.A., 2005. Numerical Modeling of the Largest Terrestrial Meteorite Craters. Solar System Research 39, 381–409.

Kellett, R.L., Rivard, B., 1996. Characterization of the Benny deformation zone, Sudbury, Ontario. Canadian Journal of Earth Sciences 33, 1256–1267.

Klimczak, C., Wittek, A., Doman, D., Riller, U., 2007. Fold origin of the NE-lobe of the Sudbury Basin, Canada: Evidence from heterogeneous fabric development in the Onaping Formation and the Sudbury Igneous Complex. Journal of Structural Geology 29, 1744-1756.

Morris, W.A., 1980. Tectonic and Metamorphic History of the Sudbury Norite: The Evidence from Paleomagnetism. Economic Geology 75, 260-277.

Morris, W.A., 1981. Intrusive and Tectonic History of the Sudbury Micropegmatite: The Evidence from Paleomagnetism. Economic Geology 76, 791-804.

Riller, U., 2005. Structural characteristics of the Sudbury Impact Structure, Canada: impact-induced and orogenic deformation – a review. Meteoritics and Planetary Science 40, 1723-1740.

Riller, U., Cruden, A.R., Schwerdtner, W.M., 1996. Magnetic fabric and microstructural evidence for a tectono-thermal overprint of the early Proterozoic Murray pluton, central Ontario, Canada. Journal of Structural Geology 18, 1005-1016.

Rosenberg, C.L., Riller, U., 2000. Partial-melt topology in statically and dynamically recrystallized granite. Geology 28, 2-7.